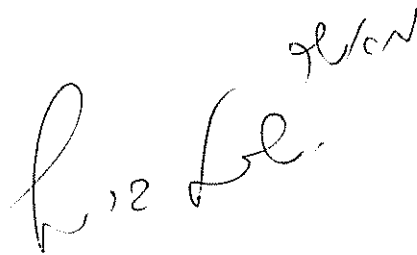


Optical Studies of Two-Dimensional Hole and Electron
Gases in Intrinsic GaAs Quantum Wells

*Thesis for the Degree of
Doctor of Philosophy by*

Shmuel Glasberg

Supervisor: Prof. Israel Bar-Joseph

A handwritten signature in black ink, appearing to read 'Shmuel Glasberg' with a stylized flourish above the name.

*Submitted to the Scientific Council of
The Weizmann Institute of science,
Rehovot, Israel.*

July 2001

Abstract

In this work we have studied the magneto-optical properties of two-dimensional hole and electron gases - mainly at low densities. We developed and refined a technique to generate the two-dimensional hole and electron gases in intrinsic quantum wells. The generation of the carrier density is based on optical excitation and space-charge separation. We show that optical generation of hole and electron gases is advantageous to doping samples in a few aspects: Having narrower spectral lines; The type of gas (hole or electron) can be changed within the same sample; Spatially separated electron and hole gases can be realized in extremely close proximities; Having control over the lateral carrier density profile.

At a low carrier density the optical properties of two-dimensional electron and hole gases are dominated by the *negatively* (X^-) and *positively* (X^+) *charged excitons*, respectively. The narrow spectral lines we achieved enabled us to obtain the spectrum of the X^+ in a magnetic field. The control over the type of gas enabled the quantitative comparison of the X^+ properties with those of the X^- within the same sample. The main finding is the near equal binding energies of the two at zero magnetic field, and the determination of their different behavior in a magnetic field. This information is valuable for understanding the three-body structure of the two exciton-ions. Another important finding is the observation of the valence band Landau levels through the X^+ shake-up spectrum.

In another part of the work we have measured the properties of the neutral exciton and charged excitons in a parallel magnetic field. The electron-hole exchange splitting and the aspherical Luttinger parameter were measured for the first time in a wide quantum well. In the closing chapter we report results on the measurements of screening in a 2DEG-hole system near $\nu=1$. These were obtained with the electron carrier density being laterally varied continuously, while performing spatial optical imaging of the Hall effect near the $\nu=1$ contour.

Acknowledgements

I wish to thank all those who helped me accomplish this research work. First and foremost, I thank Israel Bar-Joseph, my supervisor, who always provided help, guidance and momentum to the research. I also value much the intellectual spin he gained the experimental results and puzzles.

Special thanks I owe to Gleb Finkelstein who introduced me to the field of charged excitons and provided help in the first year. I would like to thank Yael Hanein who reintroduced me to the Submicron center. I'm pleased to thank Hadas for her warm and enthusiastic attitude and her involvement by providing me with the CBE samples. I enjoyed the fruitful cooperation we had with Philip Klipstein, and Adi Stern. I want to thank Guy Eytan, Yossi Yayon and Go Yusa, for their assistance, useful discussions and enjoyable lunch and coffee breaks. I also want to thank Aron and all the people at the workshop for their assistance and work. I am glad to thank Herman, Yossi, and Solomon for their quick response to my liquid helium requests. I thank all the staff members of the sub-micron center for there contribution to this research work: Diana, Late Sorina, Yoram, Olga, Misha, Vladimir, Maya, Miri and Roby. I want to thank all students that were in the sub-micron center during my work for the partnership and for creating a good and stimulating atmosphere.

Finally I wanted to thank my wife, Tal, who encouraged me throughout this period.

Table of Contents

1. Introduction	2
1.1 Two-dimensional electron and hole gases in quantum-wells	2
1.2 Positively and Negatively charged excitons	5
1.3 Experimental methods	9
2. Main results	15
2.1 Techniques to optically generate hole and electron gases in intrinsic quantum wells	16
2.1.1 Coupled 2DEG-2DHG system	18
2.1.2 A laser with separate control of N_e and N_h	20
2.2 The positively charged exciton magneto-optical spectra in GaAs quantum wells	23
2.3 Landau levels in the recombination spectrum of a low-density two-dimensional hole gas	29
2.4 Neutral and charged excitons in a parallel magnetic field	35
2.4.1 Polarization of charged excitons in a parallel magnetic field	39
2.5 Spatial imaging of the photoluminescence from a two-dimensional electron gas near filling factor $\nu=1$	44
3. Summary	49

1. Introduction

1.1 Two-dimensional electron and hole gases in quantum wells

Two dimensional electron (2DEG) and hole (2DHG) gases can be formed between two different band gap semiconductor materials such as GaAs and AlGaAs. The electron or hole carrier density is obtained by introducing a layer of dopants at a distance of a few tens of nanometers away from a GaAs/AlGaAs heterostructure. This technique, known as modulation doping, suppresses carriers scattering off the impurities and gives excellent transport properties [1,2]. Perhaps the most appealing property of the 2DEG and 2DHG is the tunability of the carrier density, all the way from zero to metallic densities. The typical Fermi energy is comparable with that a carrier can gain from modest electric or magnetic fields, characterized by eEa_B and $\hbar\omega_c$, respectively. The Fermi energy is also comparable with the typical confinement energy in a heterostructure, which is of the order of $\hbar^2/2m^*a_B^2$. Hence by applying external fields and band-gap engineering one can strongly affect the carriers properties. Another important implication of the low Fermi energy is its comparable magnitude with the characteristic carrier-carrier Coulomb interaction, $e^2/\epsilon a_B$ (which equals ~ 10 meV in GaAs), resulting in pronounced effects due to the many-body interaction.

The 2DEG and 2DHG may be treated on an equal footing, as variants of the same concept. However, part of the diverse physical implications follows from unique properties of each. The underlying differentiating property is the semiconductor band structure. Figure 1 shows the band structure for a bulk semiconductor, and for a quantum well potential. In GaAs the conduction band has s symmetry and the valence band - p symmetry. The holes are significantly heavier, and the e/h mass ratio is $\sim 1/6$ [3]. The valence band consists of three subbands: the heavy-hole and the light-hole subbands, which are degenerate at $k=0$, and the split-off subband, which has a lower energy (not shown). The introduction of a band gap discontinuity in the form of quantum-wells (QWs) modifies the band structure. As seen, the confinement causes a removal of valence band degeneracy at $k=0$, and an energy gap forms between the heavy and light hole subbands. The typical energy splitting between the two subbands ranges from a few meV in wide QWs to few tens of meV in narrow ones. External fields may mix the two

subbands; e.g. changing the relative weight of the two in the hole wave-function. This is an important source for the complicated behavior of holes.

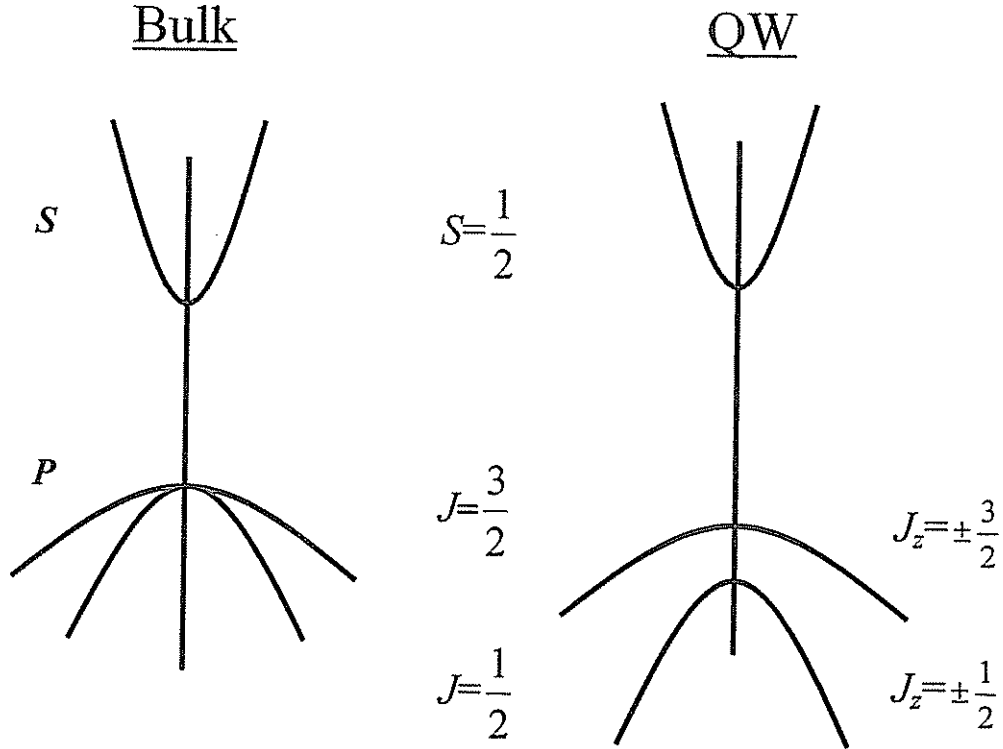


Fig. 1: Band-Structure of GaAs bulk and quantum well

A schematic diagram of a 2DEG in a modulation doped QW is shown in Fig. 2. A layer of donors is introduced into the high band-gap material; the excess electrons diffuse and are trapped by the QW, which is located at a certain distance (spacer) from the donors layer. Under steady-state conditions the bands are bent by the self-consistent potential due to the local charges. This results in a triangular-like potential, confining the electrons close to the hetero-interface. A similar drawing for a 2DHG is found in chapter 2.1.

An important issue in optical experiments is the effect of illumination on the properties of the electron and hole gases in GaAs. Usually the effects of illumination extinguish at short times after the illumination is set off. An exception is a persistent change of density at low temperatures after illumination due to photo-ionization of deep meta-stable donor levels in AlGaAs known as DX centers [4]. The electron excitation is accompanied by local lattice reformation, causing the vanishing of its binding potential.

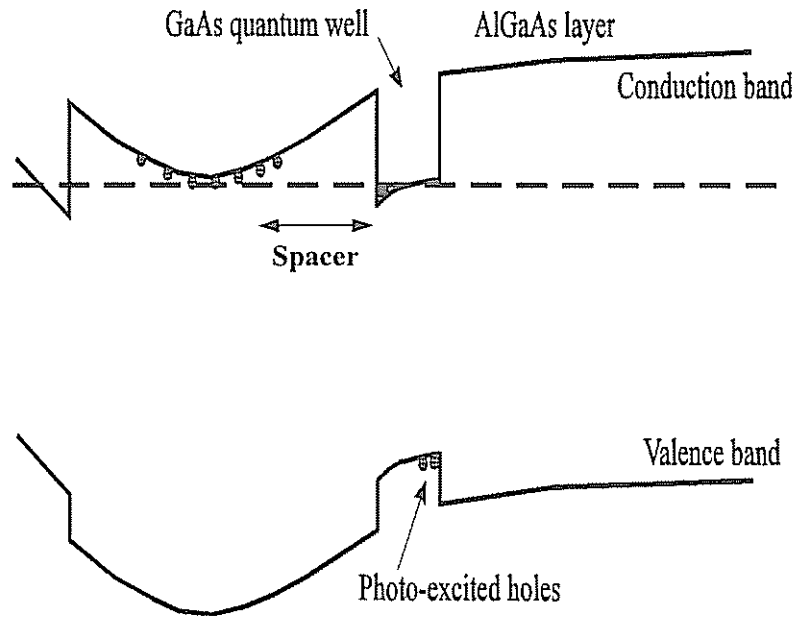


Fig2: Energy band diagram of 2DEG in quantum well.

As a result, the density of electrons originating from the DX centers persistently adds to that from the shallow dopants. Non-persistent illumination effects are mainly due to excitation above bandgap, where an electron is excited from the valance band to the conduction band, leaving a hole in the valance band. If the photon energy is above the AlGaAs barrier band-gap, carriers will be excited there as well. These electrons and holes drift in opposite directions under the effect of built-in electric fields (see Fig. 2) and could be swept into the QW, changing the 2D density. In some cases, the illumination results in the *formation* of spatially separated 2D electron and hole carrier densities – a major tool in this work (see experimental methods and chapter 2.1).

Throughout this work we use photoluminescence (PL) spectroscopy. In such experiment the photo-excited electrons and holes decay by non-radiative processes to the lowest possible energy at each band, from which they recombine by emitting a photon. As Fig. 2 shows, a minority of holes recombines with electrons from the 2DEG. If the excitation power is kept low, the perturbation to the electron gas can be small (note that the 2DEG effectively screens the holes potential). In this case the PL spectrum unravels the properties of the 2D gas.

The excited population of electrons and holes does not fully loose its excess energy, hence it can't be regarded as in thermal equilibrium with the lattice. However, since carrier scattering processes are faster than the recombination time, it is assumed that the 2DEG in the conduction band or the 2DHG in the valance band are in thermal equilibrium among themselves, and their energy distribution is described by the Fermi function.

1.2 Positively and negatively charged excitons

In QWs empty of carriers the optical properties near the band gap are dominated by the exciton (X), which is a bound state of the conduction band electron and the valance-band hole. The optical signal of modulation doped QWs containing a free dense carrier gas is substantially different. The exciton line is not observed in these structures due to the free carrier screening and the phase space filling [5]. Rather, a broad recombination line is

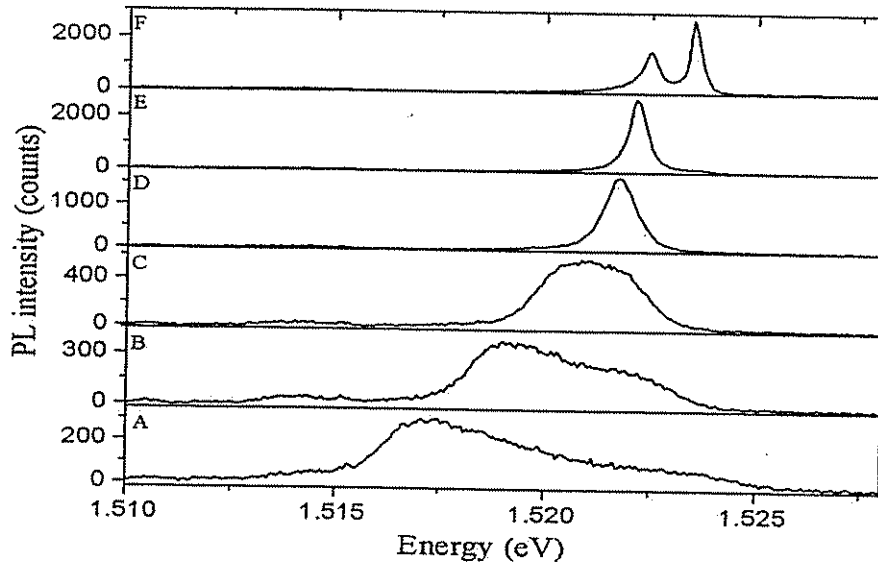


Fig. 3: The evolution of the PL spectrum from high density 2DEG (A) to depleted 2DEG (F). (after G. Eytan)

observed, whose energy-width reflects the 2D gas Fermi energy. In recent years, careful studies of the optical properties of low density 2DEG and 2DHG, resolved the existence of an intermediate state, in which the optical spectra are dominated by negatively (X^-) or positively (X^+) [6] charged excitons, respectively.

The X^- complex consists of two electrons bound to a hole, while the X^+ consists of two holes bound to an electron. These complexes were observed in II-VI [7] and III-V [6] semiconductor materials. In the PL spectrum of a GaAs QW the charged exciton manifests itself as an emission line at energy of about 1 meV below the neutral exciton line. The behavior of the PL spectrum as a function of the 2DEG density is shown for a 2DEG in Fig. 3. A similar behavior is observed for 2DHG and is given in chapter 2.2. Note that as the 2DEG density is gradually increased the charged exciton line evolves

smoothly into a free-carrier spectrum. Thus, the formation of charged excitons can be also viewed as a limiting case for the response of the 2D gas to a photoexcitation; binding a native carrier to the photo-excited e - h pair.

The effect of the 2DEG density on the X^- spectrum was a subject of several recent studies. It was shown that the appearance of excitons in the PL spectrum does not occur at a certain specific density, but is rather correlated with the drop of conductivity of the 2DEG [6]. This observation pointed to the importance of localization effects in the X^- formation. Indeed, near-field PL studies revealed strong spatial fluctuations in the X^- intensity [8]. These fluctuations were shown to be due to electron localization in the potential fluctuations introduced by the remote ionize donors. The transition from an excitonic spectrum to a free carriers spectrum was further investigated using absorption spectroscopy [9]. It was shown that the X and X^- persist in the absorption spectrum to a relatively high density, with the energy difference between the two increasing linearly with density.

While being important probes of the low-density carrier gas, the bulk of research of X^+ and X^- focuses on their properties as independent complexes. The existence of the X^+ and X^- was suggested 40 years ago based on an analogy with the H^- and H_2^+ ions [10]. The orbital structure of the H^- and H_2^+ ions is shown schematically in Fig. 4. As seen, their structure is very different. The reason for the large difference is the negligible electron to proton mass ratio. The solution for the ground state energy of the H_2^+ is essentially a single particle one, since the wavefunctions of the two heavy protons have negligible overlap [11]. The situation in the H^- is totally different. Now the two identical particles are light, and their wavefunction strongly overlap, so that Coulomb repulsion is in this case only marginally overwhelmed by attraction. Indeed, the H_2^+ binding energy is 3.6 times larger than the H^- [11]. Analytical treatment of the H^- is impossible because of the interparticle correlations. However, it may be shown that the electrons form a spin singlet ground state. One of the main goals of this work was to compare the properties of the two-exciton ions, the X^+ and X^- , based on the analogy with the Hydrogen ions. The X^+ and X^- are three-body objects, with a characteristic electron-hole mass ratio in the order of 0.15. This mass-ratio puts the X^+ and X^- in an interesting position for studying, being in between the limiting regimes of mass ratio ~ 0 (H^-) and 1 (positronium). Moreover, the large Bohr radius of the charged excitons enables their study in a magnetic field in an uncommon regime of atomic physics, where the magnetic

confinement can be increased such that the magnetic length scale is smaller than the Bohr radius ($l_B < a_B$).

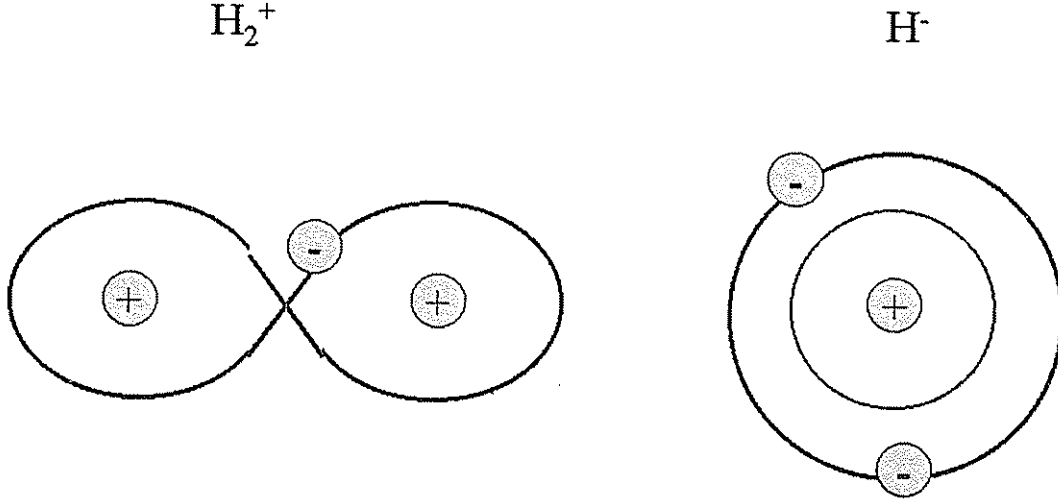


Fig. 4: An Illustration of the H_2^+ and H^- ions orbitals

The sizable electron-hole mass ratio m_e/m_h has made the modeling and comparison of the X^+ and X^- especially challenging. In the last decade there were several attempts to model these three-body complexes. One line of the theoretical work focused on calculating the second carrier binding energy as a function of the mass ratio in a zero magnetic field. Early calculations used approximations such as variational trial wavefunctions [12] or a predetermined charged exciton configuration, such as a linear chain [13]. These calculations gave the second carrier binding in the order of 0.3 to 0.4Ry, where Ry is the 2D binding energy of the 2D exciton. This value is higher than what observed experimentally (~ 0.2 Ry). Furthermore, these calculations predicted that in two dimensions the X^+ binding energy would surpass that of the X^- by $\sim 50\%$, in the case of GaAs mass ratio. This result was also in disagreement with measurements of the binding energies in various QW well widths [6,14], which gave an X^+ binding energy that exceeds that of the X^- by 15% at most. Recent calculations of charged excitons in semiconductor QWs [15] have given a binding energy difference of only 10%, in a better agreement with the experiments. The main modification did come from including the QW potential, which breaks the identity of the $e-e$ and $h-h$ interaction. We elaborate this subject in chapter 2.2.

Another line of theoretical study focuses on the calculation of the X^- spectrum in high magnetic fields. Its focus is the calculation of the singlet binding energy and tracking the

binding process of triplet states. At high magnetic fields the magnetic confinement is stronger than that from the attractive Coulomb potential ($l_B < a_B$). Hence, the models usually span the wavefunction over a Landau levels basis [16]. The numerical models treat finite width QWs by inclusion of several subbands. The main results of these calculations is the behavior of the singlet and triplet binding energies, and a recent prediction on the existence of another bound triplet state [17]. A theory of the X^+ in a magnetic field is unavailable yet. Indeed it is required in view of the different evolution of the X^+ binding energy and Zeeman splitting with magnetic field, which are observed experimentally (see chapter 2.2) as well as the recent observation of additional recombination lines in its spectrum [18].

At the time we started this work, the magneto-luminescence spectroscopy of the X^- in a low-density 2DEG was well developed. The three body-nature of the X^- has been proved by identification of its two-electron Singlet and Triplet states [6], and its shake-up spectrum in a magnetic field [19]. Furthermore, a vast literature (> 200 publications) on the properties and utilization of the X^- has been established up to date. These include its study in quantum dots [20], far-infra-red spectroscopy of its internal states [21], its spin and energy dynamics [22] and polaritons of negatively charged excitons [23]. On the other hand, the reports on the spectroscopy of X^+ [6, 24, 25] are relatively scarce and partial. The main obstacles include its discrimination from impurity spectra and its broad line-width. At present the number of works is growing slowly (still less than 10% of the publications on charged excitons), with increasing works on II-VI materials [26] and magneto-optical properties [18]. The X^+ continues to be subject of research activities since together with the X^- it constitute a model-test system to variety of phenomena in low-density carrier gas. In fact, in view of the current interest in the metal-insulator transitions in 2DHG [27], spectroscopy of the X^+ at this regime of 2DHG carrier density seems intriguing.

1.3 Experimental methods

Samples

Despite their convenience, modulation doped samples suffer from a drawback when it comes to optical spectroscopy. The ionized dopants, which are randomly distributed in the plane of doping, create a random electrostatic potential in the plane where the two-dimensional carrier gas resides [28]. This potential causes the 2D gas to be inhomogeneous, and as a result – broadens the recombination lines [8]. This problem is especially severe for 2DHG, due to the large effective mass of the heavy-holes at the top of the GaAs valance band, which results in a small Fermi energy (typically a few meV), a value which is about an order of magnitude smaller than that of a 2DEG. Hence, the screening of the random electrostatic potential from the dopants is much less effective in the case of the 2DHG.

An alternative approach, which avoids the need to dope the structures, is to use optical excitation of undoped samples, and accumulate the photo-excited electron and holes in different potential wells. Clearly, optical excitation creates the electron and hole in the same location, hence special structures are needed to separate them. In fact, one incentive to create spatially separated 2DEG-2DHG systems is to test predictions of a host of collective phenomena due their coupling [29]. Several schemes were proposed for the purpose of charge separation. One scheme consists of a p-i-n barrier diode under forward bias [30]. In this device the electrons and holes are transported to the diode junction and accumulate at opposite heterointerfaces of a larger band-gap barrier layer. Thus, the optical recombination is largely inhibited (but with some tunneling current present). Another method photo-excites e - h pairs in a wide QW, which is held in a strong electric field [31]. The strong electric field separates the electrons from holes and localizes the carrier wavefunction near the opposing barriers. This method produces equal density of electron and hole gases. The carrier densities are typically low because of efficient optical recombination. A method, which overcomes the depletion by optical recombination, employs mixed type I-II QWs [32]. In these QWs the photo-induced carriers are very efficiently spatially separated and confined in different QW potentials (see more in chapter 2.1).

In recent years several groups - including ours - have employed such schemes to sustain and control the density of electron [33] and hole [34] gases. This implementation has proven most suitable in optical spectroscopy. Specifically, we have found such methods promising in improving the quality of the 2DHG spectrum, to a quality similar of 2DEG. This subject is elaborated in chapter 2.3.

Polarized spectroscopy

The major tool we used throughout the work is the analysis of the energy and polarization properties of the recombination spectrum. In an interband recombination process the energy of the emitted photon is $h\nu = E_i - E_f \leq E_G$, where E_i and E_f are the energies of the initial and final states of the system, and E_G is the band-gap energy. The energy of photons emitted from excitonic complexes recombination is slightly lower than E_G because of the binding energy; $E_i = E_G - E_B$. Thus, different binding energies are manifested in the PL spectrum by slight energy differences of the corresponding PL lines. This is illustrated in Fig. 5 for the X and X⁻. The exciton recombination energy is smaller than the band gap by its Rydberg energy. In the X⁻, one of the electrons recombines with the hole, while the other electron final state is in the conduction band.

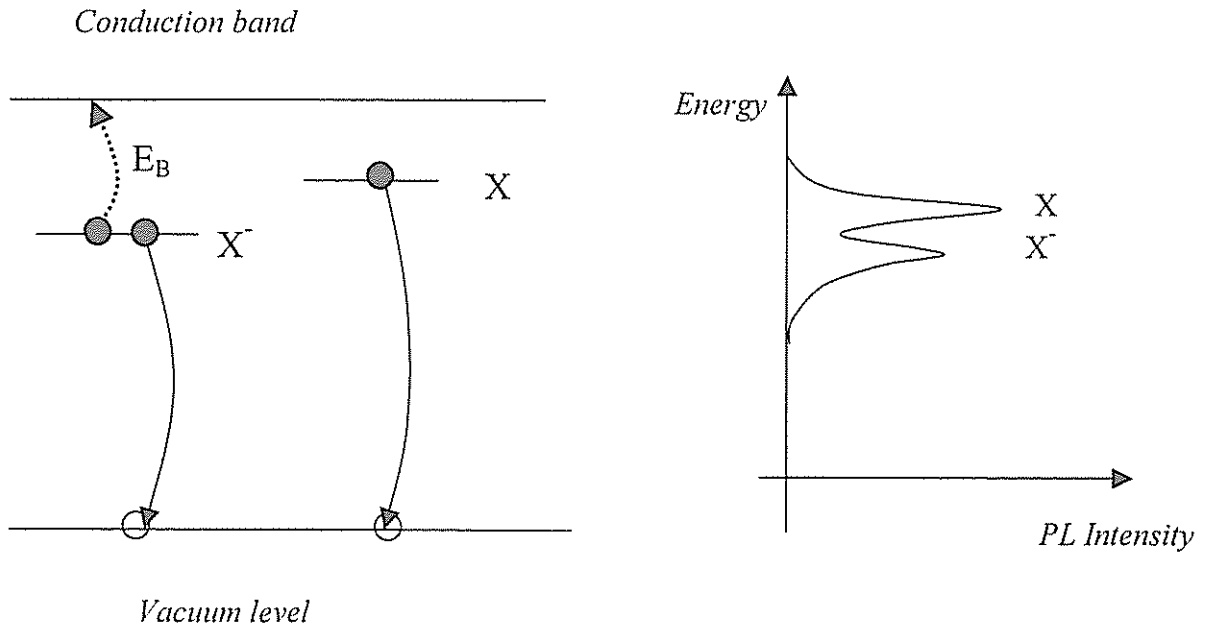


Fig. 5: Recombination process of the neutral and negatively charged excitons, and its manifestation in the PL spectra.

The resulting luminescence peak has an energy, which is E_{B2} below the X peak. Thus, the two complexes are resolved in the spectra in the form of a doublet.

In a magnetic field spin degeneracy is lifted and QW selection rules are manifested. The spectrum of charged excitons with their two-particle spin combinations becomes rich and complicated. Polarized spectroscopy is a very efficient tool for extraction and interpretation of the recombination spectrum. The magnetic field can be applied either perpendicular or parallel to the QW layer. The two geometries result in different electron and hole eigenstates. In the perpendicular geometry, the orthogonal states of the emitted photons are circularly polarized [35]. In a parallel magnetic field, the electrons and holes eigenstates are a superposition of the QW eigenstates and have zero angular momentum along z . Thus, the emitted photons are linearly polarized along x or y axis (see chapter 2.4).

We have used two low-temperature systems: A cryostat and Insert rods. The differences between these systems were manifested in the way we analyzed the PL spectrum and in particular, its polarization. The cryostat cools the sample by He flow from its reservoir. Controlling the flow (or heating the sample base) vary the sample temperature. The available temperature ranges between room temperature to 1.5K. The optical cryostat has windows to access the sample, so an external table-top optical set-up is used to collect and analyze the PL. The cryostat has a split-coil magnet, and rotating the sample holder 90 degrees does the shift from perpendicular to parallel geometries. Locating the set-up on the optical table is convenient for complex measurements; we have used the cryostat system to spatially image the PL polarization properties. This setup is described in chapter 2.5.

Our cryostat is limited by its magnet strength (7T) and measurement times between refuels. Insert rods equipped with optical fibers propose an elegant way to overcome these limitations. These rods were built with the optics and mechanical manipulation on board. The rod with the sample mounted, is inserted through a top loaded Dewar or refrigerator. The excitation and collection of light is done with the optical fibers. The rod contains also the electrical wirings for the sample and temperature sensing. The optical signal is analyzed before it is collected by the fiber and is spectrally analyzed by a table-top spectrometer and a cooled CCD (also used with the cryostats).

Using a magnet Dewar, the perpendicular and parallel field analysis geometries demand a 90 degrees reorientation of the sample, since the orientation of magnetic field is fixed. This demands rods for the different two types of experiments. Figure 6 shows the

optical path and mechanical motion in each of the rods. In the parallel geometry a prism folds the optical path and the light goes trough polarizers holder that can slide up and down between the two orthogonal linear directions. In the perpendicular geometry the relative position of a polarizer and wave-plate is rotated by 90 degrees to interchange between the two orthogonal circular polarizations. A mechanical transmission allows the external control from the top of the rods.

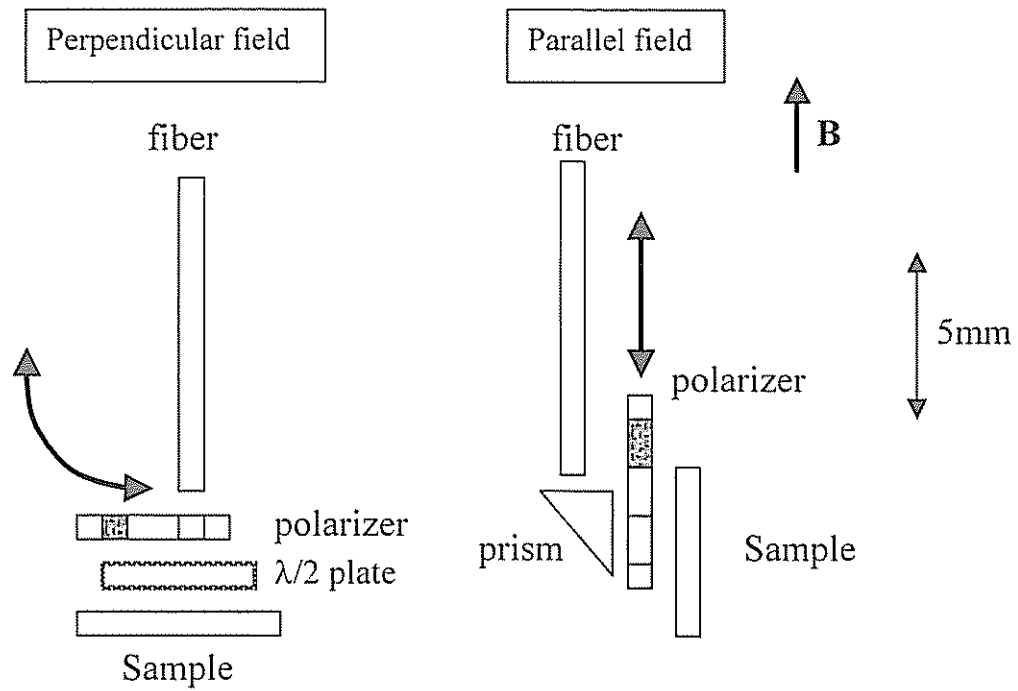


Fig 6: The optical collection setup and mechanical motion of the rods.

References

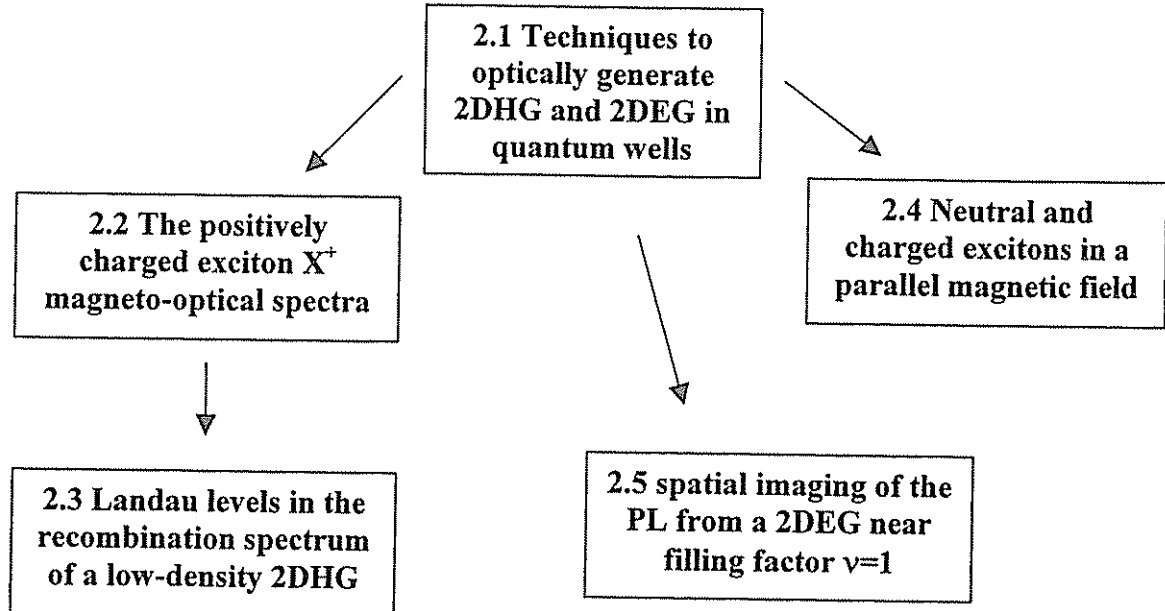
1. R. Dingle H. Stormer A. C. Gossard W. Weinmann Appl. Phys. Lett. **33**, 665 (1978)
2. T. Ando, A. B. Fowler, and F. Stern, Rev. Mod. Phys. **54**, 437 (1982)
3. *Gallium Arsenide*, Edited by J. S. Blakemore, American Institute of Physics, (1987)
4. J. M. Langer, Rev. Solid. Science (Singapore) **4**, 297 (1990); P. M. Mooney, J. Appl. Phys. **67**, R1 (1990)
5. S. Schmitt-Rink, D. S. Chemla and D. A. B. Miller, Adv. Phys. **38**, 89 (1989)
6. G. Finkelstein, H. Shtrikman and I. Bar-Joseph, Phys. Rev. Lett. **74**, 976 (1995); A. J. Shields, J. Osborne, M. Y. Simmons, M. Pepper and D. A. Ritchie, Phys. Rev. B **52**, R5523 (1995); G. Finkelstein, H. Shtrikman and I. Bar-Joseph, Phys. Rev. B, **53**, R1709 (1996)
7. K. Kheng, *et al.* Phys. Rev. Lett. **71**, 1752 (1993) (CdTe); G. V. Astakhov *et al.* Phys. Rev. B, **60**, R8485 (1999) (ZnSe)
8. G. Eytan, Y. Yayon, M. Rappaport and I. Bar-Joseph, Phys. Rev. Lett. **81**, 1666 (1998)
9. G. Yusa, H. Shtrikman and I. Bar-Joseph, Phys. Rev. B, **62**, 15390 (2000) and refs. Therein
10. M. A. Lampert, Phys. Rev. Lett. **1**, 450 (1958)
11. H. A. Bethe and E. E. Slapeter, "Quantum mechanics of one and two-electron atoms", p. 154, Springer Verlag, 1957; L. D. Landau and E. M. Lifshitz, Quantum mechanics, p. 314 Pergamon Press, 1977
12. B. Stebe and A. Ainane, Superlattices Microstruct. **5**, 545 (1989)
13. A. Thilagam, Phys. Rev. B **55**, 7804 (1997), and refs. Therein
14. J. L. Osborne, Dissertation for Ph. D. Cambridge University, p. 58, 2000
15. A. Esser *et al.* Phys. Rev. B **62**, 8232 (2000); C. Riva, F. M. Peeters and K. Verga, *ibid.* **61**, 13873 (2000); B. Setebe, A. Moradi and F. Dujardin, *ibid.*, **61**, 7231 (2000)
16. J. R. Chapman, N. F. Johnson, and V. N. Nicopoulus, Phys. Rev. B **55**, R10221 (1997); D. M. Whittaker and A. J. Shields *ibid.* **56**, 15185 (1997); A. Wojs, P. Hawrylak, and J. Quinn, Phys. Rev. B **60**, 11661 (1999)
17. A. Wojs, J. Quinn, and P. Hawrylak, Phys. Rev. B **62**, 4630 (2000)
18. O. V. Volkov *et al.* Euro. Phys. Lett. **50**, 409 (2000)

19. G. Finkelstein, H. Shtrikman and I. Bar-Joseph, Phys. Rev. B, **53**, 12593 (1996)
20. A. Gonzales and E. Menendez-Proupin, Physica E **8**, 333 (2000) and refs. therein.
21. A. B. Dzyubenko and A. Y. S. Sivachenko, Phys. Rev. Lett. **84**, 4429 (2000)
22. D. Sanvitto *et al.* Phys. Rev. B **62**, R13294 (2000)
23. R. Rapaport *et al.* Phys. Rev. Lett. **84**, 1607 (2000)
24. H. Buhmann *et al.* Surf. Sci. **362**, 447 (1996)
25. A. J. Shields *et al.* Phys. Rev. B **52**, R5523 (2000)
26. P. Kossacki *et al.* Phys. Rev. B **60**, 16018 (1999)
27. Y. Hanein *et al.* Phys. Rev. Lett. **80**, 1288 (1998)
28. A. L. Efros, F. G. Picus and V. G. Burnett Phys. Rev. B **47**, 2233 (1993)
29. X. M. Chen and J. J. quinn, Phys. Rev. Lett. **67**, 895 (1991); X. Zu *et al. ibid.* **75**, 1633 (1995) and refs. therein.
30. A. Parlangeley *et al.*, Phys. Stat. Sol. **A164**, 587 (1997); V. B. Timofeev *et al.*, Phys. Rev. B **61**, 8420 (2000)
31. T. Fukuzawa, E. E. Mendez and J. M. Hong 90, Phys. Rev. Lett. **64**, 3066 (1990); L. V. Butov *et al. ibid.* **73**, 304 (1994); F. Plentz, D. Heiman, A. Pinczuk, . L. N. Pfeiffer and K. W. West, Solid state Comm. **101**, 103 (1995)
32. P. Dawson, I. Galbraith, A. I. Kucharska, and C. T. Foxton, Appl. Phys. Let. **58**, (1991)
33. A. Ron. *et al.* Solid State comm. **97**, 741 (1996); B. M. Ashkinadze *et al.* Phys Stat. Solidi A **164**, 523 (1997)
34. Y. V. Ponomarev *et al.*, Phys. Rev. B, **54**, 13891 (1996); O. V. Volkov *et al.*, JEPT Lett. **68**, 236 (1998)
35. “*Optical Orientation*”, F. Meier and B. P. Zakharcaya, Eds. North-Holland, Amsterdam (1984)

2. The main results

In this section the most important findings of this Ph. D. work are presented in the form of journal publications. Each chapter is based on a paper, with the introduction summarizing in brief the main results and also reports related work, which was not included in the publication. We also make an attempt to reason our motivation for the specific measurements performed in each work

The first chapter presents our results on the optical generation of high quality 2DHG in intrinsic GaAs QWs, and based on that, the realization of a spatially separated ($\sim 20\text{nm}$) system of 2DHG and 2DEG. The next two chapters describe the utilization of the mechanisms described in chapter 2.1 for the comparative spectroscopy of the X^+ and X^- (Ch. 2.2), and for the observation of valance-band Landau levels in a magnetic field (Ch. 2.3). The work presented in the two following chapters uses similar QW samples, however the emphasis gradually shifts to additional experimental methods and theoretical effort. In the fourth chapter (Ch. 2.4) we study the exchange properties of the neutral and charged excitons. In the fifth chapter (Ch. 2.5) we add spatial control over the carrier density and measure the screening response of the 2DEG near filling factor $\nu=1$.



2.1 Techniques to optically realize two-dimensional hole and electron gases in quantum wells

S. Glasberg, H. Shtrikman and I. Bar-Joseph

Optical generation of spatially separated electron and hole gases in intrinsic GaAs/AlGaAs double quantum wells

Phys. Rev. B **63**, Issue 11 (2001)

We report the optical generation of a variable density two-dimensional hole gas (2DHG) in intrinsic sample. This is achieved by optical excitation of a GaAs quantum-well, which is very close to the surface, at photon energy below the AlGaAs barrier. We show that we can tune the carrier density, and even change it to a 2DEG, by exciting with an additional laser, with an energy above the barrier. By combining this structure with a mixed-type narrow quantum-well we obtain a spatially separated 2DHG-2DEG system, and we demonstrate how the density of each gas can be independently controlled.

Aside of its superior growth properties, GaAs and its derivatives are especially suited to optical manipulation, being direct band-gap materials. One of the most straightforward and non-trivial consequences of optical excitation is the creation of non-neutral carrier density in intrinsic QW [1]. This property was not emphasized in past years, where PL studies of intrinsic QWs assumed that the optical excitation would be manifested in neutral excitations only, such as the free e - h pairs, excitons and bi-excitons [2]. However, a growing number of works [3-7] have utilized photo-excitation and band gap engineering to devise means to separate the electrons from holes. One of the simplest ways to accomplish this is by illumination above the QW barriers. Let us demonstrate how the electron density in a QW is changed in such case. We utilize for that the characteristic spectrum of the negatively charged X^- in a magnetic field. Figure 2.1 shows the PL spectrum from a single QW as a function of excitation laser intensity above the barrier. As shown, at very weak excitation conditions ($I_L < 10 \mu\text{W}/\text{cm}^2$) a single recombination line of the free heavy-hole exciton is observed. However, as the illumination intensity increases, additional peaks appear

bellow the exciton line. These are the singlet and triplet X^- lines, indicating that an excess electron density is created in the QW.

In the case of illumination above the AlGaAs barrier, drift of electrons photo-excited in the barrier to the QW accounts for the build-up of their density. The exciton line dominated spectra of Fig 2.1 shows however that the 2DEG density has increased by only very little as the laser power is increased by more than three orders of magnitude. The reason for this inefficiency is the lack of confining potential for both electrons and holes. Indeed, a high-density 2DEG in intrinsic wide QWs ($L_z > 10\text{nm}$) was optically generated only with special mixed-type double QW structures grown from AlAs/GaAs [6] or InAs/GaSb [7] layers.

In the current work we developed a method which enables to optically generate a high density 2DHG of very good quality in a wide ($L_z > 10\text{nm}$) QWs. We introduced a barrier layer between the QW and the surface, which replicates the role of the spacer

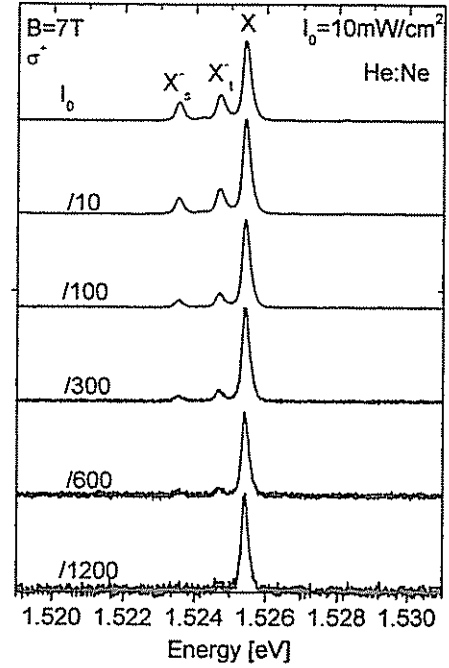


Fig. 2.1 The magneto-luminescence spectrum from a single QW as a function of laser excitation intensity.

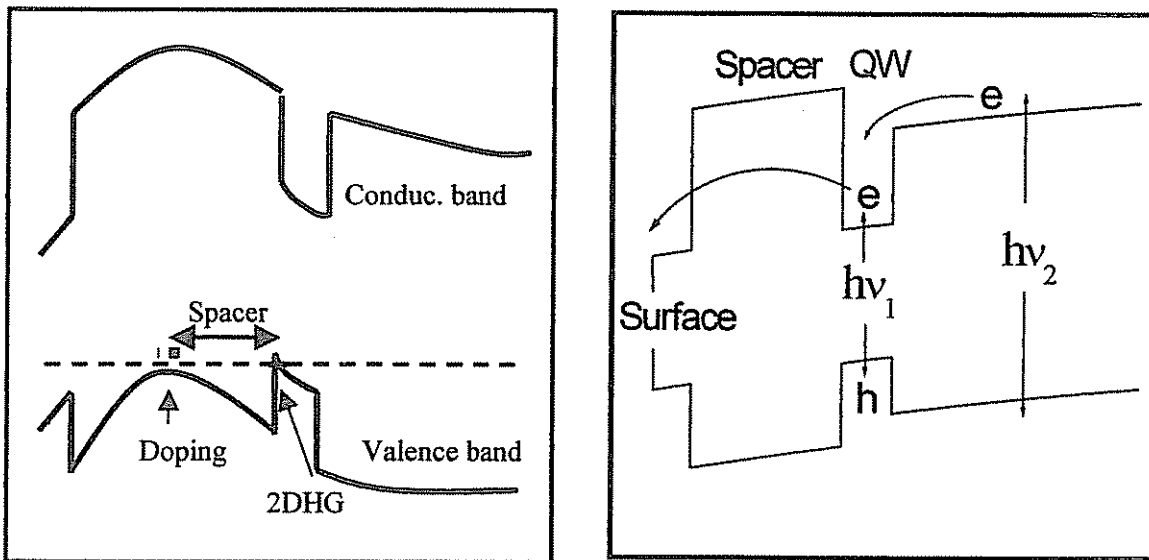


Fig. 2.2: The structure of modulation doped and intrinsic 2DHG samples. Note that the width of the Spacer is well defined in both.

layer in a modulation-doped structure. In this way we utilize the sample-surface as a potential well for the electrons. The comparison between the two structures is demonstrated in Fig. 2.2. However similar is the end result (of a dense 2DHG in the QW) the underlining mechanisms differ: while the bands are strongly curved and under equilibrium in the modulation doped structure (Fig. 2.2a), in the intrinsic structure the 2DHG is achieved under steady-state and nearly flat-band conditions (Fig. 2.2b). The ability to illuminate with photon energies bellow or above the AlGaAs band gap enables to control the type of excess carrier within the same sample. Fig. 2.3 shows a change of the PL signature from that 2DHG to 2DEG as a function of illumination conditions.

2.1.1 Coupled 2DEG-2DHG system

The second part of the paper demonstrates the realization and control of spatially separated electron-hole gases. The spatially separated 2DHG-2DEG system is attracting substantial attention and experimental effort, mainly due to being a candidate system for achieving Bose-Einstein condensation in a semiconductor [9]. Yet host of other effects were discussed, such as Fractional [10] and Wigner crystal [11] states, excitonic polarons [12], and more. A key parameter is the separation between the layers, which largely determines the strength of the inter-layer electron-hole attraction. Other important requirements are the abilities to tune the carrier density independently, to cool the carriers, and to avoid inter-well tunneling.

In this work we have realized the 2DEG-2DHG system in wide double QWs. A generic plot of the structure appears at the inset of Fig. 5 of the paper. The two wells

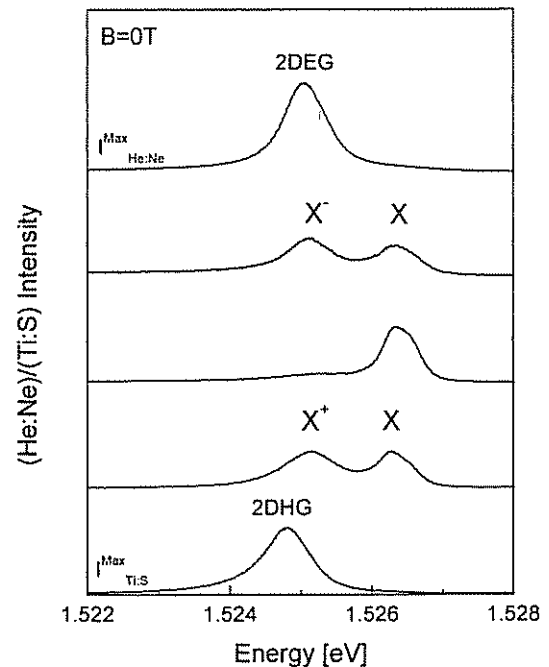


Fig 2.3: The change of PL spectrum from that of 2DHG to one due to 2DEG in the same QW, as a function of illumination conditions.

$$I_{\text{He:Ne}}^{\text{Max}} = 5 \text{ mW/cm}^2, I_{\text{Ti:S}}^{\text{Max}} = 20 \text{ mW/cm}^2$$

are of different width, hence the 2DEG and 2DHG spectral signatures could be separated. Numerous samples were grown, aiming either to maximize the attainable carrier density at a given optical excitation power, or to decrease inter-well separation. Emphasis was put on the barriers design and growth conditions to minimize defects. In general, samples closer to the surface with thicker inter-well barriers ($\sim 10\text{nm}$) gave high carrier densities ($>10^{11}\text{cm}^{-2}$), whereas samples buried deeper could sustain charge separation with thinner barriers ($\sim 5\text{nm}$) - but at lower carrier densities ($<10^{11}\text{cm}^{-2}$). The reason for that is most probably the behavior of the built-in electric field, which increases towards the sample surface. The parameters of the optimized structures are given in the paper.

We have studied the PL spectrum as a function of:

- 2DEG and 2DHG densities: between a few 10^{10}cm^{-2} to a few 10^{11}cm^{-2}
- 2DEG and 2DHG effective separation: between 15 to 30 nm
- Magnetic field: between 0 to 9T
- Temperature: between 1.5K to 4.2K

Figure 2.4a depicts the system low-density spectrum as a function of magnetic field at fixed electron and hole densities. The spectra are easily identified as being identical to these of the X^- and the X^+ in single QWs. They show clearly the singlet and triplet charged exciton states. Figure 2.4b shows the evolution of a dense 2DHG-2DEG PL spectra with increase of the 2DHG density, at a given magnetic field. We note that the spectra are similar to those obtained separately with 2DEG and 2DHG in single QWs (The appearance of a 4th Landau-level is probably due to slight increase in the 2DEG density). Generally, all the results were compared with those obtained from ‘control’ structures of optically generated 2DHG and 2DEG in single QWs. Unfortunately, we did not observe any optical signature for e - h interaction. We have found that the PL spectra of the 2DHG-2DEG were a simple superposition of the single QW spectra throughout the parameter space defined above.

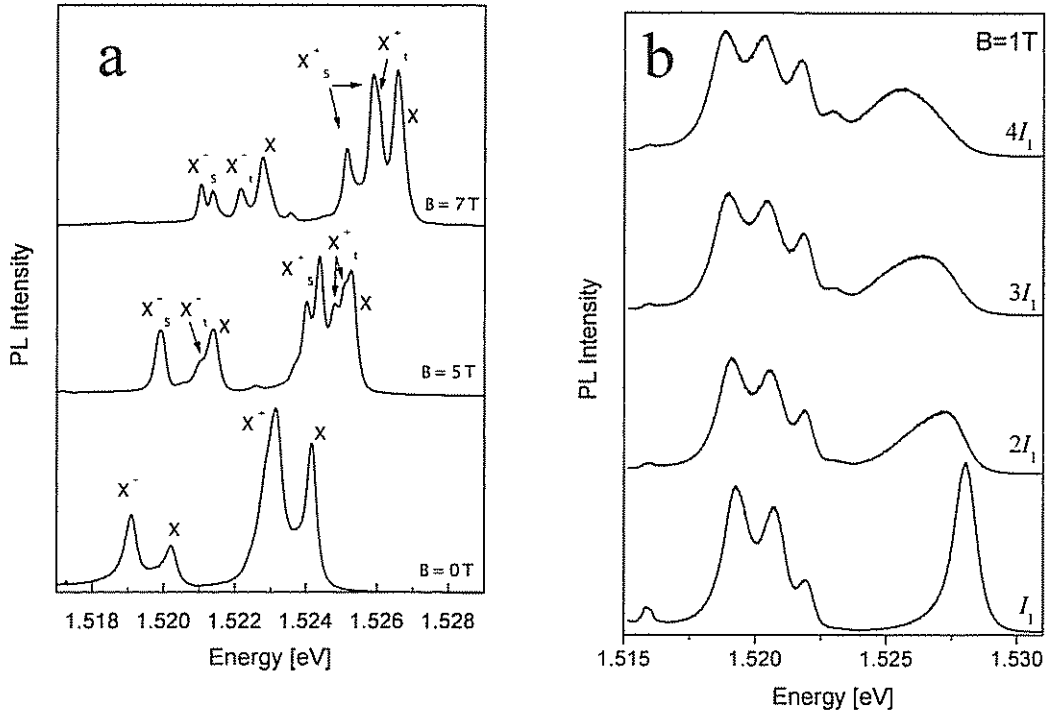


Fig. 2.4: The PL spectrum from 2DEG-2DHG systems in a magnetic field (a) at low-density, showing positively and negatively charged excitons (b) at high density, showing 2DEG Landau-levels and a 2DHG spectra. $I_1=20\text{mW/cm}^2$.

The absence of strong modifications in the spectra is surprising. We estimate the bare Coulomb interaction energy between the electron and hole layers, $e^2/\epsilon|z_e-z_h|$, to be a few meV. One would expect that this interaction energy would affect the PL spectra. We do not have an explanation for this negative result.

Other groups studied the PL from 2DHG-2DEG in parallel to our effort. A periodic modulation of PL polarization from the 2DEG as a function of filling factor was observed in narrower coupled QWs [13], and was assigned to an inter-well exciton. An inter-well $e-h$ binding energy of 1 meV was deduced from the dependence of the oscillation amplitude on temperature. In Ref. 4 changes of PL as a function of temperature led the researchers to determine several phases of the 2DHG-2DEG system. In our opinion, a simpler scenario due to changes in the steady-state carrier densities (which leads to changes in the PL spectrum) might explain those results. Another work used detection through magneto-transport [14]. The results show energy discontinuities and bistability of tunnel currents. The distinctive connection of these effects with a 2DHG-2DEG system is under study.

2.1.2 A laser with separate control of N_e and N_h

Other interesting applications of optical generation of hole and electron gases may exist when introducing extra features of band-gap selectivity. A suggestion how to optically obtain and control inversion population in a QW is illustrated in Fig. 2.5. Similarly to previous structures we discussed, the carriers are introduced to the QW, each with its own rate. The extra feature introduced here is a band-gap offset in the QW (type II QW) that decreases the electron-hole recombination rate. If this rate can be reduced below the total pumping rates R_e , R_h than population inversion is achievable. Incorporating two mirrors (an MBE grown GaAs/AlAs back mirror, and a

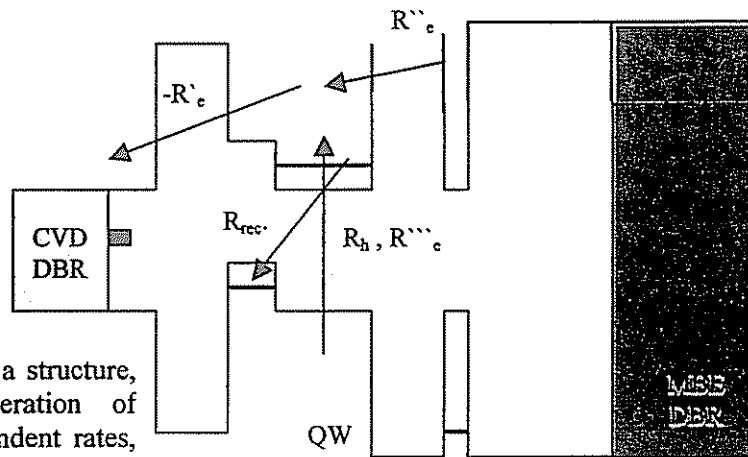


Fig. 2.5: A band gap design for a structure, which combines optical generation of electrons and holes with independent rates, suppressed recombination rate, and cavity mode for photons.

CVD deposited front mirror of alternating layers of $\text{SiO}_2/\text{Si}_3\text{N}_4$) will allow detecting induced emission from the QW, through its line-width narrowing [15]. The interesting feature here is the possibility to delicately tune this process to lower carrier densities. Note that unlike with doped samples, the only loss mechanism here, apart of the mirrors, comes from spontaneous emission, without any substantial absorption to overcome first.

References

1. C. Delalande, J. Orgonasi, M. H. Meynadier, J. A. Brum, G. Bastard, G. Weimann and W. Schlapp, *Solid State Commun.* **59**, 613 (1986)
2. S. Schmuitt-Rink, D. S. Chemla and D. A. B. Miller, *Adv. Phys.* **38**, 89 (1989); D. Birekdal *et al.* *Phys. Rev. Lett.* **76**, 672 (1996)
3. O. V. Volkov *et al.*, *JEPT Lett.* **67**, 744 (1998)
4. V. B. Timofeev *et al.*, *Phys. Rev. B* **61**, 8420 (2000)
5. E. E. Mendez *et al.*, *Phys. Rev. B* **33**, 7368 (1988); F. Plentz, D. Heiman, A. Pnczuk, L. N. Pfeiffer and K. W. West, *Solid state Comm.* **101**, 103 (1995)
6. P. Dawson, I. Galbraith, A. I. Kucharska and C. T. Foxton, *Appl. Phys. Lett.* **58**, 2889 (1991)
7. Y. B. Vasilyev *et al.*, *Physica B* **258**, 445 (1998)
8. A. Manassen *et al.*, *Phys. Rev. B* **54**, 10609 (1996); N. T. Pelekanos *et al.*, *Opt. Lett.* **20**, 2099 (1995)
9. 4.Yu. E. Lozovic and V. I. Yudson, *JEPT Lett.* **22**, 271 (1975); S. I. Shevchnko, *Phys. Rev. Lett.* **72**, 3242 (1994); S. Conti, G. Vignale and A. H. MacDonald, *Phys. Rev. B* **57**, R6846 (1998)
10. E. I. Rashba and M. E. Portnoi, *Phys. Rev. Lett.* **70**, 3315 (1993)
11. H. A. Fertig, in “High Magnetic Fields in the physics of semiconductors”, p. 416, D. Heiman Ed. World Scientific, Singapore (1995)
12. “Semimagnetic Semiconductors”, Eds. B. Mullin and H. Heinrich, Trans Tech Publ., Aedermannsdorf (1995)
13. A. Nazimove *et al.*, *Physica E* **6**, 650 (2000)
14. A. Parlangeli *et al.*, *Physica B* **256-258**, 531 (1998)
15. A. Yariv, “Quantum electronics” 3rd Ed. Wiley, NY (1989)

Optical generation of spatially separated electron and hole gases in intrinsic GaAs/Al_xGa_{1-x}As double quantum wells

S. Glasberg, H. Shtrikman, and I. Bar-Joseph

Department of Condensed Matter Physics, The Weizmann Institute of Science, Rehovot 76100, Israel

(Received 14 September 2000; revised manuscript received 3 November 2000; published 28 February 2001)

We show that optical excitation of a wide GaAs quantum well, which is located close to the sample surface, can give rise to the creation of a high-density two-dimensional hole gas in the well. Based on this mechanism, we present a double quantum well structure in which spatially separated electron and hole gases are optically created at close proximity (~ 20 nm). We demonstrate how the density of each gas can be independently controlled by the intensity of the exciting lasers.

DOI: 10.1103/PhysRevB.63.113302

PACS number(s): 71.35.Ji, 78.66.Fd, 78.55.-m, 78.66.-w

Semiconductor band-gap engineering enables the confinement of electrons or holes in two dimensions, thus forming a two-dimensional carrier gas. The experimental realization of such a system is usually based on modulation doping: a layer of dopants (donors or acceptors) is introduced into a high band-gap material, and gives rise to the formation of a two-dimensional electron (2DEG) or hole (2DHG) gas at the heterojunction, which is located at a certain distance (spacer) from the dopants layer.¹ In this way, the scattering of carriers by the dopants is suppressed and very high mobilities can be obtained. An intriguing possibility is to construct a system in which the 2DEG and 2DHG are formed at a close proximity to one another. Theoretical studies of this system predict that the interlayer electron-hole Coulomb attraction could give rise to a variety of effects, such as charge-density waves, interlayer drag, bound complexes of many particles, and interlayer-exciton condensation.² Indeed, there have been a few experimental attempts to realize such a system, and some of these effects were observed.³

An alternative approach, which avoids the need to dope the structures, is to use optical excitation of undoped samples, and accumulate the photo-excited electrons and holes in different potential wells. Clearly, optical excitation creates the electron and hole at the same location, hence special structures are needed to separate them. Two main systems were proposed and tested for this purpose. In the first, an electric field is used to localize the wave function of the electrons and holes at the two sides of a large quantum well or in two coupled quantum wells (QW's).⁴ Hence, photoexcitation would give rise to a formation of electrons and holes, which are spatially displaced. This system inherently creates an equal density of electrons and holes and does not enable independent control of the density of each carrier. Furthermore, optical recombination sets a limit on the density that can be achieved. Indeed, most of the experiments using this system focused on excitonic effects at low electron and hole densities.⁴ The other system uses a mixed type I-type II GaAs/AlAs structure, which consists of a wide and narrow GaAs QW's, having a thin AlAs barrier between them.⁵ This system makes use of the fact that the lowest Γ state in a narrow GaAs QW with a width of less than 3.4 nm is higher in energy than the X state in the AlAs barrier. This gives rise to an efficient transfer of photo-excited electrons from the narrow to the wide QW. As a result, the electrons,

which are photoexcited in the narrow QW, accumulate in the wide well, while the photo-excited holes remain trapped in the narrow well. Unfortunately, the small width of the narrow well gives rise to large fluctuations in energy, ~ 20 meV, due to well width fluctuations, and hence, to localization of the holes. In that sense, the holes may be considered to be similar to the acceptors in modulation doped structures and the thin AlAs barrier as the spacer.

In this report we present a system that enables us to create 2DEG and 2DHG in adjacent wide QW's, and to control the density of each gas independently over a wide range. Our approach is based on having two modular building blocks, one in which the 2DHG is realized, and another in which the 2DEG is realized. These building blocks maintain their independent functioning when combined together. In the first part of the report we describe the 2DHG module, which consists of a wide QW located close to the surface. We show that photo-excited electrons in the QW migrate to surface states, leaving the holes trapped in the QW. We study the optical and electrical properties of the carriers in the well and establish that, indeed, a 2DHG is formed. The 2DEG module is the mixed type I-type II structure. In the second part of the report we combine the two modules to form adjacent 2DHG and 2DEG. The different widths of the QW's, in which the 2D gases are formed, allow us to spectrally resolve their photoluminescence (PL) spectra. The electron and hole gases are excited by two different lasers. Thus, by varying the intensity of each laser, we can independently control the density of each gas.

Figure 1 describes schematically the generic structure, in which a 2DHG is formed. It simply consists of a wide GaAs QW that is separated from the cap layer at the surface by an Al_xGa_{1-x}As barrier. As will be shown later, this barrier plays a similar role as the spacer in a modulation doped structure, and we therefore denote it as the Spacer. The thickness of the QW was chosen to be 20 nm. The nominal aluminum mole fraction x of the Al_xGa_{1-x}As Spacer layer was $x=0.37$ and its thickness ranges, in the samples we studied, between 15 and 125 nm. The cap layer thickness was varied in different samples between 15 and 75 nm. Most of the results are from a sample with a 25 nm Spacer, and a 15 nm GaAs cap. The samples were grown on (100) oriented semi-insulating GaAs substrates.

PL measurements at a temperature of 4.2 K are carried out using a fiber optic collection setup. The signal is dis-

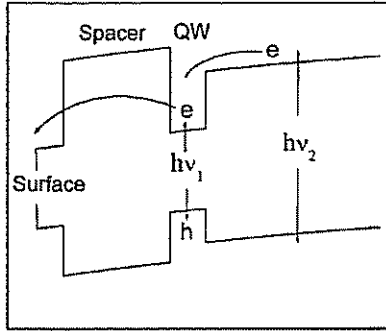


FIG. 1. The generic structure of the QW samples. Also shown are the two excitation conditions, below the ($h\nu_1$) and above the ($h\nu_2$) barrier, and the resulted electron transport.

persed in a 0.75 m spectrometer and detected in a cooled charge-coupled device detector array. The illumination source is a tunable Ti:S laser. In Fig. 2 we show the PL spectra as a function of the Ti:S laser excitation intensity at an energy $h\nu_1 = 1.590$ eV. This energy is chosen to be below the $\text{Al}_x\text{Ga}_{1-x}\text{As}$ gap, such that carriers are excited only at the QW. Under very weak excitation the observed PL spectrum (not shown) is of neutral excitons, indicating that the well is nearly empty of free carriers. As the intensity of the laser is increased, an excess density of holes is created in the well, as evidenced by the appearance of a positively charged exciton (X^+) line in the PL spectrum.⁶ As the laser intensity is further increased the X^+ line dominates the spectrum, and at yet higher intensities it turns into a broad line, characteristic of a 2DHG recombination.⁷

To establish the assignment of the type of carriers in the well, we studied the electrical properties by Hall measure-

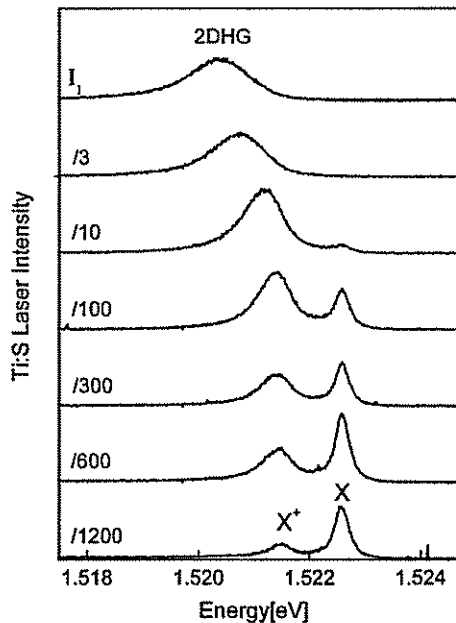


FIG. 2. The QW PL spectra at increasing the Ti:S laser excitation intensity, showing the evolution from an excitonic characteristic to that of a 2DHG ($I_1 = 30$ mW/cm²). Spacer thickness is 25 nm.

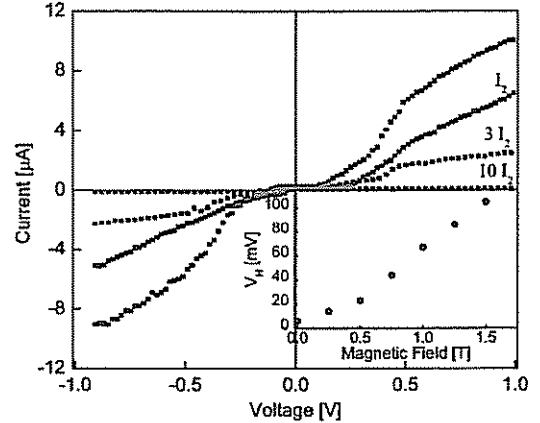


FIG. 3. Current-voltage characteristics, showing the depletion of the 2DHG channel as the He:Ne intensity is increased ($I_2 = 0.5$ mW/cm²). The Ti:S laser intensity was kept fixed ($I_1 = 50$ mW/cm²). The inset shows the 2DHG Hall voltage as a function of magnetic field.

ments while illuminating the sample with a Ti:S laser ($I_1 = 30$ mW/cm²). The sample was processed into a 300×200 μm^2 mesa, and Zn/Au contacts in a Hall bar geometry were annealed. The Hall voltage was measured up to 1.5 T and exhibited good linearity in a magnetic field (inset Fig. 3). The sign of the Hall voltage was that expected for positive charges, proving unambiguously that the carriers in the well are holes. The I-V characteristic under this illumination intensity at zero magnetic field is shown by the upper trace in Fig. 3. It is seen that the trace is not linear, exhibiting a high resistivity at low voltages. This reflects a problem with the quality of the contacts in this intrinsic sample. As a means to tune the carrier density, we added illumination with a He:Ne laser at $h\nu_2 = 1.960$ eV. This laser energy is above the band gap of the lower $\text{Al}_x\text{Ga}_{1-x}\text{As}$ barrier, but below that of the Spacer (Fig. 1). The photo-excited electrons, which are created at the low $\text{Al}_x\text{Ga}_{1-x}\text{As}$ barrier, are swept into the QW by the built-in electric field. This field is formed due to the fact that the sample unintentional background doping is *p* type, while the chemical potential is pinned to the midgap at the surface. The electrons, which are swept into the QW, recombine with the holes, thus depleting the 2DHG density.⁸ The various traces in Fig. 3 correspond to different He:Ne intensities, keeping the Ti:S laser intensity fixed. It is indeed seen that as the He:Ne intensity is increased the current decreases, until beyond a certain intensity, the channel is pinched-off. The experimental setup allows us to follow the changes in the PL spectrum induced by the He:Ne excitation. We could clearly observe a dependence, which is opposite to that seen in Fig. 2: as the He:Ne intensity is increased the spectrum changes from 2DHG-like to excitonic. This correlation between the changes in the current and PL spectrum verifies that the current is indeed due to the QW 2DHG channel.

The maximal hole density, which can be created in a given sample, is limited: as we increase the Ti:S intensity above a certain intensity, we observe that the PL does not change in shape, but only increases in magnitude. This maximal density depends strongly on the width of the Spacer

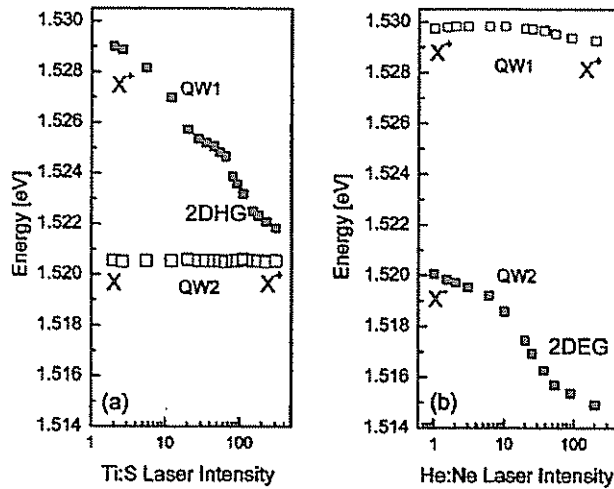


FIG. 4. The energy peaks of the PL from QW₁ and QW₂ as a function of (a) Ti:S laser intensity, varied between 1 to 300 mW/cm² (b) He:Ne laser intensity, varied between 1 to 200 mW/cm².

layer: the thinner the spacer, the higher is the 2DHG density. As the spacer width is increased from 15 to 125 nm we find that the PL spectrum exhibits a change similar to that shown in Fig. 2, from a broad line to an X-X⁺ doublet. Thus, there is a clear functional similarity between the role of the Spacer layer in our samples and that of modulation doped samples. The maximal 2DHG density that we could generate in a short Spacer sample was determined from Hall measurements to be $\sim 5 \times 10^{11}/\text{cm}^2$.

The measurements presented above clearly show that there is an excess of holes in the QW. Thus, there should be another layer with an excess of electrons. To differentiate between two candidate regions—the Spacer/cap interface and the cap/vacuum interface—we have compared two samples with a significantly different thickness of the cap layer, 15 and 75 nm. We found that the maximal achievable 2DHG density in the first sample was ~ 3 times larger than in the second one. This indicates that the electrons are accumulated at surface states in the cap/vacuum interface. We suggest that the accumulation of the hole gas occurs mainly due to the built-in electric field, shown in Fig. 1, which causes electrons to tunnel out of the well and drift to the surface, where they are trapped by surface states.⁹ The process of charge accumulation stops when the carrier density is such that a flat-band condition is met. Numerical estimates of the built-in electric field in the two samples give the observed general behavior. It should be noted, however, that the electric field values which are obtained are smaller than those required to quantitatively explain the large difference between the two samples. A more comprehensive study is needed.

We have combined the structure described above with a mixed type I-type II structure into a wide double QW configuration. The band diagram of the combined structure is shown in the inset of Fig. 5. The widths of QW₁/barrier/QW₂ are 15 nm/12 nm/25 nm, respectively. The width of the Spacer layer separating QW₁ from the cap is 20 nm. The width of the AlAs back barrier and the thin GaAs well are 15

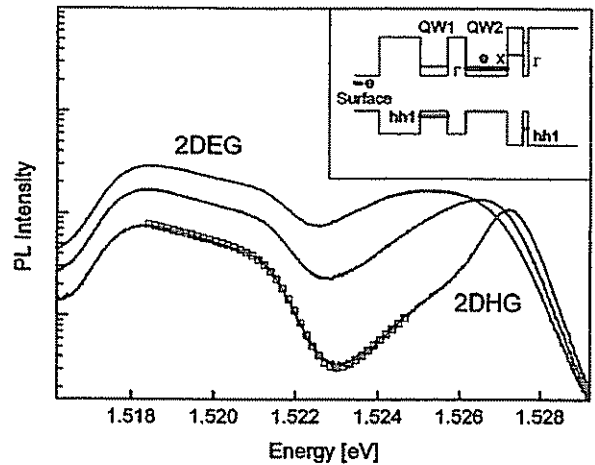


FIG. 5. The spectra of the wide double QW structure at increasing Ti:S intensity, $I_1 = 10, 20$ and 60 mW/cm^2 . The He:Ne intensity was kept fixed, $I_2 = 20 \text{ mW/cm}^2$. The spectra is characteristic of dense ($> 10^{11}/\text{cm}^2$) 2DHG in QW₁ and 2DEG in QW₂. Fit (scatter) gives $T_e = 4.2 \text{ K}$. Inset: the sample band diagram; the populated energy levels are emphasized.

and 2.5 nm, respectively. The band gap of all barriers was set above the He:Ne photon energy to eliminate absorption at that energy, and hence avoid depletion. The energy bands of the intrinsic structure are nearly flat. The presence of photo-excited carriers would only slightly modify these bands (up to a few percent of the GaAs band gap). The absence of a strong electric field between the QW's, due to the large capacitance of the double QW structure, enables in principle to realize an electron-hole system at extreme proximity—without having a breakdown.

We first show that a different 2D gas is formed by each laser; a 2DHG under Ti:S excitation, and a 2DEG—under a He:Ne. Figure 4 summarizes the response of the structure to illumination with each of these lasers. The peak PL energy of each QW is shown as a function of the Ti:S and He:Ne intensity. The shift of the peak energy to lower energies is due to band-gap renormalization, and serves as an indicator to the changes in density. As shown in Fig. 4(a), the PL from QW₁ exhibits a strong shift to lower energies with increasing Ti:S laser intensity, while that of QW₂ is unchanged. Similarly, the PL from QW₂ shifts to lower energies under increasing He:Ne illumination [Fig. 4(b)] while that of QW₁ is nearly unchanged. This behavior is consistent with that observed with each of the independent modules. We have verified that the spectra of QW₁ and QW₂ are of 2DHG and 2DEG, respectively, by studying their behavior at high-magnetic fields. Note that the effect of the Ti:S on QW₂ and that of the He:Ne on QW₁ is rather minor.

When the sample is illuminated with both lasers, both 2DEG and 2DHG are formed. Figure 5 shows the PL signal from the structure as a function of Ti:S intensity for a fixed He:Ne intensity. Two broad spectral peaks from the two QW's are clearly resolved. The high-energy peak comes from QW₁, and the low-energy one—from QW₂. It can be seen that increasing the Ti:S intensity causes a significant change in the line shape of QW₁, indicating a substantial increase in 2DHG density. The PL line of QW₂, on the other

hand, only increases in magnitude, without any significant change in line shape. Thus, we can conclude that we can tune the 2DHG density by varying the intensity of the Ti:S laser, while leaving the 2DEG density fixed. The electron density (determined from the behavior of PL in a magnetic field, which shows clear Landau levels) is $1.7 \times 10^{11}/\text{cm}^2$, whereas the 2DHG maximal density exceeds $2 \times 10^{11}/\text{cm}^2$. This result can be generalized for a variety of illumination conditions, such that to a large extent the carrier density in each of the wells can be chosen at will by a given combination of the He:Ne and Ti:S intensities.

An important question that arises is what is the carrier temperature under these nonequilibrium conditions. To determine the electrons temperature we analyzed the PL spectra of the 2DEG in QW₂ using the model proposed in Ref. 10. As can be seen in Fig. 5, the high energy part falls with a moderate slope, which becomes sharper beyond a certain energy. It was shown in Ref. 10 that this unique line shape is well described by a product $f_{\text{FD}}(\epsilon_e, T_e) \times f_{\text{MB}}(\epsilon_h, T_h)$, where f_{FD} is the Fermi-Dirac energy distribution of the 2DEG, and f_{MB} is the Maxwell-Boltzmann energy distribution of the minority holes. ϵ_e and ϵ_h are the electron and hole energies, related by $\epsilon_h = \epsilon_e m_e/m_h$, and T_e and T_h are the temperatures of the electrons and holes, respectively. We have fitted the model to the lowest PL curve of Fig. 5, where the two line shapes are well separated. The fit takes into

account the small contribution from the 2DHG tail above 1.5225 eV. We obtained an excellent fit with an electron temperature of 4.2 K. The long carriers lifetime in these structures⁵ enables this equilibration with the crystal temperature. We wish to emphasize that the fit puts a tight constrain on the electron temperature, and deviates from the measured line shape when we change it. The hole temperature appears in $f_{\text{MB}}(\epsilon_h, T_h)$ with the electron-hole mass ratio m_e/m_h as a prefactor. Assuming that $T_h = T_e$ holds in QW₂ the fit yields $m_e/m_h = 0.09$, which gives a hole mass of $0.75m_0$, in general agreement with the value found in magnetotransport and cyclotron resonance measurements.¹¹

Unfortunately, we are not aware of a similar way to assess the 2DHG temperature in QW₁. An indirect upper limit for the hole's temperature can be deduced from the heavy and light exciton PL intensity ratio. At the highest excitation intensity this ratio yields an exciton temperature of 7 K.⁷

In conclusion, we have demonstrated a technique to optically induce 2DHG in wide GaAs QW's. This has allowed us to construct a structure in which a dense 2DEG and 2DHG could be optically created at a close proximity. We have demonstrated the ability to control the density of each gas using two lasers. Further work is needed to improve the quality of the contacts.

This research was supported by the Minerva Foundation.

- ¹R. Dingle, H. Stormer, A. C. Gossard, and W. Weigmann, Appl. Phys. Lett. **33**, 665 (1978).
- ²X. M. Chen and J. J. Quinn, Phys. Rev. Lett. **67**, 895 (1991); V. I. Yudson, *ibid.* **77**, 1564 (1996); J. Fernandez-Rossier and C. T. Tejedor, *ibid.* **78**, 4809 (1997); S. Conti, G. Vignale, and A. H. MacDonald, Phys. Rev. B **57**, R6846 (1998).
- ³U. Sivan, P. M. Solomon, and H. Shtrikman, Phys. Rev. Lett. **68**, 1195 (1992); H. Rubel *et al.*, Semicond. Sci. Technol. **10**, 1229 (1995); A. Parlangeli *et al.*, Physica B **256-258**, 531 (1998); V. B. Timofeev *et al.*, Phys. Rev. B **61**, 8420 (2000).
- ⁴F. Plentz, D. Heiman, A. Pinczuk, L. N. Pfeiffer, and K. W. West, Solid State Commun. **101**, 103 (1997); T. Fukuzawa, E. E. Mendez, and J. M. Hong, Phys. Rev. B **66**, 3066 (1990); L. V. Butov *et al.*, Phys. Rev. B **60**, 8753 (1999).
- ⁵P. Dawson, I. Galbraith, A. I. Kucharska, and C. T. Foxton, Appl.

- Phys. Lett. **58**, 2889 (1991); A. Manassen *et al.*, Phys. Rev. B **54**, 10 609 (1996); A. Nazimov *et al.*, Physica E (Amsterdam) **6**, 650 (2000).
- ⁶G. Finkelstein, H. Shtrikman, and I. Bar-Joseph, Phys. Rev. B **53**, R1709 (1996); Nuovo Cimento D **17**, 1239 (1995).
- ⁷S. Glasberg, G. Finkelstein, H. Shtrikman, and I. Bar-Joseph, Phys. Rev. B **59**, R10 425 (1999).
- ⁸C. Delalande, J. Orgonasi, M. H. Meynadier, J. A. Brum, G. Bastard, G. Weinmann, and W. Schalpp, Solid State Commun. **59**, 613 (1986).
- ⁹T. E. Kazior, J. Lagowski, and H. C. Gatos, J. Appl. Phys. **54**, 2533 (1983), and references therein.
- ¹⁰R. Kuchler *et al.*, Semicond. Sci. Technol. **8**, 88 (1993).
- ¹¹H. L. Stormer *et al.*, Phys. Rev. Lett. **51**, 126 (1983); J. Ando, J. Phys. Soc. Jpn. **54**, 1528 (1985).

2.2 The positively charged exciton magneto-optical spectra in GaAs quantum wells

S. Glasberg, G. Finkelstein, H. Shtrikman and I. Bar-Joseph

Comparative spectroscopy of the positively and negatively charged excitons in GaAs quantum wells

Phys. Rev. B **59**, Rapid Comm. p. 10425 (1999)

This work studies the X^+ magneto-optical spectra, and compares the X^+ and X^- binding energies, spin configurations, and g-factors. To achieve a meaningful comparison the type of excess carriers is changed within the same sample, with minimum perturbation to the QW confinement. The comparison shows that the X^+ and X^- have nearly identical binding energies at zero magnetic field. We present our approach for quantitatively account for this behavior in view of recent theoretical models. We also find that the X^+ and X^- binding energy evolve quite differently in a magnetic field and suggest a qualitative explanation.

A comprehensive theory of charged excitons in zero and strong magnetic fields is long sought. Unfortunately, a complete description of the problem is hard to achieve, because of the comparable contributions of the $e-h$ and $e-e$ ($h-h$) interactions, and the dominance of the exchange interaction (that yields the Singlet and Triplet states). Also, the comparable Bohr and cyclotron radii ($a_B \sim l_B$) hinder a simple perturbative approach to the changes in magnetic field [1-2]. Thus, rigorous approaches that numerically solve the charged exciton Hamiltonian are largely applied (these approaches were discussed in the introduction).

A major test of any theory of charged excitons lays in its ability to reproduce the negatively and the positively charged excitons binding energies and magneto-optical spectra. At the time we published our results of nearly equal X^- and X^+ binding energies, theoretical calculations predicted a large difference between the X^- and X^+ binding energies. These calculations neglected two important effects: the finite well width and the

built in electric field due to the excess charges in the well. To understand the influence of these two let us consider the trion Hamiltonian for a finite width potential. The corresponding expressions for the X^- and X^+ are obtained by interchanging electron and hole labels in the Hamiltonian, $\{e_1, e_2, h\} \rightarrow \{h_1, h_2, e\}$. For the calculations one usually factorizes the charged exciton wave-function into an in-plane part Ψ_L and the QW sub-bands functions ϕ . Thus, the X^- wavefunction is written

$$\Psi = \Psi_L(\rho_{e1}, \rho_{e2}, \rho_h) \cdot \phi_e(z_{e1}) \phi_e(z_{e2}) \phi_h(z_h)$$

Here ρ denotes a two-dimensional vector in the QW plane. The center of mass motion can be separated from the relative motion with the charged exciton Schrodinger equation for the relative motion being [3]

$$\left[-\frac{\hbar^2}{2\mu} (\nabla_{\rho_1}^2 + \nabla_{\rho_2}^2) - \frac{\hbar^2}{2m_h} \nabla_{\rho_1} \cdot \nabla_{\rho_2} - V_{eh}(\rho_1) - V_{eh}(\rho_2) + V_{ee}(|\rho_1 - \rho_2|) - E_T \right] \Psi_L(\rho_1, \rho_2) = 0$$

where $\mu^{-1} = m_e^{-1} + m_h^{-1}$ and $\rho_j = \rho_{ej} - \rho_h$. The effective Coulomb potential in the Hamiltonian is

$$V_{ij}(\rho) = \frac{1}{\varepsilon} \iint \frac{\phi_i^2(z') \phi_j^2(z'')}{\sqrt{(z' - z'')^2 + \rho^2}} dz' dz''$$

As seen the QW sub-band functions ϕ_i determine the effective Coulomb potential - and so the binding potential. In the 2D limit, the e - e and e - h interactions will be equal. The charged excitons energies are related by the relation $E_{X^-}(\sigma) = E_{X^+}(1/\sigma)$, where $\sigma = m_e/m_h$. The results of the calculations based on this approach are shown in Fig. 2.1. The upper curves (after Ref. 4) are for a two-dimensional geometry, whereas the lower curves are for a finite width QW [3,5,6]. As seen the finite width results in a comparable binding energies for the X^- and X^+ . This result is attributed [3] to the effective potential $V_{ij}(r)$ which is different from the ideal case of a 2D Coulomb potential, especially at low mass ratios σ . We note that other calculations [5] gave equal binding energies for a width as low as 4nm, thus the effect of the QW potential is still under theoretical discussion.

Let us turn to the effect of the self-consistent potential. Figure 2.2 shows the QW electron and hole levels for low-density 2DEG and 2DHG. It demonstrates the different localization of the electron and hole wave-functions along the growth direction because of the internal electric field [7].

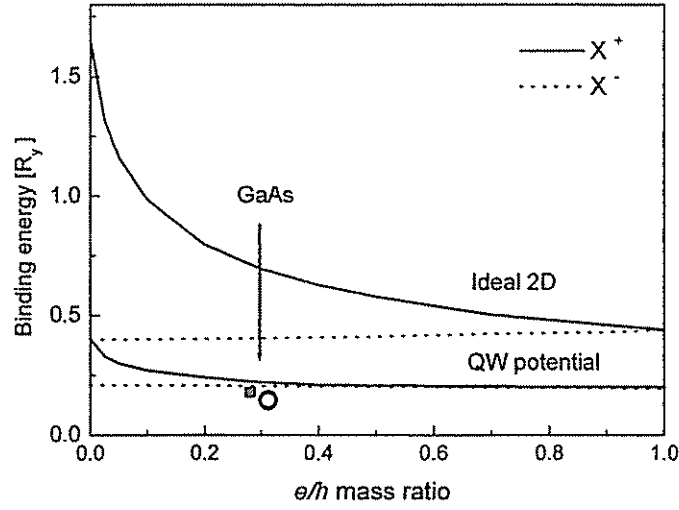


Fig. 2.1: The binding energies of X^- and X^+ as a function of mass ratio for an ideal 2D Coulomb potential and effective QW potential. Scatter shows experimental results.

Based on this result we have calculated the Coulomb interactions terms in the charged excitons Hamiltonian, for simplified uniform electron and hole charge densities $\rho_j(z) = \pm e/L_j$. The resulted Coulomb potential for the X^- and X^+ is plotted in Fig. 2.3, normalized by $V_0 = e^2/\epsilon\epsilon_0$, which is the coulomb potential between two point charges ($L_j = 0$). As seen, this rough estimate which gives $V_{ee} < V_{eh} < V_{hh}$ leads to correction downwards in the X^+ binding potential.

In view of our findings at zero magnetic fields, it is interesting to study the evolution of the binding energy in a magnetic field. The large Bohr radius of the charged excitons enables their study in a wide range of regimes: from atomic physics limit of $l_B \gg a_B$ (magnetic field as a perturbation) to the regime where the magnetic confinement dominates the binding potentials ($l_B < a_B$). The experimental results have shown that the X^-

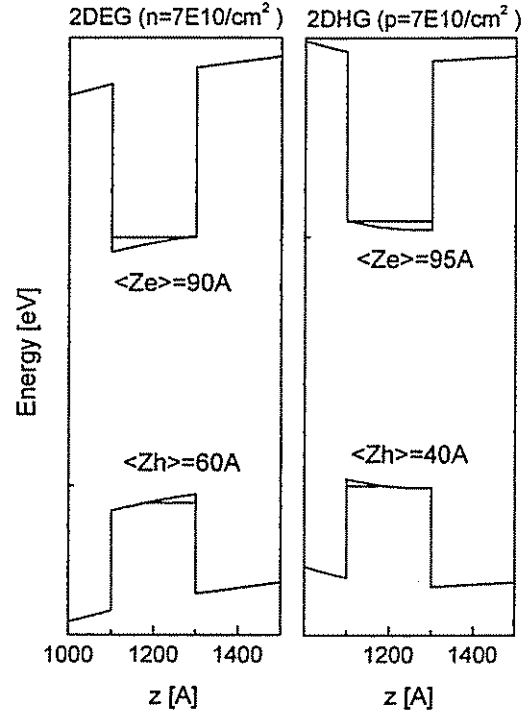


Fig. 2.2: Numerical calculation of the of the electron and hole QW levels in 2DEG and 2DHG having a density of $7 \times 10^{10} \text{ cm}^{-2}$.

exhibits a significant increase of binding energy (by 60%), while that of the X^+ remained unchanged, or even slightly decreased.

The role of the electron-hole mass ratio is significant in that phenomenon. At high magnetic fields the electron cyclotron energy ($\sim 1.75\text{meV/T}$) is large compared with the second carrier binding energy ($\sim 1\text{meV}$). Thus, the electronic wavefunction is dominated by that of the Lowest Landau level. The effect of the magnetic field on the X^- would be to quench its Bohr radius to the magnetic length. The characteristic repulsion and attraction Coulomb terms are in the form of [8, 9]

$$V_{ij=e,h}(B) = \langle \Psi_{h(e)} | \frac{e^2}{\epsilon r} | \Psi_e \rangle \propto \frac{e^2}{\epsilon l_B} \propto \sqrt{B}$$

where Ψ_i are the lowest Landau level wavefunctions. This dependence of the interaction on the magnetic field can be the root of the increase in the binding energy of the X^- [10]. Indeed, for a perfectly 2D system the X^- has a binding energy of $0.054e^2/\epsilon l_B$, which strictly increases as a root of the magnetic field [9]. Experimentally, the X^- binding energy increase as a function of magnetic field does show a square root behavior at low fields. At higher fields the increase is slower, $\sim \log B$, due to the weakening of the Coulomb interaction enhancement [8]. In the X^+ there are two holes, and their wavefunction is most likely a mixtures of Landau-levels whose relative weights in the wave function change with the magnetic field [11]. We have no qualitative means to assess the outcome of this process. Rigorous models, which take into account the Landau-level mixing, were employed, but only for the X^- [8, 12].

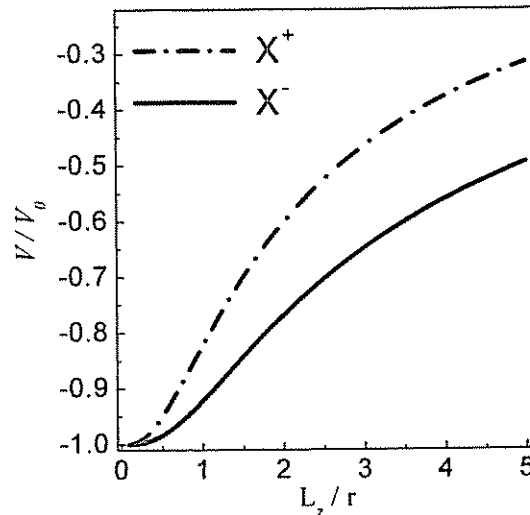


Fig. 2.3: Calculation of the Coulomb interaction term $V(r)$ as a function of the charge density along the growth direction e/L_z for the X^+ and X^- for mass ratio $m_h/m_e=8$

References

1. W. F. Xie, Commun Theor. Phys. **34**, 391 (2000)
2. A. Wojs, J. J. Quinn and P. Hawrylak, Phys. Rev. B **62**, 4630 (2000) and refs. therein
3. A. Esser, E. Runge, R Zimmermann, and W. Langbein, Phys. Rev. B **62**, 8232 (2000)
4. B. Stebe and A. Ainane, Superlattices Microstruct. **5**, 545 (1989); J. Singh et al. in EXCON'96, Germany, Ed. K. Gohrish, Dresden University Press (1996); A. Thilagam, Phys. Rev. B **55**, 7804 (1997)
5. B. Stebe *et al.*, Phys. Rev. B **61**, 7231 (2000)
6. C. riva *et al.*, *ibid.* 178, 513 (2000)
7. G. Bastard, "Wave mechanics applied to semiconductor heterostructures", France, 1988
8. D. M. Whittaker and A. J. Shields Phys. Rev. B **56**, 15185 (1997)
9. J. J. Palacios, D. Yoshika, and A. H. MacDonald, Phys. Rev. B **54**, R2296 (1996)
10. R. Suris, *Private communication*
11. U. Ekenberg and M Altraelli, Phys. Rev. B **32**, 3712 (1985); S. -R. Eric Yang, D. A. Broido, and L. J. Sham, Phys. Rev. B **32**, 6630 (1985)
12. J. R. Chapman, N. F. Johnson, and V. N. Nicopoulus, Phys. Rev. B **55**, 10221 (1997)

Comparative study of the negatively and positively charged excitons in GaAs quantum wells

Shmuel Glasberg, Gleb Finkelstein, Hadas Shtrikman, and Israel Bar-Joseph

Department of Condensed Matter Physics, The Weizmann Institute of Science, Rehovot 76100, Israel

(Received 22 June 1998)

We compare the photoluminescence spectra of the negatively and positively charged excitons in GaAs quantum wells. We use a structure which enables us to observe both complexes within the same sample. We find that their binding energy and Zeeman splitting are very similar at zero magnetic field, but evolve very differently at high fields. We discuss the implications of these observations on our understanding of the charge excitons structure in high magnetic fields. [S0163-1829(99)51516-6]

The negatively charged exciton X^- , which is a bound state of two electrons and a hole, was recently observed in the emission and absorption spectra of a depleted two-dimensional electron gas (2DEG).¹⁻³ It appears in the photoluminescence (PL) spectrum of GaAs quantum wells as a narrow line, approximately 1 meV below the neutral exciton line. This energy is the binding energy of an extra electron to an exciton. The observation of X^- triggered intensive experimental and theoretical studies of its energy spectrum and structure. A special effort was devoted to understanding its behavior in strong magnetic fields, when the cyclotron diameter becomes smaller than the X^- Bohr diameter, and the internal structure is expected to be modified. Indeed, a significant increase in binding energy and appearance of another bound state, in which the two electrons are in a triplet state, were observed in the optical spectrum in high magnetic fields.^{4,5}

Very soon after the observation of the X^- , its positive counterpart, the positively charged exciton X^+ , was observed.⁴ The X^+ consists of two holes and an electron, and is a semiconductor analogue of the hydrogen molecule ion H_2^+ . It was found that the X^+ line emerges from the two-dimensional hole gas (2DHG) PL as the hole density is decreased, very similarly to the X^- appearance in a 2DEG.⁶ In this paper we investigate the X^+ spectrum in GaAs/ Al_xGa_{1-x} As QW at high magnetic fields (0 to 9 T) and compare it to that of X^- . To obtain a meaningful comparison between the two bound complexes we design a structure where we can control the density and type of the excess carriers in the QW by changing the illumination conditions. This structure allows us to alter the carrier gas in the well from 2DHG to 2DEG, and study the X^+ and X^- spectra within the same sample.

We find that the binding energies of the two charged excitons are nearly identical at zero magnetic field. However, our results show a profound difference between the spectra of X^+ and that of X^- at a high magnetic field which is applied in a direction normal to the layers. We observe a very different dependence of the binding energy in the two complexes on the magnetic field strength: while X^- exhibits a significant increase in binding energy with increasing field (more than 60% at 7 T), X^+ binding energy remains nearly constant. A large difference is observed also between the Zeeman splitting of the X^+ and that of X^- . We discuss the implications of these observations on our understanding of

the charge excitons structure in high magnetic fields.

Two nominally undoped samples were studied. Their structure is schematically described in the inset of Fig. 1. It consists of a buffer superlattice made of 25 periods of 10 nm $Al_{0.25}Ga_{0.75}As$ and 1 nm of GaAs followed by a 20 nm GaAs well, an $Al_{0.37}Ga_{0.63}As$ layer denoted as the Spacer, and 15 nm of GaAs cap layer. The thickness of the Spacer layer is 25 and 125 nm in samples 1 and 2, respectively. The samples were grown on (100) oriented semi-insulating GaAs substrates. Under very weak excitation ($<10 \mu W/cm^2$) the observed spectrum is of neutral exciton, indicating that the well is nearly empty of carriers. However, when the intensity of the laser is increased the carrier density in the well grows, and charged excitons are observed in the spectrum. The carrier type is determined by the laser photon energy. When this energy is slightly above the GaAs gap ($h\nu_1$), carriers are created in the well and the cap layer. The built-in electric field that is due to the unintentional p -type background doping causes electrons which are excited in the well to tunnel into the cap layer. This process gives rise to electrons deficiency in the well. Similarly, the photoexcited holes in the cap layer may tunnel to the well and accumulate there. These processes are much more effective in the thinner Spacer

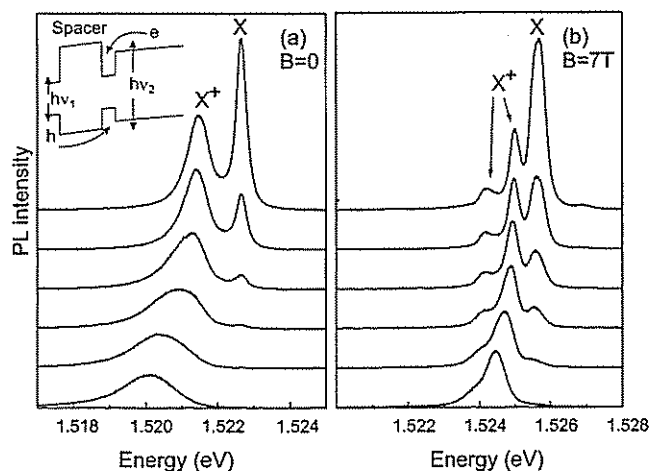


FIG. 1. The PL spectra of sample 1 for increasing He:Ne intensity, between 0 (bottom curve) and 10 (top curve) mW/cm^2 . The Ti:S intensity is $100 mW/cm^2$. (a) and (b) correspond to measurements at 0 and 7 T, respectively. Inset: The generic structure of samples 1 and 2.

sample 1, resulting in a higher hole density than in sample 2. On the other hand, when the laser is tuned to a higher energy ($h\nu_2$), slightly above the gap of the low $\text{Al}_x\text{Ga}_{1-x}\text{As}$ superlattice, most carriers are created at that region. In this case the built-in electric field causes the electrons to be swept into the well and create an excess electron density there. Thus, by changing the excitation energy we can change the carrier gas in the well from 2DHG to 2DEG. In our experiment we use a Ti:S laser at 780 nm and a He:Ne laser at 632.8 nm as the low ($h\nu_1$) and high ($h\nu_2$) energy excitation sources, respectively. The polarized PL measurements are conducted in a 7 T immersion cryostat. The PL is collected through a birefringence free optical window and analyzed through a circular polarizer. Unpolarized PL measurements are carried out in a 9 T magnet, using a fiber optic collection setup. The signal is dispersed in a 0.75 m spectrometer and detected in a cooled charge-coupled device detector.

Figure 1(a) shows the measured PL spectrum of sample 1 at zero magnetic field. The different spectra are measured with a constant Ti:S intensity of $\sim 100 \text{ mW/cm}^2$, and with an increasing He:Ne intensity, from 0 to $\sim 10 \text{ mW/cm}^2$. Under Ti:S excitation only (bottom curve) the well contains an excess hole density, and the PL spectrum is a broad line, typical of the recombination of a free carrier gas. The effect of the He:Ne laser is to reduce the hole density by supplying electrons to the well. We can see that as the He:Ne intensity is increased the width of the line decreases and it shifts to higher energies. Since the width of the line is related to the holes' Fermi energy, this narrowing of the line reflects the decrease in the hole density. Similarly, the shift to higher energy is due to a reduced band-gap renormalization and a lower built-in electric field in the well. At the largest He:Ne intensity the spectrum consists of two lines, which we identify as the neutral exciton (X) and the X^+ lines. It should be noted that this spectral signature, of two narrow peaks separated by $\sim 1 \text{ meV}$ which evolve from a broad line, is characteristic of both the $X-X^-$ and the $X-X^+$ doublets, and by itself cannot serve as a criterion for identifying the type of charged exciton. We show in the following that the PL spectrum in a magnetic field enables us to distinguish between the X^+ and the X^- .

The spectral signature of the X^- in a high magnetic field which is applied normal to the layers is rather unique.^{4,5} It consists of several lines, associated with the singlet and triplet states of the two electrons in the X^- . These singlet and triplet states have different spatial wave functions, symmetric and antisymmetric, respectively, and hence different binding energies. It is found that these lines move away from the exciton with increasing magnetic field, reflecting an increase in binding energy of the corresponding states. In addition, a series of weak satellite peaks are observed at the low-energy tail of the emission spectrum.⁷ These peaks result from shakeup processes, in which a recombination of one of the electrons in the X^- with the hole is accompanied by an ejection of the remaining electron to a high Landau level. This unique spectral signature, consisting of singlet, triplet, and shakeup lines, enables a clear identification of the X^- .

Figure 1(b) shows the PL spectra in a magnetic field of 7 T applied in the direction normal to the layers, for similar excitation conditions as in Fig. 1(a). The measured spectral signature is different than that reported for X^- .^{4,5} This is

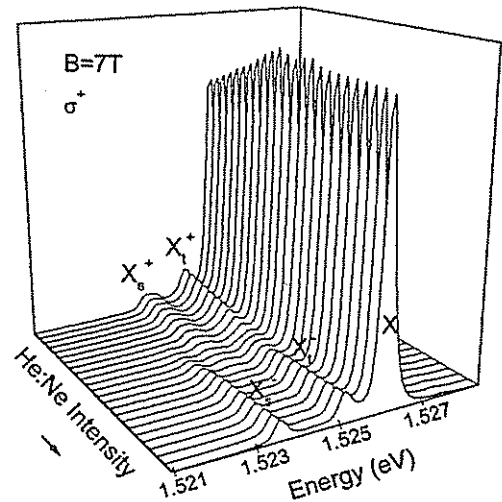


FIG. 2. Evolution of the σ^+ polarized PL spectra at 7 T with increasing He:Ne intensity for sample 2. The evolution from a X^+ to X^- spectrum through a neutral exciton gas is clearly seen. Each spectrum is normalized by its integrated intensity.

especially manifested in the energies of the two low energy lines, which evolve from the charged exciton line. These differences will be discussed in detail later in this paper. A supporting evidence for the identification of the X^+ is provided by measurements of p -type modulation doped samples which contain a 2DHG in the QW. These samples are grown on (311)A oriented GaAs substrates. The generic structure is described in Ref. 4. Different samples with different spacer widths (between 25 to 50 nm) and doping levels (5×10^{17} to $2 \times 10^{18} \text{ cm}^{-3}$) were studied. The density of holes in the QW is controlled by applying a positive voltage to a semi-transparent gate with respect to the 2DHG, and the exciting photon energy is kept below the barrier energy gap. The spectral signature, which is observed in these samples, is the same as in Fig. 1(b), only with broader lines. We therefore conclude that this is indeed the spectrum of X^+ .

Let us now turn to sample 2. The fact that the Spacer layer is much thicker than in sample 1 causes the initial density of holes in the well to be lower. Figure 2 describes the PL spectrum at 7 T for similar illumination conditions as in Fig. 1. To clarify the evolution of the spectrum we present a circularly polarized spectrum of σ^+ . The change from 2DHG to 2DEG spectrum through a neutral exciton gas is clearly visible. This change is manifested by the change of the PL spectrum from that associated with X^+ to that of X^- . Both the X^+ and X^- spectra consist of singlet and triplet lines. We can see that the strength of the X^+ lines decreases gradually with increasing He:Ne intensity, until they disappear and new lines, associated with X^- appear. These changes are accompanied by a dramatic change in the low-energy part of the spectrum, which is too weak to be seen in the figure. Together with the X^- lines we observe the familiar fan of weak shakeup satellite peaks, separated from one another by $\hbar\omega_c^e$, the electron cyclotron energy.⁷ The low-energy spectrum of X^+ is very different: the electron shakeup lines are not present and a complicated spectrum of impurity related faint lines appears. Remarkably, the energy of the exciton line is fixed in all spectra, providing a constant reference energy.

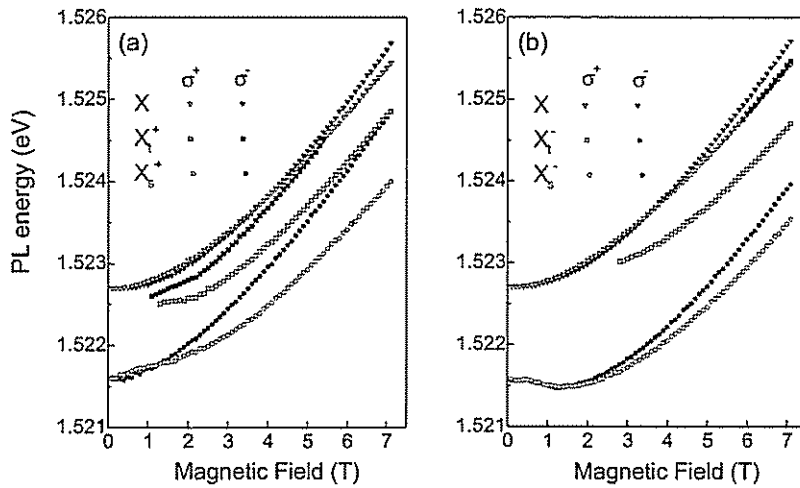


FIG. 3. The energy dispersion of the (a) X^+ and (b) X^- PL peaks as a function of magnetic field. The full and empty symbols stand for the σ^- and σ^+ polarizations, respectively.

Figures 3(a) and 3(b) show the energy dispersion of the X^+ and X^- lines as a function of magnetic field. The Zeeman split neutral exciton state appears at the highest energies, and is characterized by a change of the g factor sign at 3.5 T. The general structure of the energy spectrum is the same for X^- and X^+ : they both consist of two pairs of Zeeman split circularly polarized lines. The lowest energy pair is due to a recombination of the singlet X^- (or X^+), and the higher energy pair is due to the recombination from the triplet state (this triplet state becomes bound at a magnetic field and emerges below the exciton line).

In Fig. 4 we compare the binding energy and Zeeman splitting of the singlet state of these two complexes. The binding energy is measured relatively to the exciton state and the mean energy is taken for each Zeeman pair. It can be seen that the binding energy of the singlet X_s^- state increases between 0 and 4 T and then begins to saturate. Between 7 and 9 T it remains nearly constant. The overall increase is from 1.1 meV at 0 T to 1.8 at 9 T, more than 60%. This saturation of the X_s^- was found to persist up to 20 T.⁸ The singlet X_s^+ behavior is very different: *the binding energy remains nearly constant* between 0 and 9 T. This behavior of the X_s^+ is observed also in the modulation doped samples. It should be noted here that this observation contradicts an earlier report which found that the behavior of the X^+ binding energy is very similar to that of X^- .⁹

Let us discuss the behavior of the binding energy in the two complexes, starting with the zero magnetic-field behavior. There were several theoretical attempts to compare the zero-field binding energies of X^+ and X^- using a two-dimensional model for the structure of the charged excitons.¹⁰ These calculations yield an X^+ binding energy that exceeds that of X^- by a value which depends on the electron-hole mass ratio. Figure 4(a) clearly shows that the binding energies of X^+ and X^- are identical at zero field, with an accuracy of 0.05 meV, namely 5% of the binding energy. We have confirmed that this is not an accidental degeneracy: a similar behavior was observed in a sample with 15 nm well width. We wish to remark that the accuracy of these measurements stems from the fact that both complexes are observed in the same sample, with the exciton line appearing at a constant energy. To explain this observation within the present two-dimensional models one would have to assume a very light in-plane hole mass, close to the elec-

tron mass, which is very unlikely. For example, according to the calculations of Ref. 10 an equal binding energy implies $m_e/m_h > 0.8$. We note, however, that these models assume identical electron-electron and hole-hole interactions in the plane, i.e., $V_{ee}(r) = V_{hh}(r)$. This assumption is invalid for a triangular well, in which the 2DEG or 2DHG is confined along the growth direction z . The different electron and hole masses along z give rise to $V_{hh}(r) > V_{ee}(r)$, and hence to a larger repulsion between the holes in X^+ and lower binding energy.

Let us turn now to the behavior at high magnetic fields. Charged excitons are characterized by a delicate balance between a large Coulomb attraction and a slightly smaller repulsion. This balance is strongly affected by a high magnetic field, which squeezes the in-plane motion to a cyclotron diameter. This has a larger impact on the X^+ , where the repulsion interaction V_{hh} is larger. This can explain the fact that the X^- binding energy becomes larger than that of the X^+ at high magnetic fields. Calculations of the structure and binding energy in a magnetic field were conducted only for X^- ,

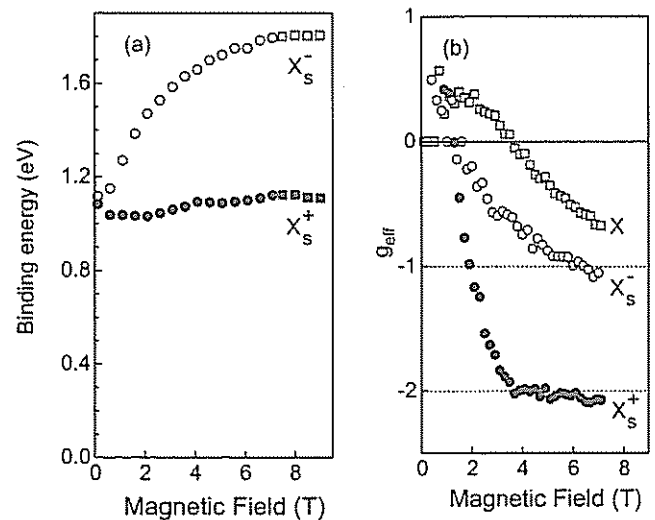


FIG. 4. (a) The binding energies of the X_s^+ and X_s^- states as a function of magnetic field. The circles and squares correspond to the polarized and unpolarized measurements, respectively. (b) The effective g factor g_{eff} of the neutral exciton; the X_s^- and X_s^+ as a function of magnetic field. Note that the neutral exciton Zeeman splitting is the same for both X^+ and X^- spectra.

using a numerical approach.^{11,8} The results agree qualitatively with the measured spectra, and show a trend of increased binding energy with magnetic field. However, the values obtained for the binding energy are smaller than those measured experimentally.

In Fig. 4(b) we show the magnetic field dependence of the g factor of the X , X_s^+ , and X_s^- recombination. The observed Zeeman splitting of a charged exciton is a sum of the electron and hole contributions, similarly to a regular exciton. Thus, one can define an effective g factor for X_s^+ and X_s^- , in the same way it is done for a regular exciton,¹² by $\Delta E = \mu_B B_z g_{X^\pm}$, where μ_B is the Bohr magneton (the sign of g is determined using the conventions of Refs. 12 and 13). The behavior of g_X in the X^+ and X^- spectra is very similar, and we show only the values obtained from the $X-X^-$ spectrum. It is seen that all exciton complexes have the same g factor value of $\sim +0.5$ at very low fields, but evolve differently as the magnetic field is increased. The behavior of g_{X^+} is especially interesting: it decreases very rapidly, changes sign, and then saturates at a value of -2 at 4 T.

The difference in g factors between the X^\pm and X indicates that at high magnetic field the electron and hole wave functions in a charged exciton are not the same as in a neutral exciton. The magnetic-field dependence of g_X is commonly understood as due to mixing with light-hole states.¹⁴

This mixing cannot explain the strong field dependence of g_{X^\pm} : it gives rise to a relatively weak field dependence of g_X , and its effect is expected to be even weaker for X^\pm , which are farther away in energy. On the other hand, the modification of the charged exciton structure in a magnetic field which was discussed above implies mixing of the electron and hole wave functions with higher Landau levels and higher subbands. This mixing gives rise to a magnetic-field dependence of g_{X^\pm} . Such mixing was indeed found to play an important role in determining the binding energy in the calculations of Ref. 11. The observed saturation in both Zeeman splitting and binding energy of X^+ can be viewed as an indication of a formation of a stable spatial structure.

In conclusion, we have provided an unambiguous identification of the X^+ spectrum at high magnetic field, and have shown that this spectrum is different from that of the X^- . Understanding the structure and the spectrum of charged excitons in this regime is still an open problem. We believe that the experimental data presented here, which compares the spectrum of X^- and X^+ within the same sample, can serve as a basis for theoretical studies of this problem.

This research was supported by the Israel Science Foundation founded by the Israel Academy of Sciences and Humanities.

¹ K. Kheng *et al.*, Phys. Rev. Lett. **71**, 1752 (1993).

² G. Finkelstein, H. Shtrikman, and I. Bar-Joseph, Phys. Rev. Lett. **74**, 976 (1995).

³ A.J. Shields *et al.*, Phys. Rev. B **51**, 18 049 (1995).

⁴ G. Finkelstein, H. Shtrikman, and I. Bar-Joseph, Phys. Rev. B **53**, R1709 (1996).

⁵ A.J. Shields *et al.*, Phys. Rev. B **52**, 7841 (1995).

⁶ G. Finkelstein and I. Bar-Joseph, Nuovo Cimento **17D**, 1239 (1995).

⁷ G. Finkelstein, H. Shtrikman, and I. Bar-Joseph, Phys. Rev. B **53**, 12 593 (1996).

⁸ D.M. Whittaker and A.J. Shields, Phys. Rev. B **56**, 15 185 (1997).

⁹ A.J. Shields *et al.*, Phys. Rev. B **52**, R5523 (1995); J.L. Osborne *et al.*, *ibid.* **53**, 13 002 (1996).

¹⁰ B. Stebe and A. Ainane, Superlattices Microstruct. **5**, 545 (1989); A. Thilagam, Phys. Rev. B **55**, 7804 (1997); J. Singh *et al.*, in EXCON'96, Germany, 1996, edited by Kurort Gohrish (Dresden University Press, Dresden, Germany, 1996), p. 107.

¹¹ J.R. Chapman *et al.*, Phys. Rev. B **55**, R10 221 (1997).

¹² M.J. Snelling *et al.*, Phys. Rev. B **45**, 3922 (1992).

¹³ H.W. van Kesteren *et al.*, Phys. Rev. B **41**, 5283 (1990).

¹⁴ G.E.W. Bauer and T. Ando, Phys. Rev. B **37**, 3130 (1988); V.B. Timofeev *et al.*, Pis'ma Zh. Éksp. Teor. Fiz. **64**, 61 (1996) [JETP Lett. **64**, 57 (1996)].

2.3 Landau levels in the recombination spectrum of a low-density two-dimensional hole gas

S. Glasberg, H. Shtrikman and I. Bar-Joseph

Observation of valence-band Landau-levels in the photoluminescence of a low-density 2DHG in a GaAs quantum-well

Phys. Rev. B **63**, Issue 20 (2001) Rapid Comm.

This chapter deals with two ways in which the spectrum of an excess density of free-holes in the quantum well is manifested. One way is through the hole shake-up spectrum from an intrinsic complex, the X^+ . The second way is through the transition of a free-hole, which weakly interacts with an impurity. The properties of the intrinsic and extrinsic complexes are multi-facial, having some fundamental similarities (three-body structure) and differences (center of mass motion, spin statistics), making their comparison informative. In this work, we compare the spectra of both, and find that they are the manifestation of the same hole Landau-level spectrum.

The photoluminescence line-shape of a 2DHG in a magnetic field is nearly feature-less, being composed of two spin-split broad lines [1]. This result stands in contrast with the 2DEG recombination spectrum that shows the quantization to Landau-levels (LLs). As discussed in the paper, the main reason for this difference is the large hole to electron mass ratio in GaAs. In this work we found that the Landau-level spectrum of free holes is manifested in the low energy part of the bound holes (X^+ and D^0h) spectra. To understand how this result occurs within objects of significant binding potential we review their structure and recombination spectrum. In Fig 3.1 we show schematically the two complexes, the intrinsic X^+ and the impurity system D^0h . Figure 3.1A shows the X^+ structure of an electron interacting with two identical holes. With all carriers having substantial overlap of wavefunction, the coulomb repulsion is only marginally overwhelmed by attraction. As a result, the inter-particle correlations are of primary

importance and it may be shown that the holes form a Singlet. This situation is analogous to the X^- [2], and a solution for the orbital radii of the holes, a and b , is shown in Fig. 3.1A where $b \gg a$. A plausible physical interpretation of this solution in the X^+ is of a hole weakly bound to an exciton. Indeed, the characteristic exciton binding energy is $\sim 6\text{meV}$, while the second-hole binding energy is $\sim 1\text{meV}$.

Figure 3.1B shows the D^0 in the presence of a hole. The donors are neutral under steady state illumination because the small number of donors in the QW recapture each a photo-excited electron. The negligible electron-donor mass ratio of this object is manifested in a binding energy that is larger by 50% than that of the exciton ($\sim 9\text{meV}$) [3]. The experimental result show that the D^0 has very shallow binding potential for the second-carrier, $\sim 0.2\text{meV}$. This energy yields a Bohr radius of 670\AA . The hole binding energy to the D^0 is smaller than the thermal energy due to ambient temperature (0.35meV). Thus, the hole can be viewed as practically free.

The major finding of this chapter is the observation of X^+ shake up (SU) lines due to valance-band LLs. Shake-up is a radiative optical process in which a recombining

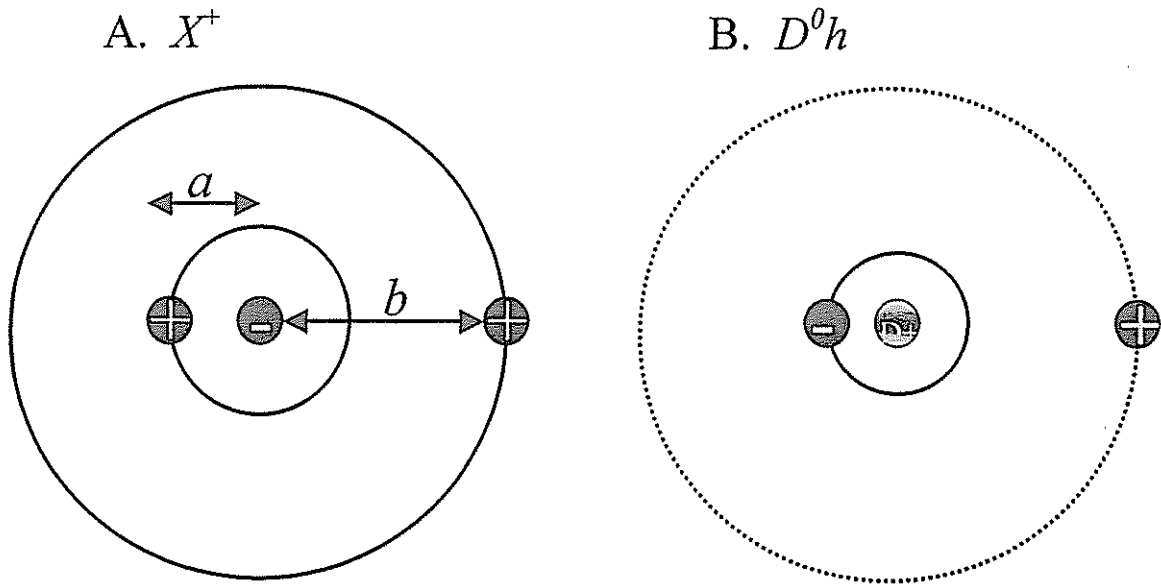


Fig. 3.1 Schematic representation of the X^+ and D^0h charged complexes

electron and hole pair excites the remaining carriers via the sudden perturbation of “shutting-off” the exciton-electron interaction. In an SU process the energy of the emitted

photon is smaller by the amount of the energy left in the excitation. At a magnetic field the SU process corresponds to e - h recombination, which leaves behind an inter Landau-level electron (with X^-) or hole (with X^+) excitation. Consequently, the SU processes give rise to a fan of discrete lines, each associated with a different LL as the final state for the shaken electron (hole). Such processes were observed in 2DEG [4, 5] and X^- [6, 7], as a series of peaks at energies which are close to an integer number times $\hbar\omega_c$ below the main recombination line. The intensity of the SU lines indicates how effectively this excitation is coupled to the recombining exciton. The SU lines can be identified by their unique energy and intensity behavior.

The X^+ SU transition intensity can be evaluated from time dependent perturbation theory. We note that a rigorous theory was employed only to the case of a 2DEG [8]. But even a sketchy perturbative description is sufficient to point to the uniqueness of this process relative to common recombination processes. We first consider a hole weakly bound to an exciton, and assume an adiabatic process. At $t < 0$ the Hamiltonian of the hole is $H_i = H_h + V_{sh}(t)$, where H_h is the LL term, $H_h|n\rangle = (n+1/2)\hbar\omega_c^h|n\rangle$, and $V_{sh}(t)$ is the hole-exciton interaction, which can be considered as a perturbation at large magnetic fields. At $t > 0$ the exciton is annihilated and the hole occupies a Landau level; $H_f = H_h$. The intensity of the process is then proportional to the matrix element of the perturbation using the eigen-states of H_h

$$I_{SU_n} \sim \frac{|\langle \psi_h^0(t < 0) | V_{sh} | \psi_h^0(t > 0) \rangle|^2}{|\varepsilon_h(t < 0) - \varepsilon_h(t > 0)|^2} = \frac{|\langle 0 | V_{sh} | n \rangle|^2}{|n\hbar\omega_c^h|^2}$$

The hole wavefunction at $t < 0$, can be approximated to first order to be the $n=0$ LL. The hole final state is in an excited LL, $|n\rangle$, with energy difference equals $n\hbar\omega_c^h$. Note that the expression for I_{SU_n} is still partially implicit; we have to assess the matrix element.

In fact, a sudden approximation is more appropriate for the SU process. The turn-off of the potential is a sudden event relative to the characteristic rate involved with the inter LL excitation energy, $\hbar\omega_c \sim 1\text{meV}$, of a few 1/ps. In the case of a sudden perturbation, the

initial state of the hole $|g.s.\rangle$ has no time to evolve, and the matrix element for the SU_n process is given by its projection on the final states of the free hole, $|n\rangle$,

$$I_{SU_n} \sim \frac{|\langle g.s. | n \rangle|^2}{(n\hbar\omega_c^h)^2}$$

This form of the X^+ SU intensity has two consequences: first, the intensity of the SU decreases with magnetic field because the energy difference in the denominator grows. Second, the higher is the LL index n , the weaker is the intensity. The suppression of high index SU process comes both from the denominator, $1/n^2$ dependence, and the numerator since the ground state $|g.s.\rangle$ is dominant by the $n=0$ LL, with some mixing with higher levels due to the binding potential. These effects were observed and reported in the paper. The assignment of the X^+ SU was supported by results obtained in the same measurement from the D^0h recombination spectrum. The hole binding energy to the D^0 of 0.2meV is smaller than the cyclotron energy of free holes at high fields (~ 1 meV). Thus, the donor site can be viewed as pinning the *guiding center* of the free-hole cyclotron motion. Note that in the case of a dense 2DHG, where free holes recombine with free photo-excited electrons the Landau fan of the holes is not observed. This is because the negligible occupation of higher conduction band LLs (since $\hbar\omega_c^e \gg k_B T$). Recombination selection rules do not allow the $n_e=0$ electron to recombine with holes at higher LLs. Hence, the only recombination line that is observed is of the $n_e=0$ and $n_h=0$. The electron in the D^0h on the other hand is localized. This breaks the restriction from LL selection rules and allows the recombination with holes at high LLs.

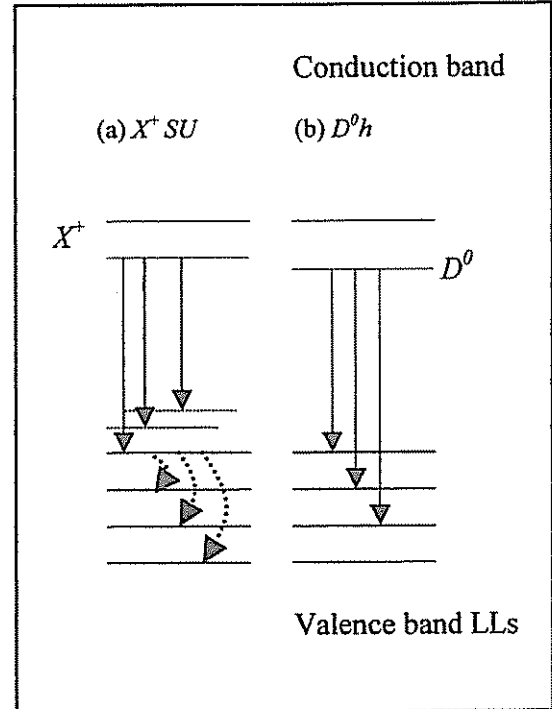


Fig. 3.2 Schematic representation of the interband transitions in the X^+ and D^0h .

The transition schemes of the X^+ SU and the D^0h are plotted in Figure 3.2. In (a) the X^+ interband transition is escorted by excitation of the remaining hole to a higher valance Landau-level. The emitted photon has consequently a reduced energy

$$E_{\text{photon}} \approx E_{X^+} - (n+1/2)\hbar\omega_c^h$$

At a field of several Tesla the cyclotron energy becomes comparable to the second hole binding energy, so the superposition of the lowest Landau level and the second orbital is very marginally perturbed by the exciton potential [9]. As a result the shift in the photon energy reflects exactly the inter Landau-level spacing.

Figure 3.2 (b) shows the transitions of the D^0h . Here the interpretation of the spectra is straightforward. The emitted photon shows the regular Landau energy fan, relative to the D^0 energy,

$$E_{\text{photon}} = E_{D^0} + (n+1/2)\hbar\omega_c^h.$$

The two last Eqs. predict that the emitted photon energy differences would both yield the hole cyclotron energy. Indeed the analysis in the paper gives that result. A constant cyclotron mass of $0.6m_0$ is deduced. We find that the cyclotron mass is rather field independent. This results somewhat differs than these from numerical calculations of the LL dispersion, that finds increased non-linearity with level index [10]. The mass is also heavier than that usually assumed for wide QWs (of ~ 0.2 to $0.3 m_0$), and is closer to that of heterostructures [11].

References

1. L. V. Butov *et al.* Phys. Rev. B **49**, 14054 (1994); We note that this doublet and the $X-X^+$ doublet are similar at low densities, being a source of uncertainty in spectra interpretation at fractional filling factors; A. G. Davies *et al.* Phys. Rev. B **51**, 7357 (1995)
2. H. A. Bethe and E. E. Slapeter, “ Quantum mechanics of one and two-electron atoms”, p. 154, Springer Verlag (1957)
3. L. E. Oliveira and G. D. Mahan, Phys. Rev. B **47**, 2406 (1993); L. E. Oliveira, Phys. Rev. B **38**, 2406 (1988); X. Liu, Phys. Rev. B **38**, 8522 (1988); R. L. Greene, Phys. Rev. B **31**, 913 (1985)
4. L. V. Butov, V. I. Grinev, V. D. Kulakovskii and T. G. Anderson, Phys. Rev. B **46**, 13627 (1992)
5. K. J. Nash *et al.* Phys. Rev. Lett. **70**, 3115 (1993)
6. G. Finkelstein, H. Shtrikman and I. Bar-Joseph, Phys. Rev. B **53**, 12593 (1996)
7. K. Kheng, K. Saminadayar and N. Magnea, Physica **E2**, 256 (1998)
8. P. Hawrylak, Phys. Rev. B **42**, 8986 (1990)
9. M. Bugajski, W. Kuszko and K. Reginski, Solid State Comm. **60**, 669 (1986)
10. S. -R. Eric Yang, D. A. Broido, and L. J. Sham, Phys. Rev. B **32**, 6630 (1985)
11. H. L. Stormer, et al . Phys. Rev. Lett. **53**, 126 (1983)

Photoluminescence of a low-density two-dimensional hole gas in a GaAs quantum well: Observation of valence-band Landau levels

S. Glasberg, H. Shtrikman, and I. Bar-Joseph

Department of Condensed Matter Physics, The Weizmann Institute of Science, Rehovot 76100, Israel

(Received 24 December 2000; published 4 May 2001)

We study the low-energy tail of the photoluminescence spectrum of a low-density two-dimensional hole gas in a magnetic field in a GaAs quantum well. A rich spectrum of lines is observed, and we show that it can be classified into two groups: the shake-up lines of the positively charged exciton (X^+), and the recombination lines of a free hole with an electron bound to a donor (D^0h). An analysis of these transitions reveals a simple picture of equidistant hole Landau levels, with a cyclotron mass of $0.6m_0$.

DOI: 10.1103/PhysRevB.63.201308

PACS number(s): 71.35.Ji, 78.66.Fd, 78.55.-m, 78.66.-w

Photoluminescence (PL) spectroscopy of GaAs quantum wells (QW's) subjected to a magnetic field normal to the layers has proven to be very effective in providing information on the conduction band electrons, but much less so for the valence band holes. QW samples containing a two-dimensional electron gas (2DEG) exhibit a rich spectrum that manifests primarily the electron Landau levels (LL's).¹ On the other hand, the PL spectrum of QW samples containing a two-dimensional hole gas (2DHG) is featureless and is characterized by two broad lines, associated with the Zeeman split levels.² The major reason is the large difference in effective mass between the electron and hole in GaAs heterostructures, which is manifested in cyclotron energies that differ by nearly an order of magnitude, 1.7 meV/T and 0.2 meV/T for the electron and hole, respectively.^{3,4} Thus, at low temperatures the photo-excited holes occupy several LL's while the photo-excited electrons reside mainly at the lowest LL. As a consequence, in 2DEG samples one observes transitions from all occupied conduction band LL's. On the other hand, 2DHG transition is allowed only to the lowest hole LL.

This inability to observe the hole spectrum in a magnetic field has significantly limited the use of PL measurements as a characterization tool of the valence band in a magnetic field. In this paper we show that this limitation can be lifted when examining the low energy tail of the PL spectrum of a low-density 2DHG. We identify two groups of recombination lines, each consisting of several equidistant peaks that are directly related to the valence band LL's. The first is the shake-up recombination lines of the positively charged exciton, X^+ . The other set of equidistant lines is related to a recombination of a free hole with an electron bound to a donor, D^0h . The important property of these two types of transitions is that they do not depend on occupation of higher electron LL's, and hence eliminate the electron contribution to the transition energies and provide direct information on the hole spectrum in a magnetic field.

Traditionally, 2DHG is obtained by introducing a layer of acceptors at a distance of a few tens of nanometers away from the GaAs/ $\text{Al}_x\text{Ga}_{1-x}\text{As}$ heterostructure. This technique, known as modulation doping, suppresses carriers scattering off the impurities and gives excellent transport properties. However, the introduction of acceptors into the structure gives rise to broadening of the PL lines, with a typical width of a few tenths of a meV. The dashed line in Fig. 1 shows a

typical PL spectrum of a modulation-doped GaAs/ $\text{Al}_x\text{Ga}_{1-x}\text{As}$ single quantum well (QW) containing a low density of 2DHG. The neutral and positively charged exciton, which characterize the spectrum at this density range, can be resolved.^{5,6} However, it is seen that the broadening is large, comparable with their energy separation. An alternative method to create an excess density of holes in the well is using optical excitation.^{7,8} The mechanism is rather simple: photo-excited electrons tunnel to the surface and leave behind the holes trapped in the well. This method eliminates the broadening introduced by the acceptors and gives much sharper PL lines. The solid curve in Fig. 1 shows the PL spectrum obtained from an optically excited 2DHG. It is evident that the lines are significantly narrower and better resolved using this method.⁹

Several nominally undoped single-QW samples were studied, all exhibiting the same qualitative behavior. Data will be shown for a particular sample. It consists of a buffer superlattice followed by a 20 nm GaAs well, a 125 nm $\text{Al}_{0.37}\text{Ga}_{0.63}\text{As}$ layer, and 15 nm of GaAs cap layer. The sample was grown on a 100 oriented semi-insulating GaAs substrate. Under very weak excitation $<10 \mu\text{W}/\text{cm}^2$ the observed spectrum is of neutral exciton, indicating that the well is nearly empty of carriers. However, when illuminating it with a higher intensity Ti:S laser at 780 nm we observe the

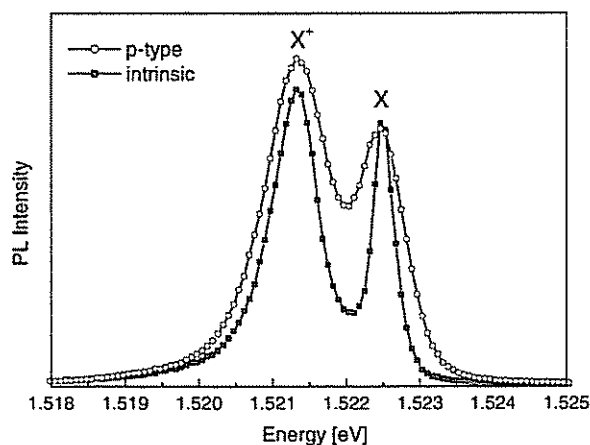


FIG. 1. The PL spectrum from two single-QW samples of 20 nm width showing the X and X^+ doublet; one sample is modulation-doped and the other is intrinsic.

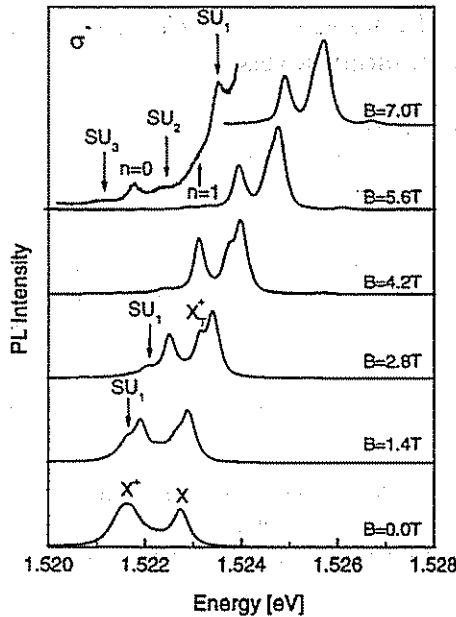


FIG. 2. The evolution of the PL spectrum with magnetic field. The tail of the spectrum taken at 7 T is magnified to show the faint peaks.

appearance of an X^+ line in the spectrum, indicating the existence of a low density 2DHG in the well. We have previously shown that the hole density can be tuned over a broad range by changing the light intensity.⁷ The PL measurements are conducted in a 7 T immersion cryostat at an ambient temperature of 3.5 K. The PL is collected through a birefringence free optical window and analyzed through a circular polarizer. The signal is dispersed in a 0.75 m spectrometer and detected in a cooled CCD detector.

Let us now present the data that sets the basis of this paper. Figure 2 shows the evolution of the X and X^+ doublet in a magnetic field for a σ^- circularly polarized PL (a similar behavior is observed for the σ^+ circular polarization). It is seen that the X and X^+ lines shift to higher energies (diamagnetic shift), and that a new line, X_T^+ , the triplet state of the X^+ , appears close to the X line.⁷ We would like to focus in this paper on the series of weak peaks, which appear at the low energy tail when a magnetic field is applied. Most of these lines are too faint to be observed on the same intensity scale, so they are magnified in the spectrum taken at 7 T. The body of this paper is devoted to the classification and identification of these lines.

Figure 3 summarizes the energy position of the recombination lines in a magnetic field. At high magnetic fields the spectrum is highly complicated as lines cross each other and a careful analysis that relies on their dispersion in a magnetic field, polarization, and intensity, is done in order to give an unambiguous identification. We find that we can divide the observed lines into two groups according to the energy to which they extrapolate at zero magnetic field. In Fig. 3(a) we show all the lines that extrapolate to the X^+ energy at zero magnetic field, 1.5216 eV, and in Fig. 3(b) the lines that extrapolate to an energy that is lower by 1.8 meV. We note that a moderate and even negative energy slope characterizes

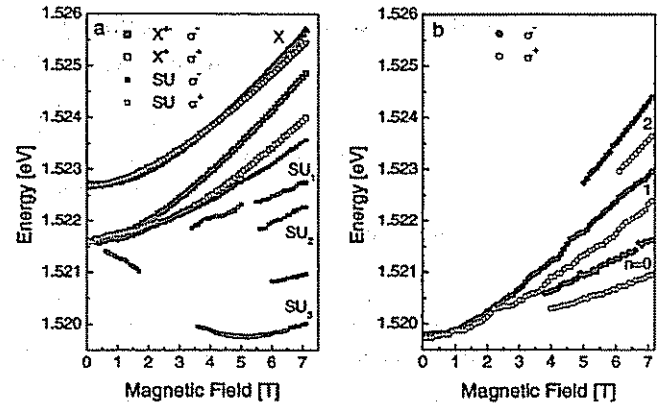


FIG. 3. The energy position of the recombination lines as a function of magnetic field. (a) X , X^+ , and the SU_n lines. (b) The D^0h lines.

the lines in Fig. 3(a). The second group exhibits a much stronger dispersion and it is seen that the slope of the higher energy lines is larger than that of the low energy ones.

We shall show that the first group of lines, which we label as SU_n , is due to a shake-up process of a hole during the X^+ recombination [Fig. 3(a)]. Shake-up lines of the negatively charged exciton X^- , in a magnetic field were previously reported.¹⁰ They are formed when the recombination of an electron with a hole creates an inter-Landau-level (LL) excitation. In the case of the X^- the final state of the remaining electron is at a high ($n \neq 0$) conduction band LL. In analogy, the final state of the hole that remains after the X^+ recombination is at a high valence band LL. Thus the energy of the emitted photon is reduced by the amount of energy taken by that hole, $n\hbar\omega_c^h$, where ω_c^h is the hole cyclotron frequency and n is the LL index. Consequently, when a magnetic field is applied a sequence of shake-up lines should appear below the X^+ , with an energy

$$E_n = E(X^+) - n\hbar\omega_c^h, \quad (1)$$

where $E(X^+)$ is the X^+ energy.

The second group of low energy lines will be shown to be related to a recombination of a neutral donor and a hole, D^0h . The binding energy of the hole at the ground state of the D^0h complex is very small, less than 0.2 meV, hence it can be considered as nearly free. The electron, on the other hand, is tightly bound to the donor with a binding energy larger than that of the free exciton, hence the recombination line of this complex appears a few meV below the exciton line.¹¹ In a magnetic field the energy spectrum of the free hole consists of equally spaced LL's. When these levels become occupied we should obtain a sequence of recombination lines with energies

$$E_n = E(D^0h) + n\hbar\omega_c^h, \quad (2)$$

where $E(D^0h)$ is the emission energy at the ground state [Fig. 3(b)].

The discussion above implies that both recombination processes give rise to a series of equally spaced emission lines with an energy spacing of $\hbar\omega_c^h$ between them. How-

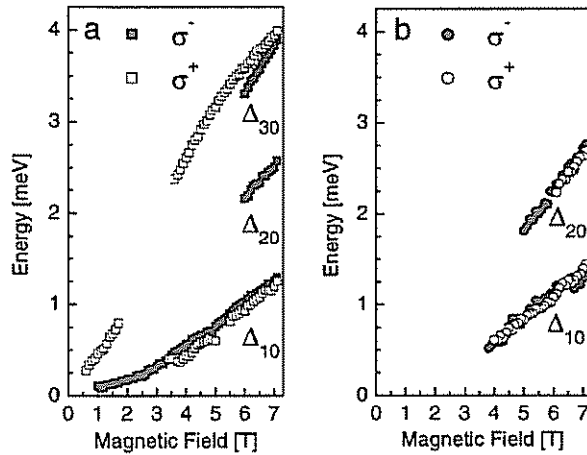


FIG. 4. The energy differences between (a) the X^+ line and the SU_n lines and (b) the D^0h lines.

ever, their evolution in a magnetic field is different. The SU_n lines emerge from the X^+ line and their energy becomes lower with increasing magnetic field. The D^0h lines, on the other hand, emerge from the main D^0h line and evolve to higher energies with increasing magnetic field, like regular LL's. In the following we study the energy dependence of the two groups and prove these assignments.

In Fig. 4(a) we plot the energy difference Δ_{n0} between the X^+ line and the n th shake-up line at the same circular polarization. A few observations can be made. First, the lines come in Zeeman pairs, one at each circular polarization. We notice that the energy differences are nearly the same at both polarizations, hence we can factor out the Zeeman energy. The second observation is that all energy differences increase monotonically with the magnetic field and extrapolate to zero at zero field. This implies that the SU_n lines indeed emerge from the main X^+ line. Finally, we note that at the high field regime $\Delta_{20} \approx 2\Delta_{10}$ and $\Delta_{30} \approx 3\Delta_{10}$, or in other words, $E_n \approx E(X^+) - n\Delta_{10}$. This behavior can be taken as a proof that this series of lines are due to shake-up processes with $\Delta_{10} \approx \hbar\omega_c^h$. Strong supporting evidence comes from the dependence of the intensity of the SU_n lines on the magnetic field. We observe that the intensity of the lines decreases with magnetic field and with the LL index n . For example, the intensity of the SU_1 line, which is clearly observed at low magnetic fields (Fig. 2), decreases by a factor of ~ 100 at the highest magnetic field. Figure 2 also demonstrates the dependence on LL index: at 7 T there is an order of magnitude decrease from SU_1 to SU_2 , and SU_3 is hardly visible. This behavior is contrary to that expected if these lines would have been due to a direct recombination process, which in that case the intensity of the lines should have increased as their energy gets lower, due to straightforward thermal equilibrium arguments. On the other hand, the observed behavior is consistent with a shake-up origin. From perturbation theory arguments the intensity of a SU_n line is proportional to $|\langle gs|n \rangle|^2 (n\hbar\omega_c^h)^{-2}$, where $|gs\rangle$ is the ground-state wave function of the hole in the X^+ , and $|n\rangle$ is the wave function of the n th valence LL. It is readily seen from the explicit dependence on ω_c^h that the intensity of the shake-up lines

should indeed fall with magnetic field. Furthermore, since at high magnetic fields the main contribution to $|gs\rangle$ comes from the lowest LL, the overlap integral $|\langle gs|n \rangle|$ should decrease with increasing n .

We turn our attention now to the D^0h spectrum. To begin with, we confirm that the lines in Fig. 3(b) are related to recombination within the QW. This conclusion is based on the fact that the recombination energy at zero field (1.5198 meV) is above that seen from the bulk GaAs buffer (1.518 meV), practically ruling out the only other candidate layer in the sample. We also notice that the D^0h lines appear at the spectrum only in the presence of a low-density 2DHG, similar to the X^+ line. As the hole density is reduced and the PL spectrum is dominated by the neutral exciton they both disappear. These two observations are consistent with the D^0h assignment. However, the main clue to the identification of these lines comes from comparison with the SU_n transitions. In Fig. 4(b) we show the energy difference Δ_{n0} between the D^0h lines at the same circular polarization. The same general behavior that is seen at the SU_n lines is observed here. Namely, the energy differences are similar in both polarizations; the energy dispersion is linear in the magnetic field; and $\Delta_{10} = \Delta_{21}$. More importantly, the energy differences at the high magnetic field limit are exactly the same as those measured for the shake-up lines, $\Delta(D^0h) = \Delta(SU)$.

The system of an ionized donor D^+ and an electron-hole pair has two distinct bound states: the D^+X , an exciton bound to an ionized donor, and the D^0h , a neutral donor bound to a hole. It can be shown from simple arguments that the binding energy of the electron-hole pair to the donor is larger in the D^0h than in the D^+X .^{12,13} Experimental findings and theoretical modeling show that the D^0h is indeed the lowest donor bound recombination line, 3 meV below the free exciton line,^{11,13} in agreement with our observations. The D^+X is 1 meV higher in energy, and at 3.5 K its occupation is lower by a factor of 30. This allows us to unambiguously assign the observed series of lines with the D^0h .

The SU_n and D^0h spectra allow us to obtain the energy difference between the various LL's, and hence the value of the heavy-hole cyclotron mass of these levels, using $m_h = eB/\omega_c^h$. We obtain from both spectra a cyclotron mass of $m_h = 0.6m_0$. This value is in good agreement with the heavy-hole cyclotron mass in GaAs heterostructures reported in Refs. 4 and 14. Note, however, that the resulting mass is heavier than that found in transport experiments. Similarly, we can extract accurately the heavy-hole Lande factor, g_h , by taking the Zeeman splitting between lines related to the same LL. We obtain $g_h = 2.05$, independent of the magnetic field strength. This value is also in good agreement with previous reports.¹⁵

Finally, the dispersion of the D^0h lines in the magnetic field allows us to estimate the small binding energy of the hole in the D^0h . Approximating the weak neutral donor potential acting on the hole by a parabolic potential, the energies of the hole in a magnetic field are given by $E_n = E_0(D^0h) + (2n+1)\hbar[\omega_0^2 + (\omega_c^h/2)^2]^{1/2}$, where $E_0(D^0h)$ is the energy at zero magnetic field, $\hbar\omega_0$ is the harmonic potential energy, and $n=0,1,2,\dots$. The D^0h lines in Fig. 3(b)

indeed exhibit a parabolic behavior at low field and become linear above 2 T. Taking the hole mass to be $0.6m_0$, and assuming the transition from parabolic to linear dispersion occurs when the two terms in the square brackets are approximately equal, one obtains a hole binding energy of <0.2 meV. This low binding energy is consistent with our assumption of the holes in the D^0h as nearly free.

In conclusion, our work is the first observation of the X^+ shake-up lines in a magnetic field. It also gives a deep insight into the behavior of the D^0h in a magnetic field. We have shown that the observation of valence band Landau levels in

the shake-up and D^0h spectrum allows us to extract the cyclotron hole mass and its g factor. These parameters were not readily available from optical measurements before. We believe that these results are important in view of the recent growing interest in the physics of low density 2DHG. They also emphasize the value of the technique of optically exciting a hole gas. The sharp PL lines that are obtained allow us to conduct spectroscopic measurements with high energy resolution, unattained with doped samples.

This research was supported by the Minerva Foundation.

-
- ¹I. V. Kukushkin and V. B. Timofeev, *Adv. Phys.* **45**, 147 (1996).
 - ²L. V. Butov, A. Zrenner, M. Shayegan, G. Abstreiter, and H. C. Manoharan, *Phys. Rev. B* **49**, 14 054 (1994); O. V. Volkov *et al.*, *ibid.* **56**, 7541 (1997).
 - ³S. Adachi, *J. Appl. Phys.* **58**, R1 (1985).
 - ⁴H. L. Stormer, Z. Schlezinger, A. Chang, D. C. Tsui, A. C. Gosard, and W. Wiegmann, *Phys. Rev. Lett.* **53**, 126 (1983).
 - ⁵G. Finkelstein, H. Shtrikman, and I. Bar-Joseph, *Phys. Rev. B* **53**, R1709 (1996).
 - ⁶Y. V. Ponomarev, A. Usher, P. J. Rodegers, B. L. Gallagher, M. Henini, and G. Hill, *Phys. Rev. B* **54**, 13 891 (1996).
 - ⁷S. Glasberg, G. Finkelstein, H. Shtrikman, and I. Bar-Joseph, *Phys. Rev. B* **59**, R10 425 (1999).
 - ⁸O. V. Volkov, I. V. Kukushkin, K. von Klitzing, and K. Ebrel, *Pis'ma Zh. Eksp. Teor. Fiz.* **68**, 223 (1998) [*JETP Lett.* **68**, 236 (1998)].
 - ⁹We have verified that this is indeed a spectrum of X^+ by observing its distinct evolution in a magnetic field.
 - ¹⁰G. Finkelstein, H. Shtrikman, and I. Bar-Joseph, *Phys. Rev. B* **53**, 12 593 (1996).
 - ¹¹R. L. Greene and K. K. Bajaj, *Phys. Rev. B* **31**, 913 (1985); X. Liu, A. Petrou, B. D. McCombe, J. Ralston, and G. Wicks, *ibid.* **38**, 8522 (1988).
 - ¹²G. Bastard, *Wave Mechanics Applied to Heterostructures* (Les Editions de Physique, Paris, 1988).
 - ¹³L. E. Oliveira and G. D. Mahan, *Phys. Rev. B* **47**, 2406 (1993); L. E. Oliveira, *ibid.* **38**, 2406 (1988).
 - ¹⁴M. Kozhevnikov, E. Cohe, A. Ron, and H. Shtrikman, *Phys. Rev. B* **60**, 16 885 (1999).
 - ¹⁵V. F. Sapega, M. Cardona, K. Ploog, E. I. Ivchenko, and D. N. Mirlin, *Phys. Rev. B* **45**, 4320 (1992).

2.4 The neutral and charged excitons in a parallel magnetic field

S. Glasberg, H. Shtrikman, P. C. Klipstein and I. Bar-Joseph

Exciton exchange splitting in wide GaAs quantum wells

Phys. Rev. B **60**, Rapid Comm. P. 16295 (1999)

We show that subtle information about spin dependent interactions in the neutral excitons is obtained when the magnetic field is applied parallel to the 2D layer. We develop a rigorous model that is applied to the neutral and charged excitons in parallel magnetic field. We report the measurements and modeling of the exciton exchange splitting, and of the Luttinger parameter which appears in the cubic term of the valence band Zeeman Hamiltonian. The spectroscopy of charged excitons in a parallel field emphasizes the role of their spatial structure. It indicates the reshape of the wave function into an oval form elongated along the magnetic field axis.

When the magnetic field is applied parallel to the QW plan, one observes three main modifications of the PL spectrum with respect to that in a perpendicular field: (i) the absence of Landau levels, (ii) the absence of the heavy-hole Zeeman splitting, and (iii) linearly polarized recombination lines (instead of circularly polarized ones). As long as the classical diameter $2R_c$ is larger than the well width, L_z , the QW potential determines the carrier properties along the growth direction. Hence, the cyclotron motion is suppressed by the QW potential, up to high magnetic fields. We illustrate this point in Fig 4.1(a). The absence of cyclotron motion in parallel field is demonstrated in Fig. 4.1(b), where the shift of the exciton recombination energy as a function of magnetic field is plotted for perpendicular and parallel fields. The behavior in a parallel field is well described by a purely parabolic function, $E = \alpha \cdot B^2$. Taking $R_y = 5 \text{ meV}$ for a 22nm QW [1] we obtain the coefficient $\alpha = 0.077$. Similar behavior is observed in Fig 4.1b for low perpendicular magnetic fields, known as the exciton diamagnetic shift [2, 3]. On the other

hand, in a perpendicular field already above 4T the exciton energy shift contains a dominant linear term.

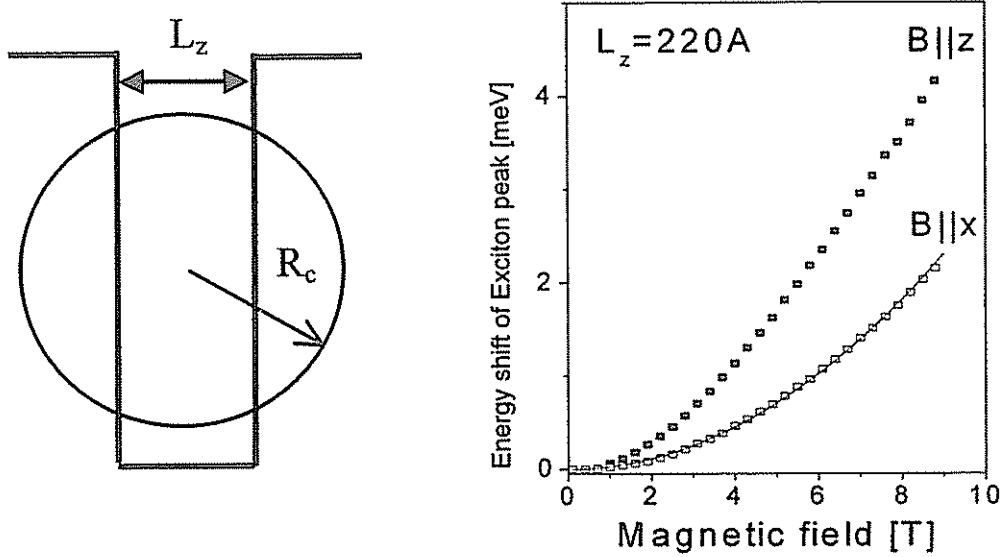


Fig. 4.1. (a) Illustration of the relative width of the magnetic motion versus the QW potential. (b) The exciton energy shift in parallel (fitted with parabola) and perpendicular magnetic fields.

Let us move to discuss the absence of heavy-hole Zeeman splitting. It is easy to see why in a parallel field this splitting vanishes: $H_{Zeeman} = -g_h^{\parallel} \mu_B B J_x = -0.5 g_h^{\parallel} \mu_B B (J_+ + J_-)$, but the heavy-hole eigenstates of $|J_z = \pm \frac{3}{2}\rangle$ satisfy

$$\langle \pm \frac{3}{2} | J_{\pm} | \pm \frac{3}{2} \rangle = 0$$

which results in the absence of this leading term in the spin Hamiltonian.

Finally, we consider the third observation, of the PL emission lines being linearly polarized. To formulate this, we start with the QW electron and hole eigenstates, which are $|\pm \frac{3}{2}\rangle$ and $|\pm \frac{1}{2}\rangle$ respectively, and are quantized along the growth direction. These

functions have spatial and spin parts and are given by: $|+\frac{1}{2}\rangle = i|s\rangle\uparrow$, $|-\frac{1}{2}\rangle = i|s\rangle\downarrow$,

$\left|+\frac{3}{2}\right\rangle = i|X+iY\rangle\uparrow$, $\left|-\frac{3}{2}\right\rangle = i|X-iY\rangle\downarrow$ [1]. In a parallel field, the diagonalization of the Zeeman Hamiltonian gives new heavy-hole and electron eigenstates, which are the superposition of the QW eigenstates (with $B\parallel x$)

$$|\pm\rangle_x^h = \frac{1}{\sqrt{2}}(|\frac{3}{2}\rangle \pm |-\frac{3}{2}\rangle)$$

$$|\pm\rangle_x^e = \frac{1}{\sqrt{2}}(|\frac{1}{2}\rangle \pm |-\frac{1}{2}\rangle)$$

We then define the exciton pair states ($|\pm\rangle_x^h$, $|\pm\rangle_x^e$). The calculation of the exciton oscillator strength is done using the dipole approximation, similarly to the calculation of the exciton oscillator strength at zero magnetic field, which uses the QW ($|\pm\frac{3}{2}\rangle_z$, $|\pm\frac{1}{2}\rangle_z$) exciton basis [1]. The linearly polarized PL lines at a parallel field result from the detailed calculation; e. g. the application of the dipole operator $-E_x \frac{\partial}{\partial x} - E_y \frac{\partial}{\partial y}$ on the X and Y spatial parts of the $|\pm\frac{3}{2}\rangle_z$ states. It can easily be shown that the ($|+\rangle_x^h$, $|+\rangle_x^e$) and ($|-\rangle_x^h$, $|-\rangle_x^e$) excitons give x-polarized emission, while the ($|+\rangle_x^h$, $|-\rangle_x^e$) and ($|-\rangle_x^h$, $|+\rangle_x^e$) gives PL polarized along the y direction.

In the absence of the leading terms (i.e. – heavy hole Zeeman energy and cyclotron energy) in the parallel field Hamiltonian, smaller terms, of a magnitude of a few tens of μeV , are manifested in the PL spectrum. These are the electron-hole exchange interaction and the heavy-hole cubic Zeeman term. Note that these small terms should be observed through their effects on spectroscopic features on the scale of few hundred of μeV , the characteristic size of the recombination line-width. Hence, the high quality intrinsic samples, with their narrow lines, were crucial for achieving the resolution needed for those measurements.

The main observable we measured was the electron-hole exchange splitting δ in the exciton [4]. The exchange interaction naturally appears when the Coulomb interaction is calculated for fermions, and has a nice phenomenological formulation [5]. Considering the case of two electrons of spin $\frac{1}{2}$. The two-electron four anti-symmetrized states are

composed of three triplet states with $S_T = S_{z1} + S_{z2} = 1$ and one singlet with $S_T = S_{z1} - S_{z2} = 0$. First we note that the eigenvalue of the Coulomb interaction differs between the triplet and singlet eigenstates, approximately by the “exchange” term

$$\langle \psi_1(r_1)\psi_2(r_2) | \frac{e^2}{\rho} | \psi_2(r_1)\psi_1(r_2) \rangle,$$

where ψ_i are the single electron wavefunctions, and $\rho = |\mathbf{r}_e - \mathbf{r}_h|$ (See Ref. 5 for detailed derivation). At the same time, the triplet and singlet eigenstates can be distinguished by the eigenvalues of the operator $2S_{z1}S_{z2} = S_T^2 - (S_{z1}^2 + S_{z2}^2)$,

which gives $3/2$ and $-1/2$, respectively. Thus, the so called triplet-singlet exchange splitting δ can be phenomenologically recovered from a Hamiltonian in the form of $H_{exch} = \delta S_{z1}S_{z2}$. In the case of exciton made of an electron and a heavy-hole the spins are $\frac{1}{2}$ and $\frac{3}{2}$ and the two-particle four anti-symmetrized states are composed of two triplet states with $J_T = S_z + J_z = 2$ and two singlet states with $S_T = |S_z - J_z| = 1$. The exchange splitting δ is phenomenologically presented by a Hamiltonian in the form of $H_{exch} = \frac{1}{2}\delta S_z J_z$. Due to the orthogonality of the hole and electron wavefunctions $\delta \propto \langle \psi_e(r_1)\psi_h(r_2) | \frac{e^2}{\rho} | \psi_h(r_1)\psi_e(r_2) \rangle$ is a small term.

The exchange interaction has important effect on the electron-hole recombination dynamics [6] and on the energy spectrum of confined systems like quantum dots [7]. To put our measurements of the exchange splitting in a wide context we compared theoretical and experimental results of numerous groups. Calculations of the exchange splitting in reduced dimensions (QWs, quantum-wire and quantum dots) predict that its value is enhanced over the bulk semiconductor value by a factor related to dimensionality. As a result, uncertainty in the bulk value translates to increasing

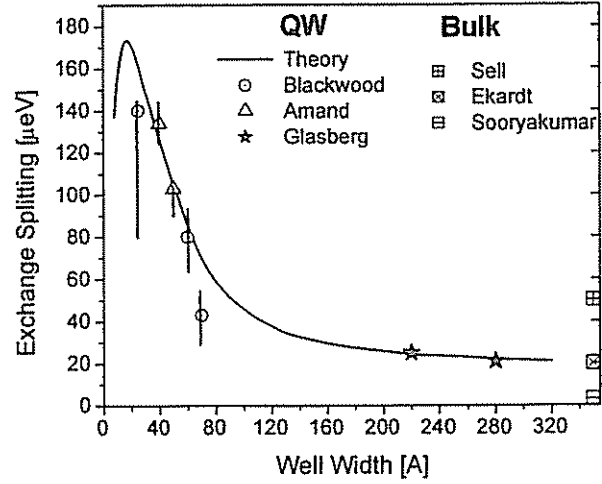


Fig.4.2: Summary of theory and experimental results for the exciton exchange splitting in bulk GaAs and quantum wells.

uncertainty at lower dimension structures. Figure 4.2 demonstrates our contribution in that respect - locking on the asymptotic behavior towards the bulk value.

The second observable we measured was the heavy-hole band cubic Zeeman splitting. The Hamiltonian of this term in a parallel magnetic field is $H_{Zeeman} = -2q\mu_B B_x J_x^3$, with q being the coefficient postulated by Luttinger in his formulation of the valence band Hamiltonian [8]. This term originates from the perturbation of the split-off band, and may be estimated from k·p theory [9]. The split-off band is 0.3eV lower in energy, a value large enough to make its effect on the heavy-hole band small. The bulk GaAs value of q is 0.04. We have measured it for the first time in a QW and found a value of 0.03. This change as a function of the QW confinement may be verified by band-structure calculations. Due to its smallness, the cubic term was overlooked for many years, however, it may have a significant importance in spin precession experiments of photo-excited holes and electrons in a parallel magnetic field [10].

2.4.1 Polarization of the charged excitons in a parallel magnetic field

We have measured the X^+ and X^- PL spectra in a parallel magnetic field. As expected, both complexes showed a linearly polarized spectrum, in directions parallel (x) and perpendicular (y) to the magnetic field. We have found that this PL is becoming increasingly polarized along the magnetic field direction x as the magnetic field is increased. This is illustrated in Figs. 4.3a and 4.3b that show the linearly polarized PL intensities I_x and I_y from the X^+ and X^- at 9T, respectively. The evolution of the X^+ and X^- intensities ratio I_x/I_y as a function of the parallel magnetic field is shown in Fig. 4.4. As seen, the PL from the two complexes develops substantial polarizability along the field direction. We found that the PL of the exciton is also polarized at high fields, but to a lesser extent.

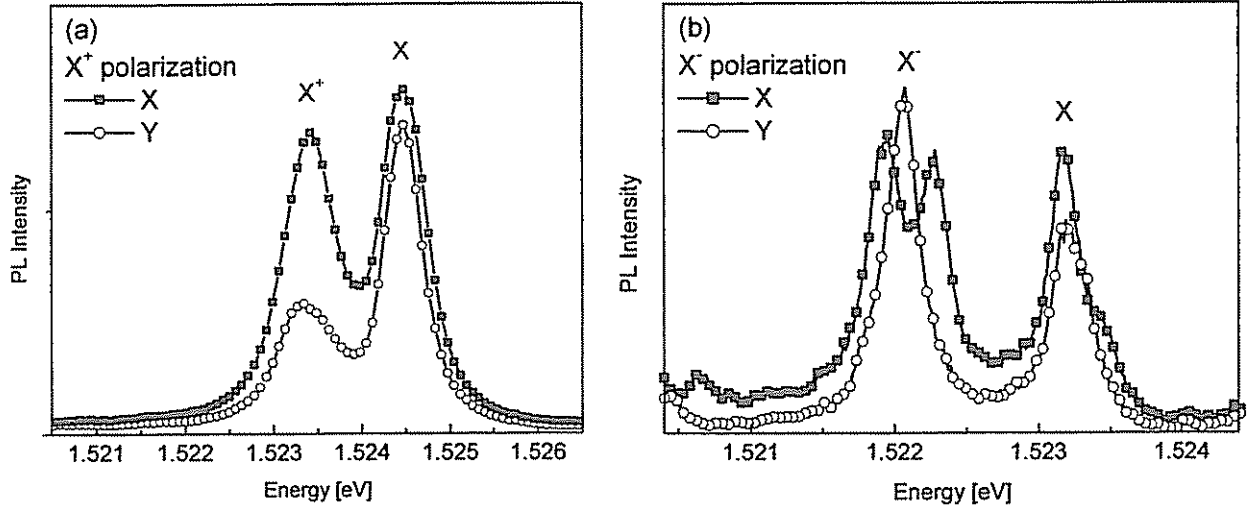


Fig. 4.3: The linearly polarized PL spectrum in a 9T parallel magnetic field along the x direction of the (a) X and X⁺ doublet L_z=22nm (b) X and X⁻ doublet L_z=26nm.

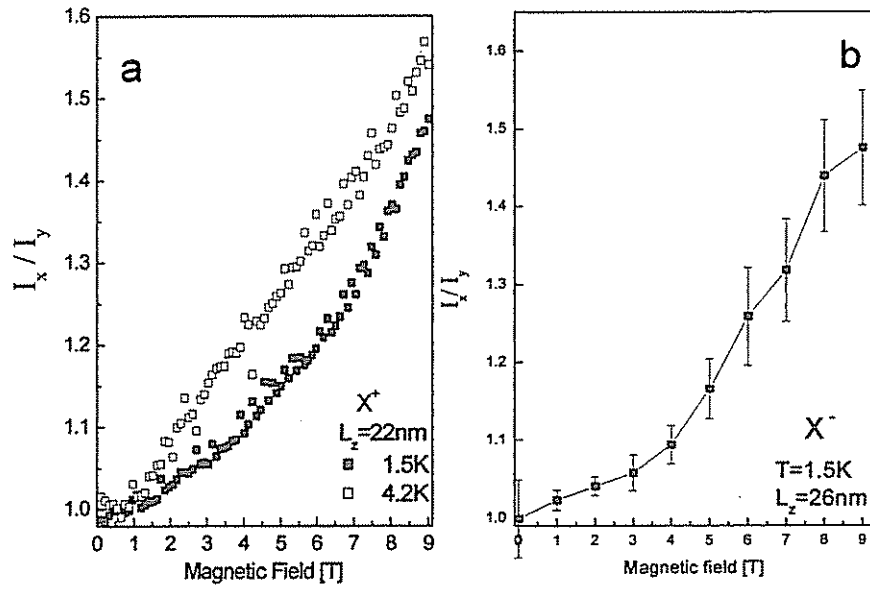


Fig. 4.4: PL intensities ratio in x and y polarization, I_x/I_y , as a function of parallel magnetic field. (a) 22nm QW X⁺ (b) 26nm QW X⁻.

We have measured the behavior of the PL polarizability for different well widths. Fig. 4.5 shows the PL polarization ratio of the X^+ in a 15nm and 22nm QWs. As seen, the polarization is much smaller in the narrower QW.

The observation of an increasing PL polarization along field direction, and its reduction with well-width lead us to suggest that the PL reflects increasing polarization of the charged exciton orbital wavefunction along the field direction. We suggest this effect yields a larger classical dipole $d=er$ along the magnetic field, which is manifested in the x and y radiative transition amplitudes via

$$|\langle c | e\mathbf{r}_x | v \rangle| > |\langle c | e\mathbf{r}_y | v \rangle|, \text{ or } \langle d_x \rangle > \langle d_y \rangle.$$

The attribution of the PL polarizability to the orbital degrees of freedom is supported by several additional observations. First, as Fig. 4.4a shows the effect is relatively insensitive to the temperature. This observation rules out changes in the occupation of *spin* states as the source of increase in the polarization of PL. Second, the exciton is affected less by the field, and only at higher fields. This result is consistent with the exciton smaller Bohr radius.

Further support comes from the dependence of the X^- binding energies upon the parallel field. We have found that the binding energy of the X^- increases by 15% at 9T (Fig. 4.6). No binding of triplet states was observed. In comparison, under

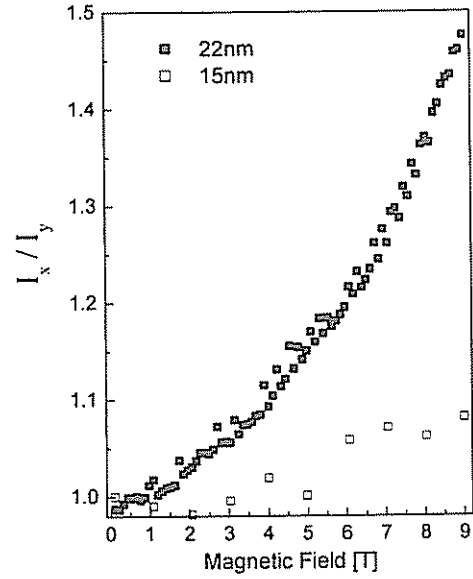


Fig. 4.5: The X^+ PL intensities ratio in x and y polarization, I_x/I_y , as a function of parallel magnetic field, for 15 and 22nm wells.

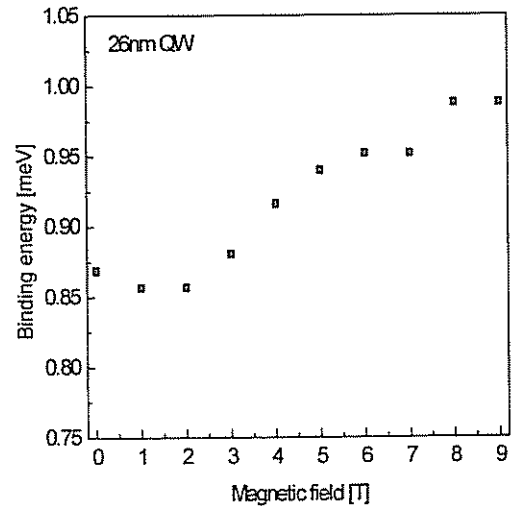


Fig. 4.6: The X^- second electron binding energy as a function of parallel magnetic field for the 26nm QW.

perpendicular field the binding energy of the X^- typically increases by 60% at 9T, and binding of triplet states was observed above $B=1T$ (see chap. 2.2). The weak change in the X^- singlet binding energy and the absence of triplet binding under parallel field are significant. They indicate the dominance of the in-plane degrees of freedom. In the perpendicular geometry, the magnetic confinement potential of $0.5m\omega_c^2 r^2$ is two-dimensional, and quenches the charged exciton Bohr radii to the magnetic length [11]. In parallel geometry the direction along the magnetic field is unaffected.

As theoretical models of the charged excitons become more comprehensive and refined - studying both finite well width and magnetic field effects - we find the observation of increased PL polarization along the magnetic field, and its interpretation as polarization of the charged and neutral excitons wavefunction, an interesting subject for these theories to explore.

Finally we address the Zeeman splitting of the X^- and X^+ - resolved at 9T in Fig. 4.7. As

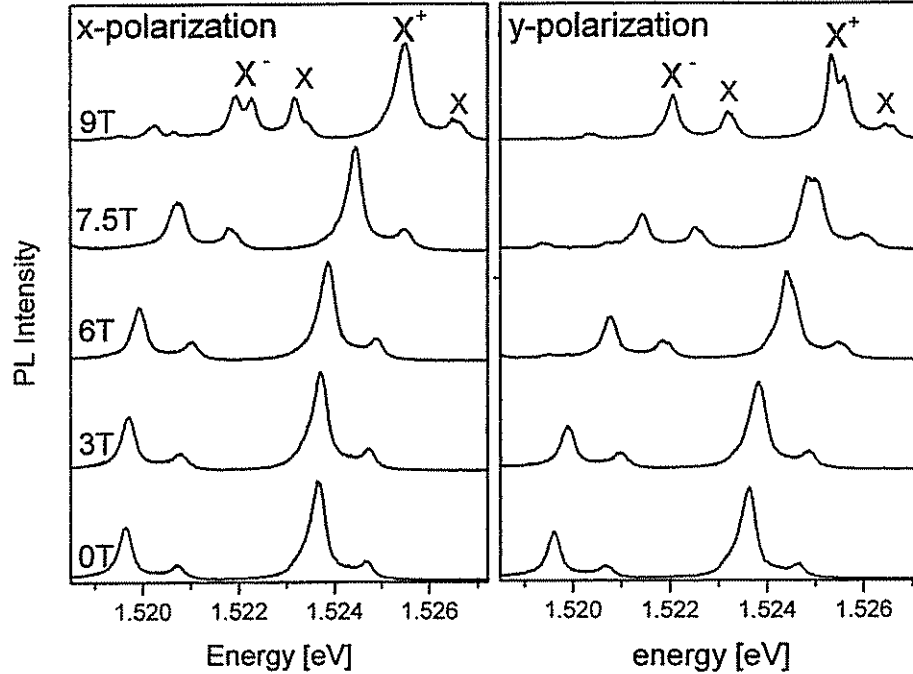


Fig. 4.7: The PL spectra from a DQW at several values of the parallel magnetic field. The wide (26nm) QW shows X^- spectrum, whereas the narrow (15nm) one shows the X^+ spectrum. $T=1.5K$.

seen the X^- PL along x direction, I_x , shows a large Zeeman splitting while the y component, I_y , shows smaller one. In contrast, the X^+ PL intensity I_x shows no splitting and a splitting is observed in I_y (see also Fig. 4.3a). This opposite behavior is surprising in view of the results for the exciton, where the difference in the Zeeman splitting between x and y components gave $\Delta_x - \Delta_y = 6q\mu_B B$ ($\sim 100\mu\text{eV}$ at 9T), with minor corrections to this value that come from mixing terms with the light-hole band. The data in Fig. 4.7 suggests that the difference $\Delta_x - \Delta_y$ *reverses its sign* between the X^- and X^+ . This may indicate of a larger contribution from *hh-lh* band mixing to the Zeeman splitting in charged excitons.

References

1. G. Bastard, "Wave mechanics applied to semiconductor heterostructures", Les Editions de Physique, France, 1988
2. H. Sakaki *et al.* Appl. Phys. Lett. **46**, 83 (1985)
3. K. Oettinger *et al.* Phys. Rev. B **52**, R5531 (1995)
4. L. C. Andreani, f. Bassini and A. Quatropiani, Nuovo Cimento **10D**, 1473 (1998)
5. N. D. Mermin and D. Ashcroft, "Solid State Physics", pp. 676-681, 1976
6. M. Z. Maialle, Phys. Rev. B **61**, 10877 (2000) and refs. therein
7. M. Bayer *et al.*, Phys. Rev. Lett. **82**, 1748 (1999)
8. J. M. Luttinger, Phys. Rev. **102**, 1030 (1956)
9. J. C. Hensel and K. Suzuki, Phys. Rev. Lett. **22**, 838 (1969)
10. J. M. Kikkawa *et al.*, Science **277**, 1284 (1997); J. M. Kikkawa and D. D. Awschalom, Phys. Today **52**, 33 (1999)
11. A. J. Shields *et al.*, Advanc. In Phys. **44**, 47 (1996); D. M. Whittaker and R. J. Elliott, Solid state Comm. **68**, 1(1998)

Exciton exchange splitting in wide GaAs quantum wells

S. Glasberg, H. Shtrikman, and I. Bar-Joseph

Department of Condensed Matter Physics, The Weizmann Institute of Science, Rehovot 76100, Israel

P. C. Klipstein

Clarendon Laboratory, Physics Department, Oxford University, Parks Road, Oxford OX1 3PU, United Kingdom

(Received 6 July 1999; revised manuscript received 15 September 1999)

We determine the exciton exchange splitting in a wide GaAs quantum well. Our method is based on applying a magnetic field parallel to the layers and measuring the oscillator strength ratio of the Zeeman split lines in two linear polarizations. We develop a theoretical model to describe the effect of the magnetic field on the exciton spectrum, and use it to determine the exchange splitting in a 22-nm quantum well to be $22 \pm 3 \mu\text{eV}$. These measurements also allow us to make an accurate determination of the value of $q=0.03$, the Luttinger parameter which appears in the cubic term of the valence band Zeeman Hamiltonian. [S0163-1829(99)51348-9]

The exchange interaction between electrons and holes in semiconductors causes an energy splitting between radiative ($J_{\text{ex}}=1$) and nonradiative ($J_{\text{ex}}=2$) exciton states.¹ This exchange splitting is an important parameter in the spectroscopy of semiconductor heterostructures, especially in the context of exciton dynamics and spin relaxation.² Recently, there has been renewed interest in the subject of electron-hole exchange in the context of quantum dot spectroscopy.³ There is a common distinction in the literature between the short-range and the long-range contributions to the exciton exchange interaction. It has been shown that in a quantum well (QW) the long-range interaction vanishes at $\mathbf{K}=0$ and only the short-range interaction gives rise to a finite energy splitting.⁴ Thus, optical spectroscopy in a QW can give direct access to the short-range exchange interaction.

During the last decade, there have been a few successful measurements of this splitting in GaAs QW's. Early measurements have used optically detected magnetic resonance (ODMR) in type II GaAs/AlAs QW's, yielding values of a few tens of μeV for the exchange splitting.^{5,6} A later measurement in narrow (<10 nm) type I GaAs/Al_xGa_{1-x}As QW's has shown that this splitting is of the order of $100 \mu\text{eV}$.⁷ This measurement was conducted at high magnetic field and studied changes in the photoluminescence (PL) intensity due to crossing of the radiative and the non-radiative exciton states. A subsequent experiment,⁸ based on PL quantum beats in a magnetic field, confirmed the results of Ref. 7.

Theoretical works predict a dependence of the exchange splitting on well width, and it is expected to increase with decreasing well width.^{4,9} Such a trend was reported in Ref. 7, where a substantial increase was observed in the exchange splitting for well widths between 7.3 and 2.5 nm. The purpose of the present work is to determine the exchange splitting in a wide QW, where a convergence towards the bulk value is expected. Unfortunately, all the above techniques cannot be applied to a wide QW. The ODMR technique cannot be used in a type I QW due to the short exciton lifetimes.^{5,6} The level crossing technique⁷ is conducted in a magnetic field normal to the layers (Faraday geometry) and

relies on knowing the heavy-hole (hh) g factor. In wide wells and in this geometry, this parameter is strongly field dependent, and there is a relatively large uncertainty in it. Finally, the quantum beats technique can not be implemented in wide wells due to the fast spin flip of the holes.⁸

The underlying idea of the present work is to apply a magnetic field in a direction parallel to the QW layer (Voigt geometry), and measure the excitonic PL spectrum. Such a magnetic field couples the $J_{\text{ex}}=1$ and $J_{\text{ex}}=2$ excitonic states. As a result, when the magnetic field is increased, the nonradiative states become increasingly radiative at the expense of the radiative states. This behavior can be fully described by a first principles calculation, and is shown to be very sensitive to the value of the exchange splitting. Thus, by fitting the measured dependence of the oscillator strength on magnetic field, one can obtain the value of the exchange splitting with high accuracy. We show that this measurement can also provide the valence band Luttinger parameter q , which gives a Zeeman energy proportional to the cube of the hole angular momentum.¹⁰ This is, to the best of our knowledge, the first determination of the cubic term in a GaAs QW.

The exciton Hamiltonian in a magnetic field parallel to the layers, $\mathbf{B}=\hat{B}\hat{x}$, is written in the form:

$$H_{\text{ex}} = H_0^B + H_e^B - H_h^B + H_{\text{exch}}, \quad (1)$$

where H_0^B is the exciton Coulomb interaction at zero field plus the orbital diamagnetic term, $H_e^B = g_e \mu_B S_x B$ is the conduction electron Zeeman term, $H_h^B = -2\kappa \mu_B J_x B - 2q \mu_B J_x^3 B$ is the valence electron Zeeman term,¹⁰ and $H_{\text{exch}} = \frac{2}{3} \delta \mathbf{S} \cdot \mathbf{J}$ is the electron-hole short-range exchange interaction term. In these, δ is the exchange splitting energy, S_x is the x component of the conduction electron spin operator \mathbf{S} , and J_x is the x component of the valence electron spin operator \mathbf{J} . μ_B is the Bohr magneton, g_e , κ , and q are the conduction and valence electron Zeeman coefficients. In Ref. 5 and subsequent papers on exchange splitting, a valence hole representation was used, whereas here we use a valence

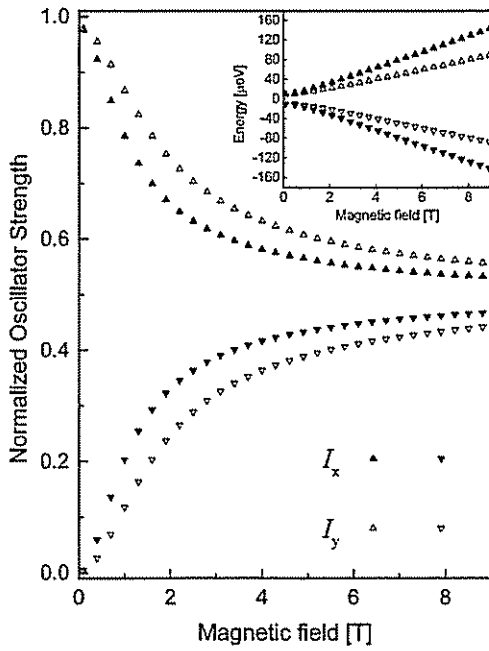


FIG. 1. The hh exciton oscillator strengths, I_x and I_y , calculated from Eq. (2), as a function of magnetic field. The inset shows the corresponding energies. The parameters used are $g_e = -0.44$, $q = 0.04$, and $\delta = 20 \mu\text{eV}$.

electron representation. This is the reason for the negative sign in front of H_h^B . The change of representation does not affect the signs of κ and q .

It is worthwhile to consider initially the case where the valence band is restricted to the heavy-hole (hh) subband alone, i.e., neglect coupling to the light-hole (lh) states. This single hole subband approximation is valid when the energy splitting between the heavy and light holes, Δ , is much larger than the Zeeman coupling energy $\sim \kappa \mu_B B$ between the two subbands. For a 20-nm-wide QW, $\Delta \approx 3 \text{ meV}$ and $\kappa \approx 0.2$,¹¹ hence at 9 T, $\kappa \mu_B B / \Delta$ is ~ 0.03 and the single subband approximation should be adequate. We use the definitions of Ref. 12 for the electron and hole Bloch functions quantized along the growth direction z . Then, by projecting along the magnetic field direction x we define exciton pair states: $(\uparrow_x^h, \uparrow_x^e)$, $(\downarrow_x^h, \downarrow_x^e)$, $(\downarrow_x^h, \uparrow_x^e)$, $(\uparrow_x^h, \downarrow_x^e)$. Here $|\uparrow_x^h\rangle, |\downarrow_x^h\rangle = [3/2 \pm 1/2]^{1/2}$, and $|\uparrow_x^e\rangle, |\downarrow_x^e\rangle = [1/2 \pm 1/2]^{1/2}$. In this basis, the Hamiltonian is separable into two diagonal blocks, $H_x = \frac{1}{2}(\epsilon_x \sigma_z + \delta \sigma_x)$ and $H_y = \frac{1}{2}(\epsilon_y \sigma_z + \delta \sigma_x)$, where $\epsilon_x = \mu_B B(g_e - 3q)$, $\epsilon_y = \mu_B B(g_e + 3q)$, and σ_x, σ_z are the Pauli matrices. In this case, the Hamiltonian can be diagonalized analytically, and the eigenvalues are $E_{x,y} = \pm \frac{1}{2}[\delta^2 + \epsilon_{x,y}^2]^{1/2}$. The exciton oscillator strength can then be calculated through the dipole approximation. We find that in each polarization there are only two transitions with finite oscillator strength, given by

$$I_{x,y} = \frac{(1 + T_{x,y})^2}{2(1 + T_{x,y}^2)}, \quad (2)$$

where $T_{x,y} = -\epsilon_{x,y} / \delta \pm \sqrt{1 + (\epsilon_{x,y} / \delta)^2}$, and the plus and minus signs are for the states which are initially radiative and nonradiative, respectively, in zero magnetic field.

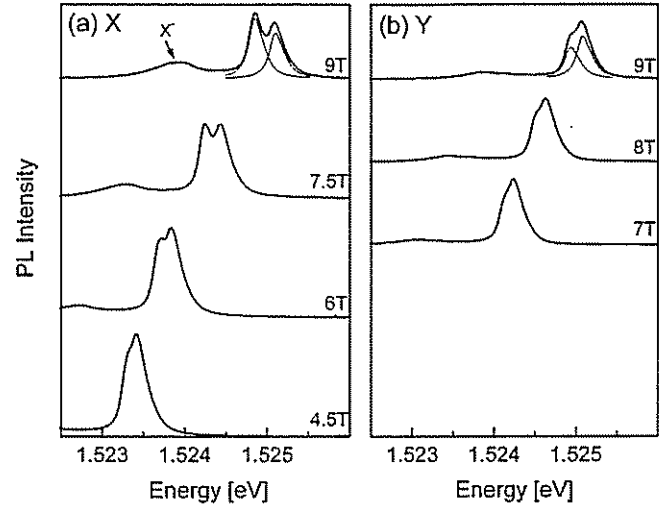


FIG. 2. The evolution with magnetic field of the x and y polarized spectra of the hh exciton in a 22-nm QW. An example of the two line shapes used for the fitting procedure is shown in the figure.

Figure 1 shows the behavior of I_x and I_y as a function of magnetic field. The corresponding eigenenergies are plotted in the inset. The parameters chosen are the bulk values $g_e = -0.44$, $q = 0.04$, and $\delta = 20 \mu\text{eV}$.¹³ Two main features can be observed in Fig. 1. First, there is an increase of oscillator strength with magnetic field of the initially nonradiative states, accompanied by a corresponding decrease of the oscillator strength of the initially radiative states. Second, there is a difference between the x -polarized and the y -polarized curves. This difference is entirely due to the cubic Zeeman term in the hh Hamiltonian. Thus, we can use the difference between the spectra in the two polarizations to determine this parameter.

Let us turn now to the experimental results. Several GaAs QW samples with well widths of 22, 28, and 40 nm were studied, all giving the same qualitative behavior. Extensive quantitative measurements and analysis were performed on the 22-nm sample, which had the smallest linewidth, and the results will be reported here in full. The details of the sample structure are given in Ref. 14. The exciton linewidth was 0.25 meV, allowing us to resolve the Zeeman split lines at moderate fields, $\sim 5 \text{ T}$. The sample was immersed in a liquid helium storage Dewar in a 9-T magnet, and oriented such that the magnetic field direction was parallel to the layers. The temperature was 4.2 K and the He:Ne laser illumination power at a wavelength of 632.8 nm was $100 \mu\text{W}/\text{cm}^2$. The PL was analyzed by sheet linear polarizers and collected by a fiber optic setup. It was then dispersed in a 0.75-m spectrometer and detected in a cooled charge-coupled device detector. The spectral resolution was $20 \mu\text{eV}$.

Figure 2 shows the evolution with magnetic field of the exciton PL spectra in x and y polarizations. The exciton line exhibits a diamagnetic shift and moves to higher energies with increasing magnetic field. It is seen that in both polarizations the spectrum evolves into a doublet, with the splitting being larger in the x polarization. It is particularly apparent that in the x polarization [Fig. 2(a)] the lower energy peak is gaining strength over its higher energy counterpart. Similarly, in the y polarization [Fig. 2(b)], a lower energy

peak is emerging with the increase of magnetic field. This behavior is consistent with the predicted dependence of the oscillator strength and energy, which is depicted in Fig. 1. In order to obtain the relative intensity and energy of each line accurately we performed peak fitting. This was done using the measured zero-field PL line shape (which is slightly asymmetric), varying only its relative intensity and energy position to yield a best fit to the doublet. The small contribution of the peak ~ 1 meV below the exciton lines, which is due to the negatively charged exciton X^- ,¹⁴ was subtracted from the data. An example of the two peaks used for the fitting procedure is shown in the figure. The sum of the two peaks matches almost exactly the measured spectrum and cannot be distinguished from the data in the figure.

In Fig. 3 we show the intensities deduced from the data in the x and y polarizations (filled and open symbols, respectively) as a function of magnetic field. The inset of Fig. 3 shows the corresponding energy splitting for each polarization. Our model predicts that these splittings are given by $[\delta^2 + \epsilon_{x,y}^2]^{1/2}$. Since $\delta \ll \epsilon_{x,y}$ for that field range, we can neglect δ and approximate these splittings by $\sim \mu_B B (g_e \pm 3q)$. The best fit to the data yields $g_e = -0.38$ and $q = 0.03$. The value for g_e is remarkably close to the value determined by PL quantum beats,¹⁵ and that of q is very close to the bulk value.¹³

In order to relate the PL intensities to the oscillator strengths, we have to take into account the Boltzman thermal occupation factors. The ratio between the intensities of two PL lines in a doublet is given by the ratio of their oscillator strengths weighted by these factors. This implicitly requires that the radiating excitonic states are in thermal equilibrium. Indeed, we performed the measurements at 9 T both at 4.2 and 2 K and found the expected scaling. We also measured the integrated PL intensity over a wide temperature range and found that nonradiative recombination does not play any significant role. We note that the absolute intensity of a PL spectrum at a certain magnetic field might depend on the magnetic field strength as well as on other experimental factors. However, we are interested only in the *relative* intensity of the two emission lines in a given field and polarization, and this can be very accurately determined from the measurements. To fit the oscillator strength, we fixed g_e and q at the values obtained from the energy curves and adjusted the

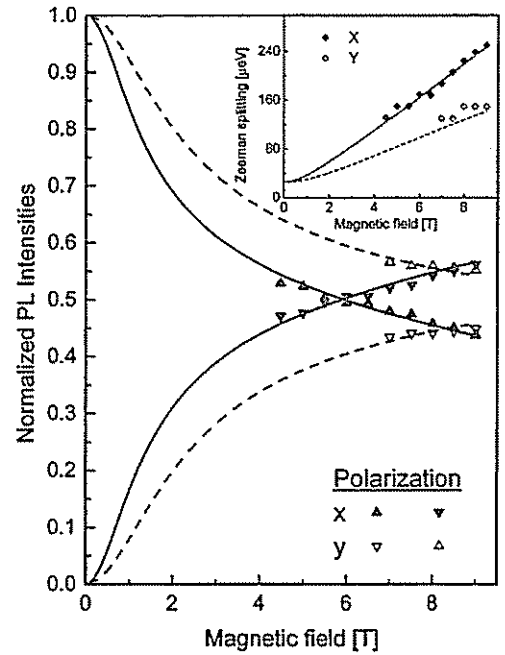


FIG. 3. The relative PL intensity in x and y polarizations as function of magnetic field. The inset shows the energy splittings. Discrete points mark the experimental results obtained from the data shown in Fig. 2. Lines are calculated using Eq. (5) with $g_e = -0.36$, $q = 0.03$, $\kappa = 0.2$, $\delta = 25$ μeV , and $T = 4.2$ K.

value of δ to obtain the best fit. This procedure gives $\delta \approx 30$ μeV . We find that the inclusion of the Boltzman factors reduces the intensities of the higher energy radiative states and reproduces the observed dominance of the low energy line above $B \sim 6$ T. While the general behavior is well described by this simple model, the quality of the fit to the oscillator strengths is not good. The good quality fitted curves shown in Fig. 3 are based on a more elaborate model which will be described below.

To improve the fit we must include the interaction with the lh1 band. This is done by writing a 4×4 matrix for the valence electron Zeeman Hamiltonian in the J_z basis $|3/2\rangle$, $|-3/2\rangle$, $|1/2\rangle$, $|-1/2\rangle$. Thus

$$H_h^B = \begin{pmatrix} 0 & \frac{3}{2}q\mu_B B_x & -\left(\sqrt{3}\kappa + 7\frac{\sqrt{3}}{4}q\right)\mu_B B_x & 0 \\ \frac{3}{2}q\mu_B B_x & 0 & 0 & \left(\sqrt{3}\kappa + 7\frac{\sqrt{3}}{4}q\right)\mu_B B_x \\ -\left(\sqrt{3}\kappa + 7\frac{\sqrt{3}}{4}q\right)\mu_B B_x & 0 & -\Delta & (2\kappa + 5q)\mu_B B_x \\ 0 & \left(\sqrt{3}\kappa + 7\frac{\sqrt{3}}{4}q\right)\mu_B B_x & (2\kappa + 5q)\mu_B B_x & -\Delta \end{pmatrix} \quad (3)$$

where the lh1 band is an energy Δ below the hh1 band ($\Delta > 0$). Equation (3) describes the energies of the hh1 and lh1 subbands close to their respective edges. No explicit dependence on the in-plane wavevector is included because the off-diagonal $k\rho$ terms are negligible for the range of in-plane wave vectors required to construct an exciton.¹⁶ Note also that in deriving H_h^B , the signs of the matrix elements depend on the choice of Bloch basis functions because of phase factors which are introduced when the basis functions are operated on by J^+ or J^- .

It is seen in H_h^B that direct coupling between the $|3/2\rangle$ and $|-3/2\rangle$ hh states is provided by the q dependent terms. On the other hand, the κ dependent term only contributes to coupling between hh and lh states. H_h^B can be diagonalized numerically to find the "hh-like" wave functions, Ψ_{h1} and Ψ_{h2} , and the "lh-like" wave functions Ψ_{h3} and Ψ_{h4} . It may be shown that at low magnetic fields, Ψ_{h1} and Ψ_{h2} approach the $|\uparrow_x^h\rangle$ and $|\downarrow_x^h\rangle$ states used in the analytical model. The Coulomb interaction, H_0^B , mixes plane-wave electron-hole pair states to create $e1$ -hh1 and $e1$ -lh1 excitons with different binding energies.¹⁷ The net effect of H_0^B is thus to change the value of Δ used in Eq. (3) from the difference in the single particle confinement energies to the difference in the observed exciton transition energies. Its variation with field is sufficiently weak for the zero field value ($\Delta = 3.1$ meV) to be used throughout.

Since the exchange splitting is very small compared to Δ , we may restrict the derivation of the exchange Hamiltonian H_{exch} to the pair state spin basis: $(\Psi_{h1}, \uparrow_x^e)$, $(\Psi_{h2}, \downarrow_x^e)$, $(\Psi_{h3}, \uparrow_x^e)$, $(\Psi_{h4}, \downarrow_x^e)$. With all parts of the total Hamiltonian now determined, H_{ex} is finally diagonalized to give the transition energies, E_n , and eigenvectors, Ψ_{ex}^n . In terms of the z -quantized states, the eigenvectors have the form ($n = 1, 2, 3, 4$):

$$\Psi_{\text{ex}}^n = \alpha_n |3/2, \uparrow\rangle + \beta_n |-3/2, \uparrow\rangle + \gamma_n |1/2, \uparrow\rangle + \delta_n |-1/2, \uparrow\rangle + \bar{\alpha}_n |3/2, \downarrow\rangle + \bar{\beta}_n |-3/2, \downarrow\rangle + \bar{\gamma}_n |1/2, \downarrow\rangle + \bar{\delta}_n |-1/2, \downarrow\rangle, \quad (4)$$

from whence the oscillator strengths are found:

$$I_{x,y}^n = \left[\frac{\alpha_n}{\sqrt{2}} \mp \frac{\delta_n}{\sqrt{6}} \pm \frac{\bar{\beta}_n}{\sqrt{2}} + \frac{\bar{\gamma}_n}{\sqrt{6}} \right]^2, \quad (5)$$

where the upper signs refer to x polarization and the lower ones to y . Using $g_e = -0.38$ and $q = 0.03$, a very good fit to the oscillator strengths is obtained for κ values between 0.2 and 0.4.¹⁸ The resulting values for δ are between 25 and 20 μeV , respectively. We wish to emphasize that the quality of the fit deteriorates significantly for values of κ and δ outside this range. Thus, we can conclude that $\delta = 22 \mu\text{eV} \pm 3 \mu\text{eV}$. This value of the exchange splitting is close to the estimates for the bulk value,¹³ and as expected is smaller than that obtained for narrow wells.^{7,8} To check the consistency of the procedure, we redo the curve fitting of the energy curves now calculated by including the light holes, using the values found for δ and κ . Taking $\kappa = 0.2$,¹¹ the best fit for g_e is slightly changed to -0.36 , a value which is in excellent agreement with that measured in Ref. 15. The best fit for q is still $q = 0.03$. The theoretical curves for the optimized parameters are shown as solid and dashed lines in Fig. 3.

We have conducted a similar analysis on the 28-nm sample, and the following values were obtained: $g_e = -0.44$, $q = 0.04$, $\kappa = 0.35$, and $\delta = 21 \mu\text{eV}$. The larger magnitude of g_e , approaching the bulk value, reflects the fact that the well is wider than in the 22-nm sample.¹⁵ The good consistency of the results on both samples provides additional support for the validity of the analysis.

We wish to comment that the contribution of the cubic term is usually neglected in the interpretation of magnetic field experiments. It should be noted that its contribution to the Zeeman Hamiltonian in our experiment is approximately a third of that of the electron. For the 4.8-nm wells in the experiment of Ref. 8, the contribution of the cubic term is approximately half that of the electron. Thus, neglecting this term is unjustified.

In summary, we have introduced a method for measuring the exchange splitting of the exciton and the coefficient of the cubic Zeeman term in wide QW's. We have determined these parameters in a 22-nm QW with good accuracy and have shown their convergence to the bulk values.

This research was supported by the Israel Science Foundation founded by the Israel Academy of Sciences and Humanities. P.C.K. acknowledges sabbatical leave from Oxford University.

¹ G. L. Bir and G. E. Pikus, *Symmetry and Strain Induced Effects in Semiconductors* (Wiley, NY, 1975).

² M.Z. Maialle *et al.*, Phys. Rev. B **47**, 15 776 (1993).

³ A. Franceschetti *et al.*, Phys. Rev. B **58**, R13 367 (1998); M. Bayer *et al.*, Phys. Rev. Lett. **82**, 1748 (1999).

⁴ L.C. Andreani and F. Bassani, Phys. Rev. B **41**, 7536 (1990).

⁵ H.W. van Kesteren *et al.*, Phys. Rev. B **41**, 5283 (1990).

⁶ P.G. Baranov *et al.*, Solid State Commun. **87**, 649 (1993).

⁷ E. Blackwood *et al.*, Phys. Rev. B **50**, 14 246 (1994).

⁸ T. Amand *et al.*, Phys. Rev. Lett. **78**, 1355 (1997).

⁹ Y. Chen *et al.*, Phys. Rev. B **37**, 6429 (1988).

¹⁰ J.M. Luttinger, Phys. Rev. **102**, 1030 (1956).

¹¹ M.J. Snelling *et al.*, Phys. Rev. B **45**, 3922 (1992).

¹² G. Bastard, *Wave Mechanics Applied to Semiconductor Heterostructures* (Les Éditions de Physique, France, 1988).

¹³ D.D. Sell *et al.*, Phys. Rev. B **7**, 4568 (1973); W. Ekardt, K. Losch, and D. Bimberg, *ibid.* **20**, 3303 (1979); R. Sooryakumar and P.E. Simmonds, *ibid.* **27**, 4978 (1983). The value of the exchange splitting δ in these papers is 100, 20, and 0 μeV , respectively.

¹⁴ S. Glasberg *et al.*, Phys. Rev. B **59**, R10 425 (1999).

¹⁵ A.P. Heberle, W.W. Rühle, and K. Ploog, Phys. Rev. Lett. **72**, 3887 (1994); R.M. Hannak *et al.*, Solid State Commun. **93**, 313 (1995).

¹⁶ G. Rau, P.C. Klipstein, and N.F. Johnson, Phys. Rev. B **58**, 7210 (1998).

¹⁷ G. Rau, A.R. Glanfield, P.C. Klipstein, and N.F. Johnson, Phys. Rev. B **60**, 1900 (1999).

¹⁸ Several authors (Refs. 5 and 7) already noticed the fact that the value of κ in a QW is significantly smaller than that of the bulk, $\kappa = 1.2$.

2.5 Spatial imaging of the photoluminescence-polarization from a 2DEG near filling factor $\nu=1$.

S. Glasberg, H. Shtrikman and I. Bar-Joseph

Photoluminescence of a two-dimensional electron gas near $\nu=1$: the screening response to a photo-excited hole

Under preparation for submission to the Phys. Rev.

We measure the degree of polarization of the photoluminescence from a two-dimensional electron gas as a function of the filling factor near $\nu=1$. The measurements are done by laterally varying the electron carrier density, and optically imaging the Hall effect near the $\nu=1$ contour. We find that the photoluminescence polarization $P = \frac{I_{\sigma^+} - I_{\sigma^-}}{I_{\sigma^+} + I_{\sigma^-}}$, shows a minimum exactly at $\nu=1$, of $P \sim 0$, with a symmetric rise away from $\nu=1$. This result is opposite to the expectation of $P \sim 1$ for a fully polarized 2DEG at $\nu=1$. We show that the behavior we observe is the result of the strong Coulomb interaction of the 2DEG with the photo-excited hole.

The quantum Hall states are characterized by their incompressibility. The incompressibility at even integer filling factors is due to the single particle cyclotron gap, whereas at odd filling factor there is a smaller Zeeman gap. In fractional quantum Hall regime the gap is formed because of electron-electron interactions. Recently, it was found that the $\nu=1$ state is similar to fractional states [1], since even in the absence of a Zeeman splitting the gap persists due to electronic correlations.

When an extra electron is added to the $\nu=1$ state, the system can minimize its energy by flipping the spin of some electrons, and forming a spin texture termed Skyrmion [1]. The existence of Skyrmions was verified by NMR [2], absorption [3], and activated transport measurements [4,5]. Similarly, the presence of a positive charge (or the lack of an electron) will produce an excitation called an "Anti-skyrmion". Evidence for the

formation of such a state in the presence of a photo-excited hole was provided by PL measurements [6].

The mechanism by which a 2DEG screens the potential of a photo-excited hole at $\nu=1$ was intensively studied experimentally [6,7] and theoretically [8-10]. In principle a single electron suffices to screen the photoexcited hole. Thus, the initial state of the 2DEG at $\nu=1$ consists of an electron at the upper Zeeman level and a ferromagnetic electron gas. This electron forms an exciton with the valance band hole. It was shown that a recombination of this exciton does not perturb the 2DEG. On the other hand, if an electron from the filled lowest landau level recombines with the hole, a spin wave excitation is created. The energy spectrum of this spin excitation is manifested in a low energy tail of the PL spectrum [7].

In the accompanying paper we study the 2DEG response to a hole at filling factors *near* $\nu=1$. We study the PL intensity at the two circular polarizations and analyze the underlying electron screening properties. The PL polarization probes the relative occupation of the spin-up and spin-down states. We show that the occupation of a spin-up state is sensitive to the compressibility of the 2DEG. We present a phenomenological model that quantifies the screening of the valance-hole potential in terms of the 2DEG screening length.

We have used spatial imaging of the photoluminescence to study the PL properties near the $\nu=1$ state. The set-up is illustrated in Fig. 5.1. The sample was mounted in a cryostat having birefringent free windows. A set-up of lenses and a polarizer collected and

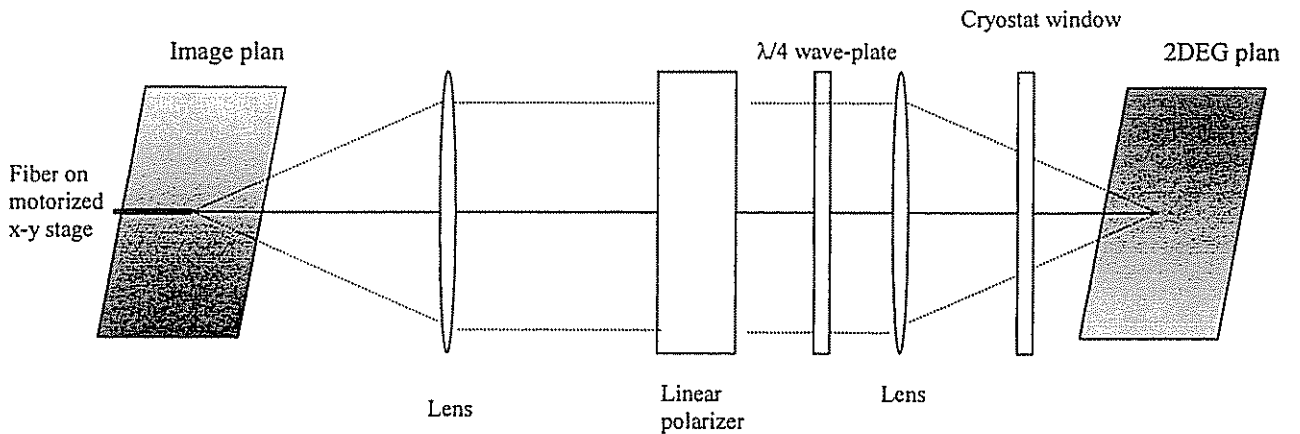


Fig. 5.1. The measurement set-up for imaging the 2DEG photoluminescence.

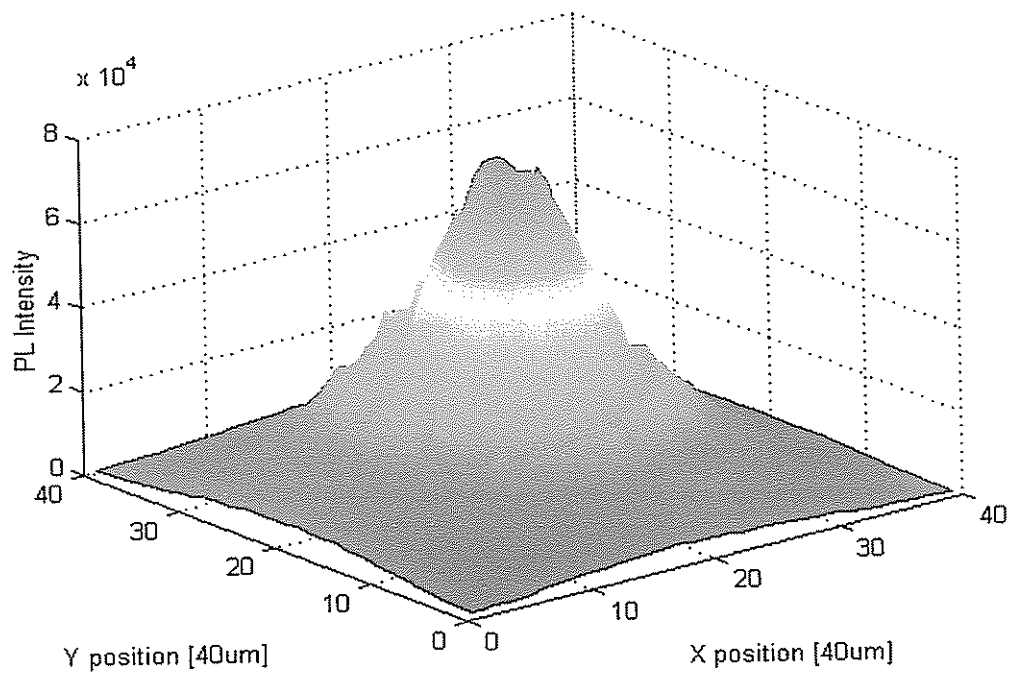


Fig 5.2. (a) 3D Image of the 2DEG spatially varying PL intensity (σ^- polarization).

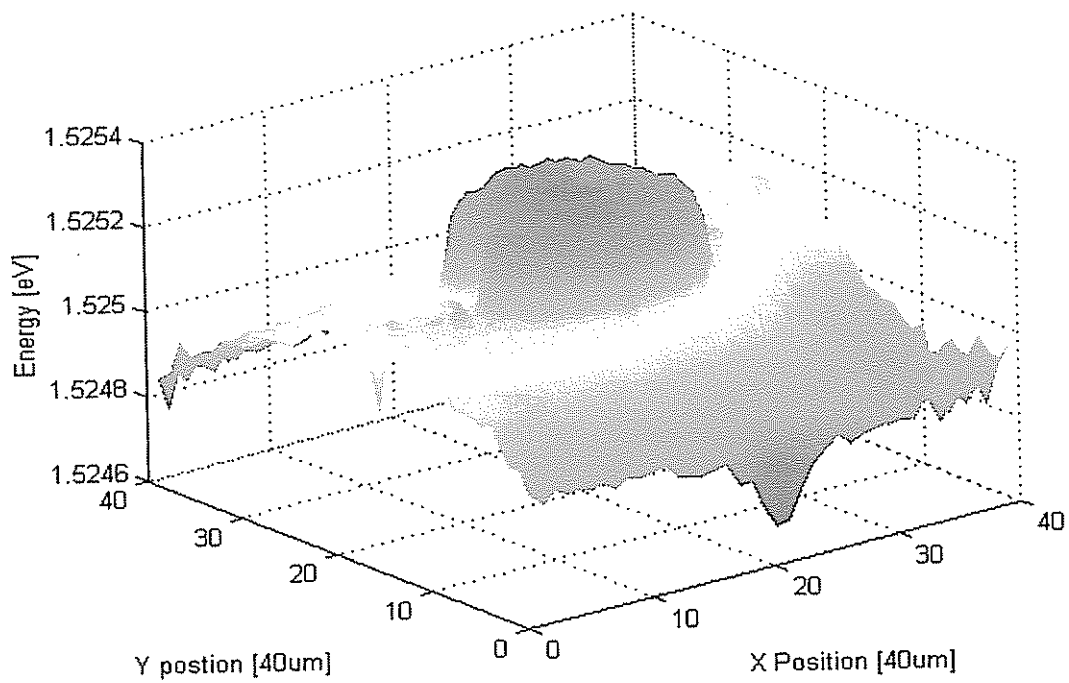


Fig 5.2. (b) 3D Image of the 2DEG spatially varying PL energy (σ^- polarization).

analyzed the spectra from a 2DEG, which was held at a temperature of 1.5K. The PL was imaged to a plane that was scanned by a fiber. The spatial imaging resolution was determined by the fiber diameter and was between $7\mu\text{m}$ to $350\mu\text{m}$. The results reported were obtained with a $50\mu\text{m}$ resolution.

The sample was illuminated by a He:Ne laser spot that created a density gradient by depletion (see chap. 2.1). The PL intensity, being linear in the excitation intensity, reflects the intensity profile of laser spot, as seen in Fig. 5.2a. The 2DEG $\nu=1$ boundary was observed through its unique energy and polarization footprint in photoluminescence (Fig.5.2b). At a given magnetic field, this boundary forms a two-dimensional contour. As seen, wherever filling factor $\nu=1$ occurs, a sharp jump in the PL energy is observed. The density profile was calibrated by detecting the $\nu=1$ jump as a function of magnetic field. This jump was studied extensively in the past [6,7]

Analysis of the intensities is done through

the degree of polarization, which is given by $P=(I_{\sigma^+}-I_{\sigma^-})/(I_{\sigma^+}+I_{\sigma^-})$ and measures the relative occupancy of the Zeeman split levels. Fig. 5.3 shows P at several magnetic fields. The depolarization towards $\nu=1$ is evident. This behavior of the PL intensity near $\nu=1$ was also seen with a 2DEG in a CdTe heterostructure [11]. It stands in sharp contradiction to the results of Ref. 12, where $P \sim 1$. There, the PL of the 2DEG was observed using recombination with acceptor bound holes. The perturbation from the photo-excited hole was minimal because the acceptors layer was remote. Thus, there is a clear indication to the source of the discrepancy. A rigorous account of the observation is

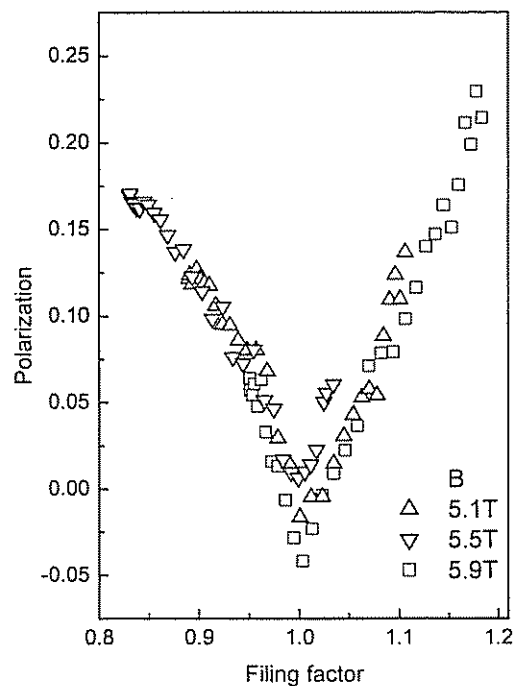


Fig. 5.3: The degree of polarization P of the PL from a 2DEG, as a function of filling factor near $\nu=1$.

not available currently. Nevertheless, a phenomenological model we outlined above is given in the paper.

References

1. S. L. Sondhi *et al.*, Phys. Rev. B **47**, 16419 (1993)
2. S. E. Barret, G. Dabbagh, L. N. Pfeiffer, K. W. West and R. Tycko, Phys. Rev. Lett. **74**, 5112 (1995)
3. E. H. Aifer, B. B. Goldberg, and D. A. Broido, Phys. Rev. Lett. **76**, 680 (1996)
4. A. Schemeller, J. P. Eisenstein, L. N. Pfeiffer, K. W. West and R. Tycko, Phys. Rev. Lett. **75**, 4290 (1995)
5. D. K. Maude *et al.*, *EP2DS-12* Workbook., 1:1 (1997)
6. J. L. Osborne *et al.*, Phys. Rev. B **58**, R4227 (1998)
7. F. Plentz, D. Heiman, L. N. Pfeiffer, and K. W. West, Phys. Rev. B **57**, 1370 (1998)
8. N. R. Cooper and D. B. Chklovskii, Phys. Rev. **55**, 2436 (1997)
9. P. Hawrylak and M. Potemski, Phys. Rev. **56**, 12386 (1997)
10. T. Portengen *et al.*, Phys. Rev. B **55**, R7367 (1997)
11. Y. Imanaka *et al.*, J. Crystal of Growth **214/215**, 240 (2000)
12. I. V. kukushkin, K. v. Klitzing, and K. Ebrel, Phys. Rev. Lett. **82**, 3665 (1999)

Photoluminescence of a two-dimensional electron gas near $\nu=1$: the screening response to a photo-excited hole

S. Glasberg, H. Shtrikman, and I. Bar-Joseph

Department of Condensed Matter Physics, The Weizmann Institute of Science, Rehovot 76100, Israel

We have measured the photoluminescence degree of polarization from a two-dimensional electron gas as a function of magnetic field and carrier density near filling factor $\nu=1$. We found that the photoluminescence degree of polarization poses a minimum exactly at $\nu=1$, with a symmetric rise away from that filling factor. We suggest that the depolarization of the photoluminescence at $\nu=1$ manifests the creation of an exciton in the incompressible two-dimensional electron gas. The gradual recovery of PL polarization away from $\nu=1$ manifests the increasing compressibility of the electron gas.

PACS: 71.35.Ji, 78.66.Fd, 78.55.-m, 78.66.-w

The behavior of the two-dimensional electron gas (2DEG) in the magnetic field regime near filling factor $\nu=1$ is a subject of intensive research in recent years. At this filling factor all the electrons reside at the lower spin-level, and the 2DEG is in an incompressible state. It was predicted, however, that away from this filling factors, at $\nu<1$ or $\nu>1$, the 2DEG could minimize its energy by exciting electrons to the higher spin level. This excitation, which is called a Skyrmion [1], is manifested as a rapid decrease of the spin-polarization of the electrons in both sides of the $\nu=1$ state. This behavior was indeed observed by NMR measurements of the electron magnetization [2].

It is well known that the spin polarization of a 2DEG can also be determined by an optical measurement. The underlying idea is based on the selection rules for interband transitions: σ^+ or σ^- circularly polarized photons can be absorbed by a transition to the spin up or down electron state, respectively. Thus, absorbance at each of the two polarization should be directly related to the occupation of these spin states. Similar arguments hold for a photoluminescence (PL) measurement. In that case, the PL polarization P , defined by $P=(I_{\sigma^+}-I_{\sigma^-})/(I_{\sigma^+}+I_{\sigma^-})$ where I_{σ^+} and I_{σ^-} are the intensities at the σ^+ and σ^- , respectively, provide a measure of the electron spin

polarization. These selection rules were recently used to determine the electron spin-polarization in an absorption [3] and PL [4] measurements at various integer and fractional filling factors.

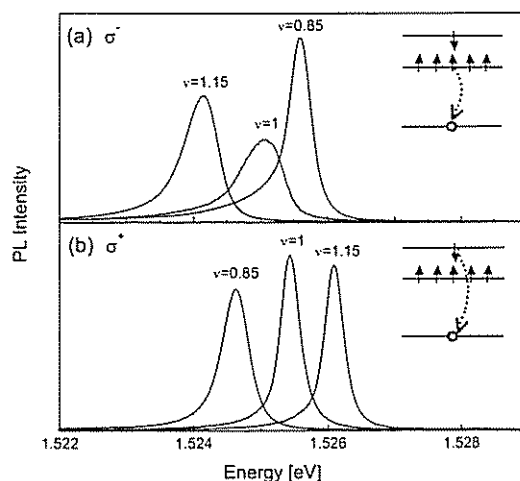


Fig. 1: The PL intensity as a function of filling factor, near $\nu=1$. Recombination is from (a) the LLL σ^- and (b) the next Zeeman split LL σ^+ . Insets show the different recombination processes.

An important factor that should be taken into account in an optical measurement is the photo-excited hole. This hole, which is positively charged, may modify the state of the

2DEG. The understanding of its role in a PL experiment around $\nu=1$ is the focus of this work. We find that the PL polarization P exhibits a behavior opposite to that anticipated for a 2DEG: it is nearly zero at $\nu=1$ and increases symmetrically at both higher and lower fillings. We show that this behavior manifests the screening of the hole potential by the 2DEG: the electrons at $\nu=1$ are at an incompressible state and screening can only be achieved by an electron at the higher spin level. This electron, which can be the photo-excited electron, could fully screen the hole charge. At $\nu \neq 1$ the electrons become compressible and partial screening can be achieved by the electron redistribution. As a result, the occupation in the higher spin level at the vicinity of the hole is lower. Since the PL intensity is proportional to overlap between the electron and hole it serves as a measure for the *local* occupation of the electron spin levels near the hole.

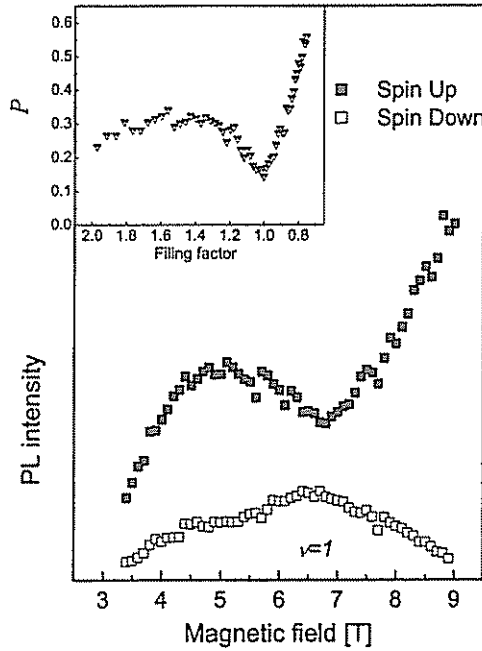


Fig. 2: The σ^+ and σ^- PL intensities from the Zeeman split LLLs, as a function of magnetic field. Inset: The corresponding degree of polarization of the PL intensity as a function of the filling factor.

Our measurements were conducted on a single well sample, consisting of a single sided modulation doped 20 nm quantum well with a 50 nm spacer. The electron density of $1.6 \cdot 10^{11} \text{ mW cm}^{-2}$ was deduced from the magneto-optical spectrum. We performed two kinds of measurements: one in which the density is fixed and we change the magnetic field, and another in which the magnetic field is kept constant and the density is tuned. Both techniques enabled us to vary the filling factor, but also allowed us to separate between the dependence on magnetic field or density and that which is due to the filling factor. Polarized PL measurements as a function of magnetic field were carried out at a temperature of 1.5K using a pumped helium refrigerator. The sample was illuminated by He:Ne laser intensity of 0.1 mW cm^{-2} . The emitted PL was

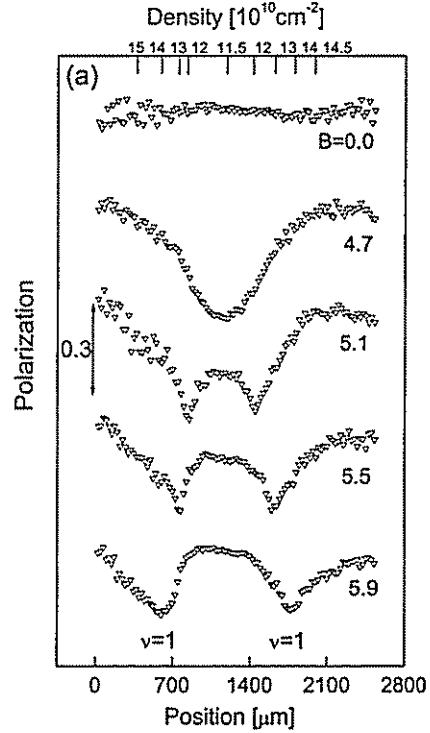


Fig. 3: The degree of polarization of the PL Intensity from the Zeeman split LLLs, as a function of the position (density).

analyzed with a circular polarizer and collected with an optical fiber. The signal was dispersed in a 0.75m spectrometer and detected with a cooled CCD detector-array. The measurements as a function of density were done using a novel technique: we have previously shown that the illumination of the sample by light at energy that is below the bandgap of the barriers causes a depletion of the electron density in the well. The amount of that depletion depends on the density - the higher the illumination intensity the lower is the electron density. As a result, when the sample is illuminated by a light beam with a Gaussian intensity profile, we expect the electron density to be the lowest at the center and highest at the edges. Thus, by imaging the PL from the illuminated area and measuring the PL from each point separately we can obtain the PL spectrum over a wide range of electron densities. To conduct this measurement we used a 1.5 K cryostat having birefringent free windows.

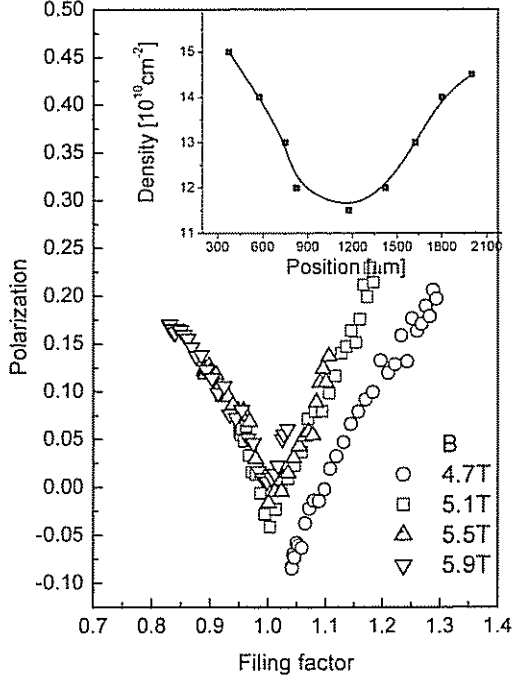


Fig. 4: The degree of polarization as a function filling factor. Inset: the carrier density as a function of position. (Both obtained from analysis of the data presented in Fig. 3).

The sample was illuminated by a He:Ne laser beam with a spot size of $\sim 1 \text{ mm } 1/e^2$ diameter. The average laser intensity was 1 mW cm^{-2} . A set-up of lenses, quarter wave plate and a polarizer analyzed the spectra from the 2DEG and imaged it into a plane. The PL was collected by an optical fiber whose position at the imaging plane was controlled using step motors. The fiber diameter ranged between $7 \mu\text{m}$ to $350 \mu\text{m}$ in various measurements. The spatial imaging resolution is directly given by the diameter of the collecting fiber, since the magnification of the lens system was unity. The results shown were obtained with a $50 \mu\text{m}$ diameter fiber. This resolution was found sufficient, with the collected PL signal being mechanical scans. Figure 1 shows the PL spectrum from the lowest Landau level for several filling factors near $\nu=1$ at two circular polarizations. The filling factor was varied by a magnetic field. A different dependence on filling factor is seen at the two polarizations: large enough to have sufficiently low noise. Care was taken to ensure the repeatability between the different polarizations and the σ^- recombination line at $\nu=1$ is relatively broad, with a low energy tail and it becomes narrower as ν is changed to both lower and higher values. The σ^+ recombination line, on the other hand, remains narrow throughout the filling factor range. (In both circular polarizations we observe some asymmetry around $\nu=1$, with the lineshape at $\nu>1$ being broader than $\nu<1$). This behavior was already reported in several earlier experiments [5], [6], and was analyzed theoretically [7], [8]. It was shown that the recombination lines at the two polarizations correspond to two different processes. To see that let us consider the insets of Fig. 1. We assume that the system is initially at $\nu=1$, with a single additional photo-excited electron at the upper spin level. It is evident from the figure that the final state of the system is not the same for the two recombination processes. In the σ^+ process the additional electron is removed and the final state is a filled lower spin level. The σ^- process, on the other hand, removes an electron from the lower spin level, leaving a quasi-hole in the filled spin level and an electron at the upper one. This final state is

in fact equivalent to a spin-flip excitation of the $\nu=1$ state, and since the relative position of the electron and quasi-hole can be different, we get a spin-wave excitation. This excitation is manifested as a broad low energy tail of the σ^- line.

We notice, however, that in addition to the changes in lineshape around $\nu=1$ there are some significant changes in peak intensity, especially at the σ^- polarization. To quantify these changes we study the behavior of the PL polarization P as a function of ν . We first do that by changing the magnetic field, keeping the density fixed. The results are shown in Fig. 2: a clear and strong dip is observed at $\nu=1$ (corresponding to $B=6.7$ T). This behavior is opposite of that of the 2DEG spin polarization, which has a *maximum* at $\nu=1$ and *decreases* at higher and lower filling factors. It is instructive to compare this result with the recombination spectra of a 2DEG with a remote acceptor [4]. In this experiment the PL showed a monotonic *increase* its polarization until it reached the value $P=1$ at $\nu=1$. The main difference between the two experiments is the location of the valence band hole relative to the 2DEG along the growth direction. In our experiment, which is done in a quantum well, the hole is very close (few nm) to the 2DEG plane while in Ref. 4 the hole is bound at a distance of 25 nm from the heterostructure. The discrepancy between our results and that of Ref. 4 points to the importance of the electron-hole Coulomb interaction in determining the PL polarization. This interaction is much stronger in our quantum well sample.

We next studied the behavior at a constant magnetic field while varying the electron density using our PL imaging setup. The $\nu=1$ boundary was observed through its unique PL peak energy footprint: at this filling factor (as in other integer and fractional filling factors) there is an abrupt jump in peak energy which reflects a jump in the chemical potential [6, 9]. By conducting this measurements at several magnetic fields and identifying the $\nu=1$ boundary at each field we obtain a calibration of the electron density at each spatial location (see inset of Fig. 4). Let us use this calibration to study the behavior of the PL polarization P

as a function of ν . Figure 3 shows several cuts through the center of a two-dimensional image of the PL polarization, taken at different magnetic fields. Two clear minima are observed as filling factor $\nu=1$ occurs (the symmetric carrier density profile produces two minima in the polarization curve). We note that the Zeeman splitting does not show similar behaviour. Hence the changes in the intensities can not originate from changes in the thermal occupation. Rather, as shown in Fig. 4, a clear *symmetric* and linear dip is obtained. Its slope is about 1.3 spin/flux quantum, nearly independent of the magnetic field.

Let us track the origin of the behavior of the PL polarization near $\nu=1$. To do so we would like to obtain the electron occupation near the photoexcited hole. The occupation of the Zeeman split LLs is determined by the minimum energy state, which screens the hole. There are two distinct ways by which a hole is screened: by a single electron or by collective response of the 2DEG. At $\nu=1$ all electrons occupy the lowest LL hence the screening by a single electron requires occupation of the next LL with an energy price of E_z^* , which is the exchange enhanced Zeeman splitting. This energy is the sum of the bare Zeeman energy splitting and the correlation energy paid for having two electrons occupying a given site with identical spatial wave-functions. The total energy splitting is linear with the magnetic field, and written as $g^*\mu_B B$. The enhanced g -factor depends on density and equals about 6 at $n=1.6 \cdot 10^{11}$ mW cm⁻² [10], which results in E_z^* being about 2.5 meV.

Let us consider the opposite limit where the gas is highly compressible. We approximate the hole as a positive charge disc of diameter $\sim l_B$, where l_B is the magnetic length. The electronic charge density near that hole, ρ_{sc} , can be calculated from linear response theory. The classical capacitance energy it costs to screen the hole potential is given by $\epsilon \int V_0(r) \rho_{sc}(r) d^2r$, where ϵ is the dielectric constant and $V_0 = -e^2/\epsilon l_B$. The integral gives $E_{sc} = 3e^2 \lambda_{TF} / 2\epsilon l_B^2$, where λ_{TF} is the Thomas-Fermi screening length.

To model the 2DEG response we construct a phenomenological energetic function

$$E(\alpha) = \alpha E_z^* + (1 - \alpha) E_{sc}$$

with an amplitude α . This function is the sum of the energy associated with a spin flip of a net charge αe , and the classical capacitance energy associated with screening the remaining positive charge $(1 - \alpha)e$ spread over a radius of l_B . Thus α falls in the range $0 < \alpha < 1$.

For an ideal 2DEG, the screening length diverges at $\nu=1$. However, localization and temperature broaden the δ -function response and decreases λ_{TF} to several times the magnetic length [11]. Taking $\lambda_{TF} \sim l_B$, E_{sc} is in the order of 10 meV, which is much larger energy than E_z^* . Hence, $\alpha \sim 1$ minimizes the electron energy. Away from $\nu=1$ $\lambda_{TF} \ll l_B$ so E_{sc} will be smaller than E_z^* . As a result one expects α to tend to 0.

Based on the analysis above we interpretate the experimental results as follows: At $\nu=1$ the incompressible 2DEG does not screen the potential of the photoexcited hole. Rather, an extra (spin flipped) electron is required to neutralize the hole. The identity of electron and hole lowest LL wave-functions at high magnetic fields guarantees that the cancellation would be good. As a result, the valance hole can recombine with either an 'up' or 'down' electron with similar probabilities. Averaging over many recombination events one indeed observes at $\nu=1$ a degree of polarization close to zero (Fig. 4). As the filling factor shifts away from $\nu=1$, the electron gas becomes increasingly compressible. Thus, a screening via 'rearrangement' within the levels may be energetically favorable relative to spin flip. Thus, the recombination from the next spin

level would diminish and strongly polarized PL occurs (note that at the relevant range of filling factors the lowest LL is always dominantly occupied; $0.8 < \nu < 1.2$). At $\nu > 1$ and $\nu < 1$ an electron-hole symmetry holds, and screening by a minority of electrons at $\nu > 1$ is equivalent to that from a minority of empty states in the lowest LL at $\nu < 1$. Stated more accurately, both yield the same expression for the 2DEG compressibility wave-vector, $q_{TF} = 2De^2 n$. This symmetry is the underlining mechanism that results in a symmetric variation of the PL polarization about $\nu=1$.

Changes in the PL polarization near $\nu=1$ may be also related to the relaxation of the photoexcited electrons into the lowest LL. At low temperatures the LLL is fully occupied for $\nu > 1$, while it becomes increasingly vacant for $\nu < 1$. Thus, one may expect an increased rate of relaxation of the photoexcited spin-up electrons at $\nu < 1$. As we observe a symmetric behavior of the PL about $\nu=1$, such a mechanism has to incorporate symmetric reduction in the occupation of the LLL for $\nu > 1$ and $\nu < 1$, which requires the formation of spin textures [1, 5]. The screening picture we presented is certainly consistent with the formation of spin textures, but does not require such.

Finally we note that similar behavior of the PL intensity (and hence polarization) near $\nu=1$ was recently reported for a 2DEG in CdTe QW [12].

We acknowledge useful discussions with Adi Stern.

-
1. L. Sondhi *et al.*, Phys. Rev. B **47**, 16419 (1993)
 2. S. E. Barret, G. Dabbagh, L. N. Pfeiffer, K. W. West and R. Tycko, Phys. Rev. Lett. **74**, 5112 (1995)
 3. E. H. Aifer, B. B. Goldberg, and D. A. Broido, Phys. Rev. Lett. **76**, 680 (1996)
 4. I. V. Kukushkin, K. v. Klitzing, and K. Ebrel, Phys. Rev. Lett. **82**, 3665 (1999)
 5. F. Plentz, D. Heiman, L. N. Pfeiffer, and K. W. West, Phys. Rev. B **57**, 1370 (1998)
 6. J. L. Osborne *et al.*, Phys. Rev. B **58**, R4227 (1998)
 7. N. R. Cooper and D. B. Chklovskii, Phys. Rev. **55**, 2436 (1997)
 8. P. Hawrylak and M. Potemski, Phys. Rev. **56**, 12386 (1997)
 9. R. J. Nicholas *et al.*, Physica B **249**, 553 (1998); K. Asano and T. Ando, Physica B **256**, 319 (1998)
 10. D. R. Leadley, R. J. Nicholas, J. Harris, and C. T. Foxton, Phys. Rev. B **58**, 13036 (1998); V. T. Dolgoplov *et al.*, Phys. Rev. Lett. **79**, 729 (1997)
 11. J. P. Eisenstein, L. N. Pfeiffer, and K. W. West, Phys. Rev. B **50**, 1760 (1994)
 12. Y. Imanaka *et al.*, J. Crystal Growth **214/215**, 240 (2000)

3. Summary

1. Optically generated hole and electron gases

We have demonstrated a new technique to optically generate 2DHG in wide GaAs QWs. A functional analogy of the new structure with modulation-doped structures was established. The 2DHG was found to have narrower recombination line-widths, which we utilized in subsequent works (see chaps. 2.2 and 2.3). The new mechanism has enabled the realization of a dense spatially separated 2DEG-2DHG system. We have demonstrated the ability to control the density of each of the gases independently using two lasers. Measurements and analysis of the system magneto-optical spectrum as a function of density and inter-well separation showed it is a simple superposition of the individual gases spectrum. Namely, we did not observe a manifestation of an inter-well Coulomb interaction. We conclude that further refinements are sought for this system to show delicate interactions, mainly reducing the optical excitation power.

2. The X^+ magneto optical spectra and its comparison with that of the X^- .

We have identified the X^+ spectral signature in a magnetic field, which consists of spin singlet and triplet states. We have demonstrated the ability to change the type of excess carriers from holes to electrons and thus the spectra changed from X^+ to X^- within the same sample. This enabled us to accurately compare the properties of the two complexes. We found that the binding energies of the two complexes are nearly identical at zero magnetic field, in contrast with predictions from existing models at the time. In a magnetic field we found that the X^+ binding energy remains constant, while that of the X^- increases substantially. The modeling of charged excitons at zero and finite magnetic fields is presently evolving through rigorous theories and comparison of experimental results with these models shows improved agreement at zero field.

3. Identification of the X^+ shake-up process and the valance band Landau-levels.

This work gave the first observation of the X^+ shake-up lines in a magnetic field. It has also gave a deeper insight into the behavior of the neutral Donor in the presence of a free hole (D^0h) in a magnetic field. The observation of valance-band Landau levels through the X^+ shake-up and D^0h recombination spectrums allowed us to extract the

cyclotron hole mass and its g factor. These parameters were not readily available from optical measurements before. These results were obtained with optically generated hole gas in intrinsic an QW. The sharp PL lines were critical for the high resolution spectroscopy. In that regard it would be interesting to try and observe delicate features as the center-of mass Landau-levels of charged excitons, and the 2DHG Landau-levels at an increased carrier density.

4. The neutral exciton, and the X^- and X^+ in a parallel magnetic field.

We have provided a first principle model of the exchange interaction in the neutral exciton. Experimentally, we have measured the exchange splitting between singlet and triplet excitons in a regime of weak quantum confinement. The importance of a measurement at such regime is that it gives values close to those from bulk samples but avoids the complexity of the analysis of the bulk results. In addition to this result, we have also measured at the same time the Luttinger parameter q in a GaAs QW for the first time. We have observed a strong linear degree of polarization of the X^+ and X^- PL spectrum along the magnetic field axis. We suggest this behavior is the result of the X^+ and X^- being polarized along the field. A rigorous calculation of the charged excitons orbital structure in a parallel magnetic field is needed to verify this result.

5. The screening response of a 2DEG near $\nu=1$ to a photo-excited hole.

We have measured the 2DEG PL intensity and extracted its degree of polarization near $\nu=1$. We used a set-up that spatially imaged the PL from a 2DEG. The results show that the photo-excited hole depolarizes the 2DEG differently at $\nu=1$ and $\nu \neq 1$. We have phenomenologically modeled the screening response of the 2DEG. The model explain the results assuming that at $\nu=1$ a single electron screens the photo-excited hole, whereas at $\nu \neq 1$ the screening must involve partial contribution from larger number of electrons. An interesting challenge is to determine if a skyrmion-like electronic texture is involved in the screening at $\nu \neq 1$.

תקציר

בעבודת דוקטורט זו פותחה טכניקה חדשה למימוש של גזי חורים ואלקטרונים בבורות קוונטיים ללא אילוח, באמצעות הארה והפרדת מטענים. טכניקה זו מרחיבה את יכולת המחקר של גזים אלקטרוניים דו-ממדים מעבר לאפשרי בדגמים מאולחים במספר אופנים: הצרת הקווים הספקטראליים, שליטה בסוג נושא המטען (חור או אלקטרון) באותו הדגם, מימוש גזי אלקטרוניים וחורים המופרדים לאורך ציר הגידול בסמיכות רבה, ושליטה מרחבית על פרופיל צפיפות נושאי המטען בבור הקוונטי.

בצפיפויות גז נמוכות, התכונות האופטיות של גזי האלקטרוניים והחורים נשלטות על ידי אקסיטונים טעונים שלילית וחיובית בהתאמה. הקווים הספקטראליים הצרים והיכולת לשנות את סוג נושא המטען אפשרו לראשונה את הספקטרוסקופיה של האקסיטון הטעון חיובית בשדה מגנטי ואת ההשוואה הכמותית של תכונותיו עם זה של האקסיטון הטעון שלילית. הממצא העיקרי הוא שוויון אנרגיות הקשר בהעדר שדה מגנטי, ותלות שונה בשדה המגנטי. מידע זה חיוני להבנת המבנה התלת-גופי של שני יוני האקסיטון. ממצא מרכזי נוסף הוא מדידת רמות לנדאו של פס הערכיות באמצעות ניתוח ספקטרום תהליכי העירור של האקסיטון הטעון חיובית.

בחלק אחר של העבודה נמדדו תכונות האקסיטון הנייטרלי והאקסיטונים הטעונים בשדה מגנטי המקביל למישור הבור הקוונטי. אנרגיית החילוף של האלקטרון והחור ופרמטר לוטינג'ר הא-ספרי נמדדו לראשונה בבור קוונטי רחב. בפרק האחרון אנו מדווחים על תוצאות מדידת תכונות המיסוך של גז האלקטרוניים בנוכחות חור ליד $v=1$. תכונות המיסוך נמדדו על ידי שינוי מרחבי רציף של צפיפות הגז והדמיה אופטית מרחבית של אפקט הול סביב קו הגבול המוגדר על ידי המילוי $v=1$.

ספקטרוסקופיה אופטית של גזי חורים ואלקטרונים
דו-ממדיים בבורות קוונטיים של GaAs אינטרינזי

חיבור לשם קבלת התואר
"דוקטור לפילוסופיה" מאת

שמואל גלסברג

מנחה: פרופ' ישראל בר-יוסף

מוגש למועצה המדעית של
מכון וייצמן למדע
רחובות, ישראל

תמוז תשס"א